TOPICAL REVIEW — Fundamental physics research in lithium batteries

Lithium-ion transport in inorganic solid state electrolyte*

Jian Gao(高健)[1,2], Yu-Sheng Zhao(赵予生)[3], Si-Qi Shi(施思齐)[4,2,†], and Hong Li(李泓)[1,‡]

[1] Institute of Physics, Chinese Academy of Sciences, Beijing 100190, China
[2] Materials Genome Institute, Shanghai University, Shanghai 200444, China
[3] Department of Physics and Astronomy and High Pressure Science and Engineering Center, University of Nevada, Las Vegas, Nevada 89154, USA
[4] School of Materials Science and Engineering, Shanghai University, Shanghai 200444, China

(Received 18 May 2015; revised manuscript received 22 July 2015; published online 7 December 2015)

An overview of ion transport in lithium-ion inorganic solid state electrolytes is presented, aimed at exploring and designing better electrolyte materials. Ionic conductivity is one of the most important indices of the performance of inorganic solid state electrolytes. The general definition of solid state electrolytes is presented in terms of their role in a working cell (to convey ions while isolate electrons), and the history of solid electrolyte development is briefly summarized. Ways of using the available theoretical models and experimental methods to characterize lithium-ion transport in solid state electrolytes are systematically introduced. Then the various factors that affect ionic conductivity are itemized, including mainly structural disorder, composite materials and interface effects between a solid electrolyte and an electrode. Finally, strategies for future material systems, for synthesis and characterization methods, and for theory and calculation are proposed, aiming to help accelerate the design and development of new solid electrolytes.

Keywords: lithium-ion batteries, solid state electrolyte, ionic conductivity, ion transport mechanism

PACS: 82.47.Aa, 65.40.gk **DOI:** 10.1088/1674-1056/25/1/018211

1. Introduction

The early definition of solid state electrolytes (SSE) is usually indistinguishable from fast ion conductors (FICs) or super ion conductors (FICs), which are grouped as solid materials with ionic conductivity approaching (or in some cases exceeding) that of molten salts or electrolytic solutions. This implies a peculiar liquid-solid dual property, i.e., "some atoms have nearly liquid like mobility while others retain their regular crystalline arrangement."[1]

With the great attention paid to lithium-ion batteries (LIBs), their potential applications in electric vehicles and large-scale smart grids demand an urgent enhancement of safety, which results in today's broadened interest in inorganic solid state electrolytes. Some of their issues are as follows: (i) Composite solid electrolytes have higher conductivity at interphases. (ii) Solid electrolyte interphase (SEI) growing on electrodes (especially anions) is of critical importance for the performance of LIBs. However, Li_2CO_3, the main inorganic component, has much lower conductivity than the first defined superionic conductors.[2–5] In addition, electrode coatings, core-shell electrode particles and self-organized surfaces formed during synthesis also have functions similar to SEI. (iii) The conductivity of LiPON is of the magnitude 10^{-6} S/cm, which is much lower than found before; however, a thin film all-solid-state cell structure enables over 30000 charge–discharge cycles.[6] Considering all of the above, the general discussion of solid state electrolytes in this review is focused on their role in a working cell (to convey ions while isolating electrons), but not for their conductivity and the ion transport mechanism.

This review will concentrate on the ion diffusion mechanism in inorganic solid state matter, and the ion diffusion in polymers is mentioned as an aside to clarify the perspective. Although the review will focus on solid state electrolytes working in LIBs, the theoretical models and treating processes can be applied to those working in fuel cells, solid oxide fuel cells (SOFC), Li–air batteries, Li–S batteries, electrochemical sensors, electrochromic devices, oxygen separation membranes, and so on.

The superionic phase can typically be distinguished from the usual phase because of the following properties, which are summarized in Ref. [1]: high ionic conductivity, low activation, an open structure with an interconnected network of vacant sites available to ionic species. Besides, the phase can be characterized by dynamic and collective effects: the absence of well-defined optical lattice modes, the presence of a pervasive, low-energy excitation, an infrared peak in the frequency-dependent conductivity, unusual NMR prefactors, phase transitions and a strong tendency for mobile ions to be found be-

*Project supported by the National Natural Science Foundation of China (Grant No. 51372228), the Shanghai Pujiang Program, China (Grant No. 14PJ1403900), and the Shanghai Institute of Materials Genome from the Shanghai Municipal Science and Technology Commission, China (Grant No. 14DZ2261200).

†Corresponding author. E-mail: sqshi@shu.edu.cn
‡Corresponding author. E-mail: hli@aphy.iphy.ac.cn

© 2016 Chinese Physical Society and IOP Publishing Ltd

tween allowed sites. High ionic conductivity often conflicts with high structural stability, because higher ionic conductivity requires weak chemical bonding energy, which leads to opposite effects on the structural stability. As a compromise between the two aspects, a sort of "dual structure" will work: two separate sub-lattices provide, respectively, a rigid frame and a soft part that may undergo the phase transition to the higher symmetrical characteristic structure (disordered state) for mobile ions.

Atypical ionic conductors without "dual structure" or independent superionic phase can also be of interest as solid state electrolytes, as defined and interpreted above. Their characteristics usually lie between the normal thermally activated defect crystals and typical superionic conductors. Moreover, atypical ones often exist as thin film with nanometer scale thickness to make up for their deficient conductivity. Then the complexity of defects gives rise to the challenges of theoretical models and experimental characterization.

2. Brief history of the development of solid electrolytes[7–11]

In 1833, Michael Faraday discovered an abnormal enhancement of electrical conductivity in Ag_2S with the stimulation of temperature that could not be interpreted as arising from electronic conductivity. He then proposed Faraday's laws of electrolysis.[12] After that, Faraday,[13] Hittorf,[14] Gaugain,[15] etc. found that many inorganic solids exhibit similar behaviors. In 1884, Warburg[16] tested and verified Faraday's laws of electrolysis, and this work is regarded as a significant breakthrough for putting forward the probability of ionic (other than electronic) conductivity, overturning the conclusion of Arrhenius that neither pure salt nor pure water can be a conductor, but only salt dissolved in water.

In 1897, Nernst invented stabilized ZrO_2 as an electric lighting device (Nernst glower),[17,18] and it is still one of the most important oxygen sensitive solid electrolyte materials. The flow of electrical current was suggested to be essentially oxygen ion conduction, although the underlying mechanism was not illustrated until 1943 by Wagner.[19] During the period, Haber,[20] Katayama,[21] etc. actively promoted the investigation of glass/ceramic solid state electrolytes. In 1935, on the basis of the stabilized ZrO_2 discovered by Nernst, Schottky applied for the first patent on solid electrolytes used for fuel cells.[22] Subsequently, several other solid electrolytes suitable for fuel cell were proposed by Baur and Priess.[23] The performance of stabilized $ZrO_2$was not surpassed until the 1960s, when Takahashi discovered CeO_2–La_2O_3 solid solutions.[24] Nowadays, materials mentioned above remain the most widely utilized in SOFCs.

Other than the oxygen ion conductors mentioned above, in 1914, Tubandt and Lorenz studied the silver and thallium halides, among which AgI is important for its phase transition to high-conductive α-AgI below the melting point, exhibiting conductivity similar to its liquid phase.[25] The mobility was measured to identify Ag ions other than electrons as mobile species.[26] In 1935, by means of x-crystallography, strock studied the structure and put forward the sublattice melting model to interpret the abnormal high conductivity for Ag ions.[27]

On the theoretical side, the ion diffusion mechanism cannot be separated from defect chemistry. In 1923, Joffé concluded that "even pure crystals are partly dissociated and present an intrinsic conductivity";[28] in 1926, by assuming the presence of point defects, Frenkel suggested two basic diffusion mechanisms through interstitials and vacancies separately.[29] In 1930, Wagner and Schottky deduced from statistical thermodynamics that "in equilibrium at a finite temperature, some defects exist, even in a crystal of exact stoichiometric composition." In addition, nonstoichiometricity of a compound, i.e., having an excess of some component, can lead to extra interstitials or vacancies.[30,31] In 1962, Wagner extended the concepts of defect chemistry to the multicomponent system.[32] On the experimental side, Wagner contributed quite a lot during the 1950s, including the Hebb–Wagner direct-current polarization technique. And Wagner and Hebb proposed "blocking electrodes", electrodes that can distinguish the partial ionic and electronic current carriers of mixed conductors.[33]

At the end of the 1960s, some novel inorganic solid electrolytes were obtained via innovative synthesis strategies, and they attracted much attention due to their high conductivity and potential applications in electrochemical devices such as batteries. Two successful attempts were the synthesis of $RbAg_4I_5$ via doping, and stabilizing the high-temperature, high-conductivity phase α-AgI at room-temperature.[34] In another breakthrough, the Cu ion conductor $Rb_4Cu_{16}I_7Cl_{13}$ was synthesized and is even now the solid electrolyte with highest conductivity.[35] In 1973, Kunze discovered fast ion-conduction behavior in a glassy system with Ag,[36] which leaped over the earlier limitations of ceramic fields. While their conductivity is quite high, the above compounds are expensive, due to their Ag constituent and their Gibbs free energy is too low, causing low energy capacity at open-circuit voltage. Moreover, composition with excess Cu is usually accompanied by electrons or holes generating current, leading to mixed conductors, rather than a pure Cu ion conductor. As a result, neither Ag nor Cu ionic conductors can satisfy the application requirements.

In view of the above situation, attention was gradually turned to the alkali metal solid state electrolytes. In 1967, β-Al_2O_3 was found to be a solid electrolyte with two-dimensional conduction pathways,[37] and it reached the apex

of its reputation with the coming of the American oil crisis, when it was successfully applied in Na–S batteries. As an alternative to organic electrolyte solutions, solid state electrolytes are safer, so they have huge application prospects, motivating the investigation of solid state ionics.

Lithium is the lightest alkali metal with the smallest atomic number, indicating an extremely high gravimetric energy density, which attracts much attention, although the Li–ion solid electrolyte shows lower gravimetric energy density than the Ag or Cu counterpart, as shown in Figs. 1 and 2.

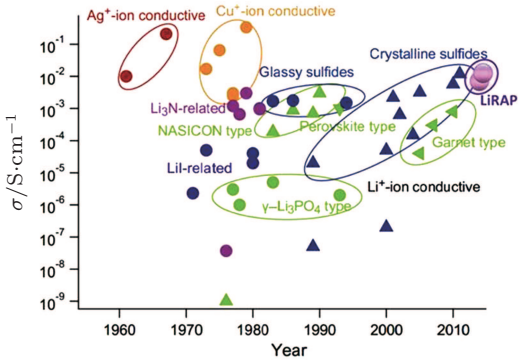


Fig. 1. Research progress map of solid electrolytes (adapted from Ref. [8], LiRAP is added).

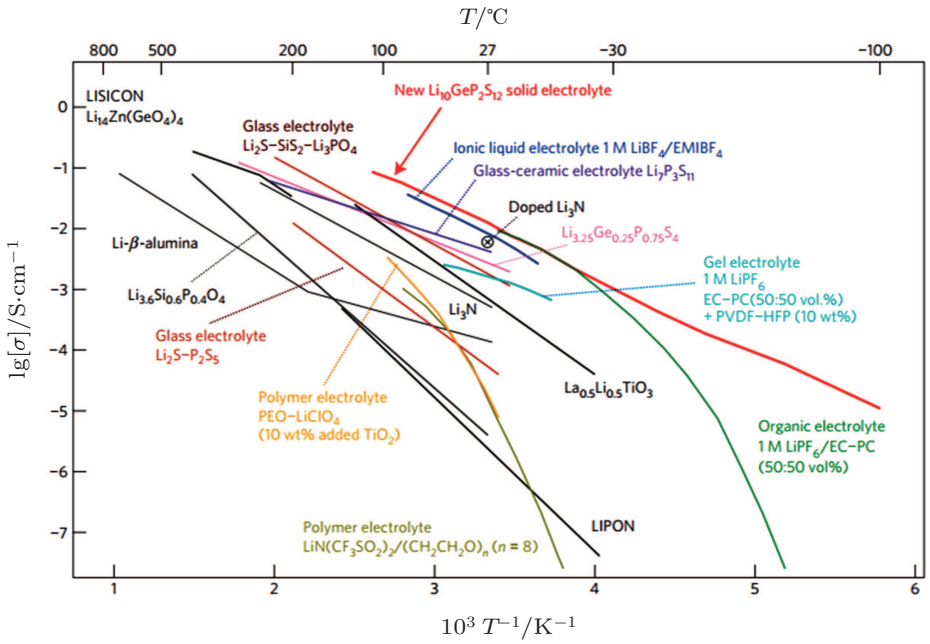


Fig. 2. Arrhenius plot of available lithium solid electrolytes, organic liquid electrolytes, polymer electrolytes, ionic liquids, and gel electrolytes.[38]

Lithium nitride was first reported in 1935,[39] and became intriguing as an ion conductor for its high lithium content and its open structure.[40,41] In 1973, Liang dispersed Al_2O_3 particles into a LiI solid matrix, and obtained a mixture with conductivity 50 times higher than that of LiI alone.[42] The "space charge layer" theory was proposed by Wagner[43] and Maier[44] in succession to interpret the abnormal phenomenon, guiding followers to optimize conductivity by designing the micro- or nano-complex. In 1980, LiI was used as a solid electrolyte in commercializing cardiac pacemakers.[45] In 1981 and 1982, lithium halide hydrate solid state electrolytes with an anti-perovskite structure were proposed,[46–48] as was their mixture with Al_2O_3.[49] Besides, $LiBH_4$[50,51] (and the mixture with lithium halides[52]) has high conductivity. The decomposition voltage of lithium-ion nitrides and iodides is too low to satisfy one of the usual criteria, which requires a really high cathode voltage involved in lithium-ion secondary batteries for high energy capacity. Despite the intrinsic disadvantage of instability, these discoveries and potential applications stimulated enthusiasm for researching inorganic solid state electrolytes, which motivated the discovery of oxide and sulfide systems with wider electrochemical windows and higher chemical and electrochemical stability.

Early attempts with lithium-ion oxide salts did not result in adequate performance as solid state electrolytes.[53,54] In 1976, Goodenough and Hong were first to report a fast sodium ion conductor $Na_{1+x}ZrP_{3-x}Si_xO_{12}$, which was later named NASICON (Na superionic conductor).[3,55,56] In 1977, $LiM_2(PO_4)_3$ compounds with the same structure and general formula as $LiM^{I}M^{II}P_3O_{12}$ were found to have high conductivity.[57] The three-dimensional (3D) $[M^{I}M^{II}P_3O_{12}]$ skeleton of NASICON is composed of MO_6 octahedra linked to PO_4 tetrahedra; mobile Li ions are distributed in skeletons with two types of occupied sites (A_1, A_2). The Li ion must struggle through a bottleneck when it jumps between two sites, and the bottleneck size depends greatly on the types and

character of skeleton ions,[58] and is influenced by the distribution or concentration of mobile ions at sites (A_1, A_2).[59] The abundant variety of dopants and substitutes makes NASICON a typical case for studying the relationship among chemical composition, crystal structure and ionic conductivity.[60] For example: if M is Ti, then Ti can be doped with Mg, In, Ga, Sc, Al, La, Y, Sn;[61–67] if M is Zr , then Zr can be doped with Nb, Ta, Y, In;[68] if M is Ge, Ge can be doped with Al, Ga, Sc, In,[69,70] and if M = Hf, then Hf can be doped with In, Sc.[71–73] Among all possible compounds, $Li_{1.3}Al_{0.3}Ti_{1.7}(PO_4)_3$ has the highest conductivity, whose M is fixed to Ti and doped by Al.[65,66] Although there have been many studies on NASICON superionic conductors, the inherent reasons for the doping-induced enhancement of ionic conductivity still remain open. Aono suggested that the high conductivity of $Li_{1.3}Al_{0.3}Ti_{1.7}(PO_4)_3$ may not be determined by the intrinsic structural character, but contributed by the higher density and smaller grain boundary resistance, which are both due to the Al doping.[74] The shortcoming of the large grain boundary resistance for the NASICON system can be overcome by preparing it into lithium-ion conductive glass ceramics (LIC-GC).[75–77] LIC-GC enhances total ionic conductivity by eliminating grain boundary resistance and is relatively easy to fabricate at a large scale by a melting method. In addition, glassy products are easier to mold and can be shaped into thin films. Note that LIC-GC has already been commercialized by the OHARA company.[78]

Another Li superionic conductor (LISICON) with 3D conduction pathway, $Li_{14}Zn(GeO_4)_4$, was developed by Hong in 1978.[79] However, the pure solution phases for this kind of oxysalt can be formed only within limited ranges of concentration and temperature.[80] The general formula is extended to $xLi_4M^{IV}O_4$–$(1-x)Li_3M^{V}O_4$ (M^{IV} = Ge, Ti, M^{V} = As, V) as a γ-Li_3PO_4-type solid electrolyte, which also has the solid solution limit (x = 0.4–0.6), and conductivity is not more than 10^{-4} S/cm.[81] Benefitting from the development of computer science and information techniques, it is feasible to screen solid state electrolytes for those possibly having excellent performance, via high throughput calculation. Fujimura *et al.* investigated LISICON systematically by calculating a series of conductivities of a wide compositional phase space at high temperature. Together with the machine learning technology, theoretical and experimental datasets are combined to predict the conductivity of each composition at certain temperatures. Limited by the actual solution range, the conductivity of the optimized composition is still less than 10^{-4} S/cm.[82] Although this system has low conductivity, its amorphous film can be applied in thin film batteries[83,84] for a shorter distance and smaller resistance between cathode and anode. Moreover, the glass or glass-ceramic state extension of the system usually has the higher conductivity. In 1993, as another extension of γ-Li_3PO_4 system,[85] the thermodynamically stabilized LiPON thin film was fabricated with radio frequency (RF) sputtering by Bates *et al.*[86] LiPON thin film has been widely used as thin film solid electrolyte[6,86–90] for its wide electrochemical window within 0–5.5 V[91] and its compatibility with high-voltage cathodes (above 5 V) such as $LiN_{i0.5}Mn_{1.5}O_4$, with a long life of more than 10000 cycles.[92] The Li_2PO_2N crystal was synthesized and calculated by *ab initio* calculation, comparing it to amorphous LiPON.[93]

The Thio-γ-Li_3PO_4 system often has higher conductivity, the study of which has been encouraged by the investigation of glass states of this system.[94] Highly polarized S ions interact with Li ions weakly, which results in sulfide solid electrolytes having higher conductivity than oxysalts.[94–98] As a result, sulfide solid electrolytes have become the current preference for integration into all-solid-state batteries.[99,100] Although the conductivity can be further increased by adding the composites such as LiI,[95–98] as mentioned above, the low decomposition voltage of LiI narrows the electrochemical window. Further studies indicate that adding oxides to the system can also enhance conductivity without affecting the working voltage,[101,102] and the resulting system can be applied in solid state batteries with 4 V cathodes.[103–105] Besides the glass-state systems, there has been much progress in the research of crystalline-state Li–P–S systems.[106–108] In 2000, Kanno discovered pure sulfides with a structure similar to LISICON, called thio-LISICON.[109] By optimizing the composition, $Li_{3.25}Ge_{0.25}P_{0.75}S_4$was found to exhibit the highest conductivity[110] among the thio-LISICON compounds. The system includes Li–Ge–P–S,[109–111] Li–Si–P–S,[112,113] and some thin films,[114] and it can be extended to general γ-Li_3PS_4[115] and β-Li_3PS_4[116,117] systems. The general system is one of the most widely investigated as solid state electrolytes,[113,118,119] but usually in combination with cathodes of lower voltage than common commercialized cathodes (e.g., $LiFePO_4$ and $LiCoO_2$) to ensure stability of the system. Besides, similar to the case of NASICON systems, the conductivity of LISICON can be enhanced by crystallizing the glass state to form a glass-ceramic system,[120–124] and the glass-ceramic electrolytes can be used in all-solid-state batteries.[125,126]

It is worth mentioning that in 2011, Kamaya *et al.* reported that a novel crystalline sulfide state solid electrolyte, $Li_{10}GeP_2S_{12}$, exhibiting conductivity of 1.2×10^{-2} S/cm at room temperature, which is the highest so far among the inorganic solid electrolytes.[38] It can be applied in all-solid-state batteries incorporating $LiCoO_2$ as the cathode (in contrast to sulfides mentioned in the last paragraph)[38,127] and Li–In alloy,[38] $Li_4Ti_5O_{12}$,[128] or Si[129] as the anode. In addition, it was found that batteries with Li metal as the anode and $LiFePO_4$ or $LiNi_{0.5}Mn_{1.5}O_4$ as the cathode can work, and

the corresponding voltammetric profiles were measured, although the cycling performance was not presented.[130] One possible reason is that $Li_{10}GeP_2S_{12}$ is not stable when in contact with Li metal, as has been confirmed by *ab initio* calculations,[131] cyclic voltammetry (CV) and *ex situ* x-ray diffraction (XRD) results.[132] The crystal skeleton structure was first obtained from XRD and synchrotron radiation x-ray data, combined with *ab initio* calculation,[38] and the Li occupation pattern was analyzed from refining the neutron diffraction[38] and single crystal x-ray data.[133] Furthermore, the thermodynamic stability of $Li_{10}GeP_2S_{12}$ was investigated by *ab initio* calculation,[134] and the Li ion diffusion mechanism was studied by classical[135] and *ab initio*[131] molecular dynamic (MD) simulations. Given the strong Coulombic interaction among the mobile ions, the string like cooperative ionic motion pattern is found to be energetically favorable,[136] leading to a one-dimensional ionic channel with low activation energy and high conductivity.[134,136] Interestingly, the consideration of van der Waals (VdW) interaction resulted in a three-dimensional ionic channel.[137] Combining two measurement methods with a distinct specific timescale, AC impedance spectroscopy (IS) and pulsed field gradient NMR (PFG-NMR), the conduction pathway dimension was identified separately according to the time-scale.[138] A totally different collective diffusion process was observed using nanosecond quantum molecular dynamics simulations of non-stoichiometric $Li_{4-x}Ge_{1-x}P_xS_4$, which leads to drastically reduced activation energy.[139] Experimental results also indicate higher conductivity, up to 1.42×10^{-2} S/cm, at room temperature for non-stoichiometric $Li_{10+\delta}Ge_{1+\delta}P_{2-\delta}S_{12}$ ($0\leq\delta\leq0.35$); in addition, when temperature is increased, the activation energy was reduced, and the respective three- and one-dimensional conduction pathways at high and low temperatures were visualized through the neutron diffraction data refined by the maximum-entropy method (MEM).[140] Enlightened by the discovery of $Li_{10}GeP_2S_{12}$ in 2011, Ong *et al.* studied the phase diagram, electrochemical stability and ionic conductivity of the $Li_{10\pm1}MP_2X_{12}$ (M = Ge, Si, Sn, Al, P, X = O, S or Se) family, finding that smaller lattice parameters lower the conductivity significantly, while larger parameters had less effect. Oxygen-substituted samples are stable, in contrast to their sulfide counterparts with lower conductivity. Note that for wide acceptance, electrolytes containing Ge are usually not stable with Li anodes, and both Si and Sn attract attention as substitutes with cheaper prices.[141] Before long, both of them (Sn,[138,142] Si[129,142,143]) were authenticated by experiments. By the way, elastic properties of $Li_{10}GeP_2S_{12}$, which are important for practical application as solid state electrolytes, were systematically studied by *ab initio* calculations.[144]

$Li_{3x}Ln_{2/3-x}[U+FFFF]_{1/3-2x}TiO_3$, usually abbreviated as LLTO, presents a definite percolation diffusion mechanism based on Li sites and vacancy sites, because of its simple perovskite structure and obvious intrinsic vacancies arising from the primary $Ln_{2/3}[U+FFFF]_{1/3}TiO_3$. When Ln is doped by Li, the original vacancies are occupied by excess Li as charge compensation. The discovery of perovskite solid electrolytes can be traced back to 1984, when Latie *et al.* found that substituting Li for Ln and substituting Ti for Nb simultaneously in $Ln_{1/3}NbO_3$ could result in $Li_xLn_{1/3}Nb_{1-x}Ti_xO_3$, the conductivity of which is enhanced with the increase of Li content, and the activation energy is reduced by the larger bottleneck of the Li-ion channels.[145] Following the hint to maximize the low valence Ti for relatively more Li content, x can be fixed as 1, then replacing an adequate proportion of Ln can control the Li content, i.e., $Li_{3x}Ln_{2/3-x}[U+FFFF]_{1/3-2x}TiO_3$ ($0<x\leq1/6$, for the vacancy density must not be less than 1). Within the years 1993–1994, Inaguma and Liquan Chen found that the bulk conductivity of $Li_{3x}La_{2/3-x}[U+FFFF]_{1/3-2x}TiO_3$ at ambient temperature could reach up to 10^{-3} S/cm when $x=0.11$, which is related to the product of Li-ion and vacancy concentrations as the rudiments of percolation model, and that Ba and Sr doping into Li-vacancy sites enlarge the bottleneck size and thus increase ionic conductivity.[146,147] In addition, because of the so-called lanthanide contraction, in lanthanides, increasing atomic number corresponds to decreasing atomic radius, doping with a heavier lanthanide element leads to a narrower bottleneck and lower ionic conductivity.[148] To revise the percolation model, Inaguma *et al.* proposed that it benefits ionic conductivity only when the Li content x is more than the threshold x_c, i.e., $\sigma\propto(x-x_c)^{\mu}$.[149] Considering all of the foregoing, the conductivity σ of $Li_{3x}Ln_{2/3-x}[U+FFFF]_{1/3-2x}TiO_3$ can be expressed by a relationship among the Li content, vacancy content and that threshold[150]

$$\sigma\propto\frac{3x(1/3-2x)}{(3x+1/3-2x)^2}(3x+1/3-2x-x_c)^{\mu}, \qquad (1)$$

where $x_c=0.3117$ for the cubic structure and $\mu=2$ for three-dimensional conduction pathways. It was found that the fitting results can conform well to the experimentally determined dependence of Li content on ionic conductivity.[150] One abnormal phenomenon was found, however: for some doping cases, an increase of lattice parameters results in a reduction of ionic conductivity. In view of this, it has been speculated that the difference between the atomic radii of the dopant and the primary lattice atoms leads to local lattice distortion. A further correction is that the second term in the right hand side of Eq. (1) is replaced with $(n+n'-\alpha nx-x_c)^{\mu}$, where n and n' are the respective numbers of Li atoms and vacancies in the crystal lattice unit.[151] Besides, the 2D conduction mechanism is found at relatively lower temperature directly by neutron powder diffraction study,[152] while higher

temperatures increase the oxygen vibration and open up the originally blocked bottleneck to enable the third dimension for Li-ion diffusion[153] and delocalizes Li ions from the 2D La-poor layer to realize a higher degree of disorder.[154] Considering the quasi-2D conduction mechanism and the preferential La distribution, equation (1) can be further revised as: $\sigma \propto n_{\rm eff}(n' - n_{\rm c})^{\mu} = 12x(1-12x)(0.5 - g({\rm La2}))^{1.3}$.[152] The deviation from Arrhenius can be explained by the long-range correlation of mobile carriers, which can be inferred both from the abnormal activation energy measured by IS.[153,155] as well as from activation energy discrepancies between IS and measurements of ^{7}Li NMR spin-lattice relaxation.[156] The total conductivity of $Li_{3x}Ln_{2/3-x}[U+FFFF]_{1/3-2x}TiO_3$ is limited by grain boundary resistance, which can be reduced by high temperature sintering; however, the high-temperature, long-duration thermal process leads to Li evaporation, making accurate control of Li content difficult. Therefore, this system can hardly be applied in all-solid-state batteries.

The Li-ion compounds $Li_5La_3M_2O_{12}$ (M = Ta, Nb), with garnet structure, were reported in 1988, and the structure was examined by x-ray diffraction, without knowing the Li distribution, due to limited experimental resolution of Li atoms.[157] However, this system did not attract much attention as a solid electrolyte until 2003, when Thangadurai and Weppner found that it is a good Li-ion conductor with high conductivity and a wide electrochemical window.[158] In contrast to the common perovskite or NASICON solid state electrolyte, the garnet family excludes Li-reducible Ti^{4+}, so it can directly contact Li metal without damage, which has been viewed as its distinguishing advantage.[159] In 2004, Thangadurai and Weppner, together with Adams, used the bond valence sum method to verify the structure, and they minimized the mismatch of the Li-bond valence state as the isosurface to map the conduction pathways visually. It was concluded that Li ions occupy the octahedral sites other than tetrahedral vacancies.[160] The Li-ion occupation pattern is of great importance for understanding the diffusion mechanism but was not located precisely until 2006, by Cussen. It was revealed from neutron powder diffraction data that Li ions occupy both tetrahedral (80%) and octahedral sites (43%), and the latter are responsible for the mobile carriers via a clustering mechanism.[161] NMR results indicate that the Li-ion distribution depends on the annealing temperature; that is, the high annealing temperature implies that more Li ions can be quenched at the octahedral sites as mobile carriers, which leads to higher ionic conductivity.[162] In 2012, Han and Yusheng Zhao utilized variable-temperature neutron diffraction (HTND), combined with the maximum-entropy method (MEM) for data refining, to estimate the Li nuclear-density distribution and visualize the conduction pathway experimentally for the first time. These results confirm that displacement is directly driven by temperature.[163] More efforts in calculation have gradually elucidated the Li-ion diffusion mechanism; for example, conductivity and distinct mechanisms for different M elements and various Li concentrations,[164] structural phase transition,[165] concerted[166,167] or asynchronous phenomena,[168] point defects,[169] local structure and dynamics performance,[170] often in combination with experimental data. Other efforts focused on enhancing conductivity. Substituting and doping with lower-valence elements, e.g., replacing La by Sr[171] or Ba,[172] replacing M (= Nb, Ta) partly[173] or totally[174] by Zr, can increase Li content and thus improve conductivity. The highest conductivity found was 4×10^{-4} S/cm in $Li_7La_3Zr_2O_{12}$ (LLZO),[174] the most attractive composition so far. LLZO has cubic and tetragonal phases. Cubic phase LLZO has higher conductivity and can be synthesized by doping Al or Ga, or by pulsed laser annealing.[175–179] Cubic phase thin film can be obtained from epitaxial growth[180] or aerosol deposition (AD).[181] The latter method prevents the electrolyte from reacting with the active electrode by avoiding the annealing process, although the obtained electrolyte exhibits extremely low conductivity (1.0×10^{-8} S/cm@140 °C) and worse cyclic performance if applied in all-solid-state batteries. Nebulized spray pyrolysis results in a thin-film hybrid of both phases.[182] The disadvantages of LLZO used in sandwich-structure all-solid-state batteries include high interface resistance and poor cyclic stability,[183] both of which can be ameliorated by introducing a thin Nb interlayer between the electrolyte and cathode ($LiCoO_2$).[184]

In 2012, a novel class of solid electrolyte, called lithium-rich anti-perovskites (LiRAP) was reported by Zhao *et al.*[185] LiRAP is named for the following reasons: It has a structure similar to perovskites with electronically-inverted ions located in the corresponding lattice sites. In other words, as compared with the traditional perovskite ABX_3, X is occupied by Li^+ with positive charge, leading to a high concentration of Li ions (i.e., "Li rich"), A and B by halogen$^-$ (F^-, Cl^-, Br^-, I^-) and chalcogen^{2-} (O^{2-}, S^{2-}) separately with negative charges.[185] Almost at the same time, Li_3OCl happened to be discovered as a byproduct during synthesizing Li_5OCl_3.[186] In the following year, phase diagram calculation results indicated that Li_3OCl was in a less stable state (metastable phase) than Li_2O and LiA (A = Cl, Br) at 0 K[187] and could be stabilized by exerting a certain temperature.[187,188] By accommodating dopants and substitutions (e.g., halogen mixing, Li sites doped by higher-valence-state elements, and depletion of lithium halides) as well as local disorder from thermal treating process without phase transition, (anti-) perovskite has greater tolerance for structure modulation[189] to ensure structural stability and enhance conductivity. In this case, $Li_3OCl_{0.5}Br_{0.5}$ has room temperature conductivity of 6.05×10^{-3} S/cm.[185]

The underlying reasons are summarized as follows: (i) With point defects, LiRAP undergoes sublattice melting at adequate temperature;[190] (ii) Concerted diffusion contributes to low activation energy;[187,190] (iii) Excess defects produced during synthesis process may be of critical importance for abnormally high conductivity.[187,190] Seen from either the original intention of materials design or the experimental and calculation results, it can be said that that higher-valence dopants and disordered state (amorphous or glassy state) account for the higher conductivity. For instance, divalent-cation doping gives amorphous LiRAP extremely high conductivity (25 mS/cm at room temperature).[191] The theoretical electrochemical window of LiRAP remains controversial, ranging from 5 eV[185] to 6.44 eV,[191] and cyclic voltammetry measurements illustrate that it can be stable up to 130 °C with 8 V applied voltage.[191] Note that despite the band gap of 5 eV, LiRAP tends to decompose into Li_2O_2, LiCl, and $LiClO_4$ under 2.5 V bias voltage.[187] The stability of Li_3OBr when exposed to common battery solvents was investigated for many applications beyond all-solid-state LIBs.[192]

Lithium-ion inorganic solid state electrolytes have enormous advantages over traditional organic electrolytic solutions, as follows.

(I) Resists flame, explosion, leakage and corrosion, and it is a radical approach to solve the safety problem.

(II) Prevents batteries from swelling.

(III) Avoids the collapse of cathode structure resulting from a high concentration of organic molecules embedded during charging and discharging.

(IV) Solves the increasing growth of SEI, which causes capacity loss.

(V) As illustrated in (II), (III), and (IV), all-solid-state batteries potentially offer superior service life and cycle life.

(VI) The Li-ion mobility approaches 1, implying higher ionic conductivity with equivalent total conductivity, as well as higher power density; on the other hand, extremely low electronic conductivity prevents batteries from self-discharge, which ensures longer shelf life.

(VII) Service life is not affected by high temperature. Moreover, such batteries can work within a wide temperature range, maintaining adequate ionic conductivity and electrochemical stability. With these advantages, they can potentially be applied in rugged environments, so they may be of the great significance for national security.

(VIII) Wide electrochemical window, high decomposition voltage, compatibility with high-voltage cathodes.

(IX) Higher densification and better mechanical strength can suppress the formation of Li dendrites, and make Li metal anodes possible.

(X) (VIII) and (IX) will both improve energy density.

The performance of solid state electrolytes, such as cyclic performance, rate performance, and low temperature behavior, is always constrained by having lower conductivity than liquid electrolytes. Assuming that the voltage-drop across the electrolyte is U(mV), the current density is j(mA/cm^2), the thickness of the electrolyte pellet is l(cm), the conductivity can be written as: $\sigma = (jl)/U$ ($\Omega^{-1}\cdot$cm^{-1}). The battery capacity per unit area is about 1–3 mAh/cm^2; thus the current density with discharge rate of 1 C is 1–3 mA/cm^2. The area of an 18650 battery is usually about 560 cm^2. As a result, the total battery resistance is less than 2 m·Ω, or no more than 10 m·Ω for an enterprise level battery or even at a lower level. So the inner voltage drop across a traditional battery is estimated to be about 2–10 mV, which can be used as a benchmark to evaluate all-solid-state batteries. Note that $\sigma = (0.2 \sim 1) \times l(\Omega^{-1}\cdot\text{cm}^{-1})$, so the solid electrolyte with conductivity of $10^{-6}(\Omega^{-1}\cdot\text{cm}^{-1})$ should have thickness of about the order of magnitude of μm (e.g., LiPON), while conductivity of $10^{-3}(\Omega^{-1}\cdot\text{cm}^{-1})$ corresponds to the thickness of mm (e.g., sandwich-structure sulfide electrolyte all-solid-state batteries). Here, only the bulk resistance is considered in the estimation, despite the possible interphase resistance, which is usually higher and can be the principal source of the full cell's total resistance.

3. Theoretical models for characterizing the ion transport mechanism in lithium-ion solid state electrolytes

3.1. The defect and phase transition in solid state electrolytes

According to the classification given by Funke,[193] the state of totally ordered crystal is defined as level one. In this state, ions cannot leave their lattice sites, as shown in Fig. 3(a). Once thermodynamics-driven point defects occur, this point disorder state is defined as level two; here ionic diffusion consists of random walks along a static energy landscape of separate point defects, as shown in Fig. 3(b). In fact, modern materials science is usually based on this level. However, in a disordered structure, involving crystals with structural disorder, glasses, polymer electrolytes, and nanosized systems (nanocomposites and thin films), which are shown in Figs. 3(c1)–3(c3), respectively, the diffusion mechanism is dramatically different, and this state is defined as level three. In this state, the separate point defects lose their isolated nature and interact with each other. As a result, complicated many-body problems should be considered, including the interaction among mobile carriers, as well as interaction between mobile ions and the surrounding matrix.[193,194]

Solid state electrolytes can be grouped into three general categories according to their defects type and phase transition mechanism, as illustrated in Fig. 4:[195] (i) point defect category: simple thermal activated ionic defects coinciding with

Arrhenius behavior, e.g., Li_3N, LISICON and β-Al_2O_3; (ii) first-order category: the first-order transition is attributed to sublattice melting, which usually exists in the familiar superionic conductors, including Ag and O ionic conductors. When it comes to Li-ion conductors, the following are mainly included: NASICON family such as $LiZr_2(PO_4)_3$,[196] LiRAP family,[185,191] and $LiBH_4$[50] (and its composite with lithium halide[52]); (iii) glass transition or the second-order transition: more disordered structure caused by a further increase of temperature, and exhibiting non-Arrhenius behavior; often found in silicates, phosphates and chalcogenide glasses; $Li_{0.33}La_{0.56}TiO_3$ or garnet family can behave within a wide enough range of temperature. The conductivity–temperature relationship for various materials is shown in Fig. 2,[195] which indicates that although most inorganic solid state electrolytes abide by the Arrhenius equation, it is unclear whether the phase transition occurs or not, for a wide enough temperature range. The thermodynamic effect related to ionic transport and to melting have a certain correlation.[9]

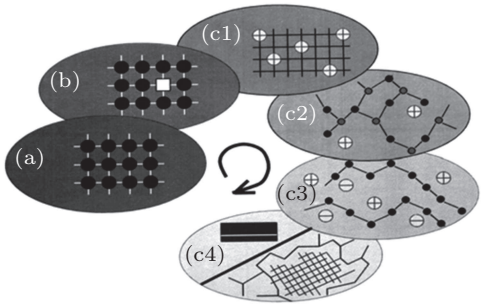


Fig. 3. An evolving scheme of materials science: (a) ideally ordered crystals; (b) point disorder in crystals; (c1) crystals with structural disorder; (c2) ion-conducting glasses; (c3) polymer electrolytes; (c4) nano-sized systems such as nano-composites and thin films.[193]

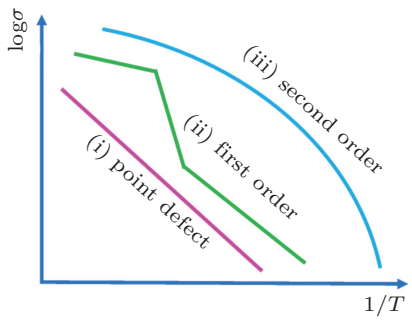


Fig. 4. Arrhenius plot of ionic conductivity for three types of solid state electrolytes.

Reference [1] introduced the modern transition theory established by Landau, although the nature of the parameters related to the superionic phase transition remains unclear. To theoretically explain the critical behavior, a quasi-chemical model and a lattice gas model were adopted, but neither of them is sufficient. Alternatively, the critical behavior can be understood via experimental measurements as follows: (i) conductivity and activation: the performance of critical interest and its characterization methods will be introduced in Section 4; (ii) specific heat:[185,191,197–199] its anomaly is one of the key indications of a phase transition; (iii) acoustic properties: the presence of an order parameter with the same symmetry as strain components results in a renormalization or softening of the elastic constant for the strain[200] or an anomaly in ultrasonic attenuation.[200–202] The study of these critical behaviors helps to make clear the features of order parameters and understand the interactions among ions.

3.2. Overview of the development of the theory of ionic transport in solids[203–205]

In ordinary solids, particle diffusion is based on the Brownian motion of thermally activated defects in the periodic potential barrier. The point defect transport mechanism follows the random walk mode[206–210]

$$D_r = \langle R_n^2 \rangle / (6t_n) = 1/6(\nu a^2 c), \tag{2}$$

where D_r is the random diffusion coefficient, indicating a hypothetical diffusivity arising from uncorrelated jump sequences, R_n is the net displacement after n steps, $\langle\ \rangle$ is the average value for all processes, t_n is the corresponding time, a is the hopping distance or free path, c is the defect concentration, and ν is the average hopping frequency.

Correlation factor f can be defined as

$$f = D^*/D_r, \tag{3}$$

where D^* is the tracer diffusion coefficient, indicating the diffusivity of tagged atoms, and f is determined by the geometric structure and diffusion mechanism.[203]

Assuming that the lattice particles' vibration submits to the thermal activation, the frequency can be expressed as

$$\nu = \nu_0 \exp\left(-\frac{\Delta G}{k_B T}\right) = \nu_0 \exp\left(\frac{\Delta S}{k_B}\right) \exp\left(-\frac{\Delta H}{k_B T}\right), \tag{4}$$

where ν_0 is called the attempt frequency, which is the order of the Debye frequency; ΔG, ΔS, and ΔH, respectively denote the changes of Gibbs free energy, enthalpy and entropy from the ground state to active state; T is the temperature of the Kelvin unit, and k_B is Boltzmann constant. According to Eqs. (2)–(4),

$$D^* = \frac{1}{6} f a^2 c \nu_0 \exp\left(\frac{\Delta S}{k_B}\right) \exp\left(-\frac{\Delta H}{k_B T}\right). \tag{5}$$

Note that D^* is also called the self-diffusion coefficient because it describes single-particle diffusion.

When the chemical composition varies in the diffusion zone across a certain range, a polynary diffusion couple needs to be considered. Then the diffusion particles experience various chemical environments and have different diffusion coefficients, which is usually formulated by Darken equation.[211] Taking a binary system for example:

$$\tilde{D} = (N_2 D_1^* + N_1 D_2^*)\left(1 + \frac{\partial \ln \gamma_1}{\partial \ln C_1}\right), \tag{6}$$

where $\tilde{D}$ is called the interdiffusion coefficient or chemical diffusion coefficient. However, equation (6) cannot be used to characterize ion diffusion, which comprises various complications such as electric neutrality. Note that unlike solid state electrolytes with a single mobile Li^+, electrode materials involve intricate non-neutral defects, especially enormous interacting vacancies when charged, and electronic conductivity cannot be ignored. As a result, what is obtained by measuring the electrode, including cyclic voltammetry (CV),[212,213] galvanostatic intermittent titration technique (GITT),[214,215] potentiostatic intermittent titration technique (PITT),[213,216–218] electrochemical impedance spectroscopy (EIS),[6,212,213,215,218,219] is usually about the chemical diffusion coefficient.[220] Since this review focuses on the ion diffusion in solid electrolytes, the relevant terms are only itemized here without further description.

For both pure and mixed ion conductors, diffusing particles experience a drift motion in addition to random diffusion if an external voltage is applied as the driving force. So the relationship between the ionic DC conductivity σ_{dc} and the diffusion coefficient D^{σ} can be written according to the Nernst–Einstein equation as

$$D^{\sigma} = \frac{\sigma_{dc} k_B T}{cq^2}. \tag{7}$$

Here, c is the particle-density of the charge carriers and q is their charge. Note that since D^{σ} is not derived from Fick's first law, it is not the real diffusion coefficient defined exactly, but a derivation from Eq. (7) with the same dimension as the diffusion coefficient. To build up the relationship between D^{σ} and D^*, the ratio of D^* in Eq. (5) and D^{σ} in Eq. (7) is defined as

$$H_R = D^*/D^{\sigma}, \tag{8}$$

where H_R is called the Haven ratio, and it indicates the displacement effects during the ionic diffusion process, in which it is assumed that an ion can hop not only into a nearest neighboring vacant site, but also into an occupied site. The latter movement is equivalent to a hop toward the same direction. This concerted displacement with successive jumping will continue until the ion hops into a vacancy site. When the cooperative effect from the interaction among mobile carriers is considered, the description of the process will become more complicated.[221] Given a simple but inaccurate interpretation, if the mobile ions interact with each other, or if the electrons contribute to the diffusion process, $H_R < 1$; if defects like vacancy pairs or impurity–vacancy pairs participate in diffusion that does not directly act on conductivity, $H_R > 1$.[204] The exact value of H_R can be obtained by measuring σ_{dc} and D^*, and the further interpretation details can be found in Refs. [204], [205], and [221]. In the case of solid state electrolytes with a melting sublattice, or glassy or polymer conductors with highly disordered structure, the Haven ratio is of great significance for identifying the ion diffusion mechanism. Accordingly, it is more difficul to analyze the possible factors affecting the Haven ratio value.[203]

The limitation of random walk theory lies in the requirement that the ionic transport should not be affected by other accompanying defects, which seems hard to satisfy in solid state electrolytes with their relatively high conductivity. This is because of the following: (i) In the static energy landscape for most solid state electrolytes, the energy valley sites (equivalent positions for mobile ions) are more numerous than the actually occupied sites (the number of mobile ions in fact).[1,9] The maximum of the equivalent sites leads to the sketch of sublattice melting, of which the mobile ions can diffuse "freely" like liquid. (ii) Concerted ion migration always leads to lower activation energy because the energy landscape is dynamic instead of static. In a sketch of dynamics, time scale is of critical importance.[1,9,195]

3.3. Four theoretical models for characterizing diffusion in solids[1,9,222]

3.3.1. Two-state model[1,223]

The ion diffusion process in a fixed lattice's energy landscape can be simplified and viewed as a two-state model, i.e., a bound state and an approximately free-ion state, and an energy barrier exists between them depending on an effect of the static skeleton lattices. Once an ion has energy above the barrier threshold, it can be excited from the bound state to the approximately free-ion state with a certain life time and can transport with the velocity of free ions. This model can be characterized with several different mathematical formulations. Herein, by introducing the conditional probability $P(\boldsymbol{l}t|00)$ to describe the case of finding a particle at time t and site $\boldsymbol{l}$ for the initial condition at time 0 and site $\mathbf{0}$, Γ is the transition rate, the master equation is adopted as follows:

$$\frac{\mathrm{d}}{\mathrm{d}t} P(\boldsymbol{l}t|\mathbf{0}0) = \Gamma \sum_{\langle l,l'\rangle} \left[P(\boldsymbol{l}'t|\mathbf{0}0) - P(\boldsymbol{l}t|\mathbf{0}0)\right], \tag{9}$$

and can be written in a compact form:

$$\frac{\mathrm{d}}{\mathrm{d}t} P(\boldsymbol{l}t|\mathbf{0}0) = -\sum_{\boldsymbol{l}'} \Lambda_{\boldsymbol{l},\boldsymbol{l}'} P(\boldsymbol{l}'t|\mathbf{0}0), \tag{10}$$

$$\Lambda_{\boldsymbol{l},\boldsymbol{l}'} \sim \begin{cases} z\Gamma, & \boldsymbol{l} = \boldsymbol{l}', \\ -\Gamma, & \boldsymbol{l},\boldsymbol{l}' \text{ nearest neighbour}, \\ 0, & \text{otherwise}, \end{cases} \tag{11}$$

where z is the number of nearest neighbors. Equation (10) in the direct space can be transformed to Fourier space as

$$\frac{\mathrm{d}}{\mathrm{d}t} P(\boldsymbol{k},t) = -\Lambda(\boldsymbol{k}) P(\boldsymbol{k},t), \tag{12}$$

$$\Lambda(\boldsymbol{k}) = \Gamma \sum_{\boldsymbol{l}-\boldsymbol{l}'} \mathrm{e}^{-\mathrm{i}\boldsymbol{k}\cdot(\boldsymbol{R}_{\boldsymbol{l}}-\boldsymbol{R}_{\boldsymbol{l}'})}. \tag{13}$$

Then the solution is

$$P(\boldsymbol{k},t) = P(\boldsymbol{k},0)\exp[-\Lambda(\boldsymbol{k})], \quad t \geq 0, \tag{14}$$

with the initial condition as $P(\boldsymbol{k},0) = \sum_{\boldsymbol{l}} \mathrm{e}^{-\mathrm{i}\boldsymbol{k}\cdot\boldsymbol{R}_{\boldsymbol{l}}} P(\boldsymbol{l}0|\boldsymbol{0}0) = 1$. Combined with symmetric continuation, $P(\boldsymbol{k},-t) = P(\boldsymbol{k},t)$, the frequency domain solution is

$$P(\boldsymbol{k},\omega) = \frac{2\Lambda(\boldsymbol{k})}{\omega^2 + \Lambda^2(\boldsymbol{k})}, \tag{15}$$

which is a Lorentzian function, whose width $\Lambda(\boldsymbol{k})$ can be measured by a quasielastic Mossbauer spectrum and quasielastic neutron scattering, as will be illustrated in Section 4.3.2. Then the diffusion coefficient can be derived from $\Lambda(\boldsymbol{k})$ as

$$D = \frac{1}{6}\langle \boldsymbol{R}^2 \rangle = -\frac{1}{6}\sum_j \frac{\partial^2 \Lambda(\boldsymbol{k})}{\partial k_j \partial k_j}\bigg|_{k=0}. \tag{16}$$

As mentioned in the dynamics sketch, for solid state electrolytes, the release time τ_{r} is not infinitely short and the trapping time τ_{t} is not infinitely long. In two-state model, the conditional probability can be divided into the free part and trapped part as

$$P_l(t) = P_l^{\mathrm{free}}(t) + P_l^{\mathrm{trapped}}(t). \tag{17}$$

Then the differential equations are

$$\begin{aligned} \frac{\mathrm{d}}{\mathrm{d}t}P_l^f(t) &= \Gamma \sum_{\langle l,l'\rangle} [P_{l'}^f(t) - P_l^f(t)] \\ &\quad - \frac{1}{\tau_{\mathrm{t}}}P_l^f(t) + \frac{1}{\tau_{\mathrm{r}}}P_l^t(t), \end{aligned} \tag{18}$$

$$\frac{\mathrm{d}}{\mathrm{d}t}P_l^t(t) = -\frac{1}{\tau_{\mathrm{r}}}P_l^t(t) + \frac{1}{\tau_{\mathrm{t}}}P_l^{\mathrm{f}}(t). \tag{19}$$

Note that it is difficult to solve $P(\boldsymbol{k},t)$ in complicated cases.[224] One of the underlying reasons is that the potential barrier and potential well can vary within a certain energy range in the disordered structure.[224–227] Figure 5 shows the common complicated models, in which Γ_{fi} ((f)-final, (i)-initial) is the hopping rate resulting from random lattice potential.

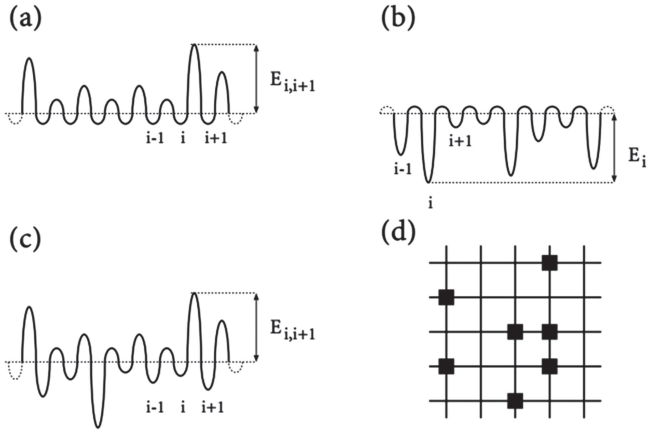


Fig. 5. Models of disordered potential barriers and wells.[223] (a) RB, (b) RT, (c) RB+RT, and (d) RBS.

(I) Random barriers (RB)

$$\Gamma_{ij} = \Gamma_{ji} = \Gamma_0 \exp\left(-\frac{\mathrm{E}_{ji}}{k_{\mathrm{B}}T}\right), \quad E_{ji} \geq 0. \tag{20}$$

(II) Random site energies (RT)

$$\Gamma_{ji} = \Gamma_0 \exp\left(-\frac{\mathrm{E}_i}{k_{\mathrm{B}}T}\right), \quad E_i \leq 0. \tag{21}$$

(III) RB+RT

$$\Gamma_{ji} = \Gamma_0 \exp\left(-\frac{\mathrm{E}_{ji} - \mathrm{E}_i}{k_{\mathrm{B}}T}\right), \quad E_{ji} \geq 0, \quad E_i \leq 0. \tag{22}$$

(IV) Random blocked sites (RBS)

A special case of the percolation model indicates the condition that the lattice sites are randomly blocked and cannot accept the hopping ions,

$$\Gamma_{ji} = \begin{cases} \Gamma, & \text{if } j \text{ is "open"}, \\ 0, & \text{if } j \text{ is blocked}. \end{cases} \tag{23}$$

3.3.2. Lattice gas model[1,223]

In this model, the crystal volume is divided into a substantial number of units; each unit can be occupied by no more than one particle. Comparison between the lattice gas model and the two-state model suggests that the latter indicates single-particle transport along the energy landscape; whereas the former indicates many-particle diffusion, in which the interaction among mobile particles is introduced by assuming unit exclusion.

In the case of ordered structure, particles can hop into the nearest-neighbor non-blocked sites at a constant rate Γ. This model was introduced by Spitzer,[228] and the exact results can be found in Ref. [229]. The master equation is

$$\frac{\mathrm{d}}{\mathrm{d}t}P(\boldsymbol{l},t) = \Gamma \sum_{\langle l,l'\rangle} \Big[P(\boldsymbol{l}',\bar{\boldsymbol{l}},t) - P(\boldsymbol{l},\bar{\boldsymbol{l}}',t)\Big], \tag{24}$$

where $P(\boldsymbol{l}',\bar{\boldsymbol{l}},t)$ is the joint probability that site $\boldsymbol{l}'$ is occupied ($\boldsymbol{l}'$) and site $\boldsymbol{l}$ is empty ($\bar{\boldsymbol{l}}$) at time t. By taking into account

$$\begin{aligned} P(\boldsymbol{l}',\bar{\boldsymbol{l}},t) + P(\boldsymbol{l}',\boldsymbol{l},t) &= P(\boldsymbol{l}',t), \\ P(\boldsymbol{l},\bar{\boldsymbol{l}}',t) + P(\boldsymbol{l},\boldsymbol{l}',t) &= P(\boldsymbol{l},t), \end{aligned} \tag{25}$$

the master equation can be rewritten as

$$\frac{\mathrm{d}}{\mathrm{d}t}P(\boldsymbol{l},t) = \Gamma \sum_{\langle l,l'\rangle} \Big[P(\boldsymbol{l}',t) - P(\boldsymbol{l},t)\Big], \tag{26}$$

which has a similar form to Eq. (9), and can be solved analogically. The collective diffusion coefficient is $D_{\mathrm{coll}} = \Gamma a^2$. Note that the site-exclusion lattice gas concentration is not included in Eq. (26).

In the case of disordered structure, the space correlation occurs; thus even the simplified site-exclusion model is complicated. Some solutions of specific cases can be found in

Ref. [223]. Three common models are listed as follows (here an energy ε_i is assigned to each lattice site i).

(I) Percolative disorder

$$\varepsilon_i = \begin{cases} 0, & \text{probability} \quad p, \\ \infty, & \text{probability} \quad 1-p. \end{cases} \tag{27}$$

(II) Gaussian disorder

$$P(\varepsilon) = (2\pi\sigma_\varepsilon^2)^{-1/2}\exp(-\varepsilon/2\sigma_\varepsilon^2). \tag{28}$$

(III) Randomly placed counterions

$$\varepsilon_i = -\sum_{\boldsymbol{R}} \frac{n_{\boldsymbol{R}} e^2}{|\boldsymbol{r}_i - \boldsymbol{R}|}. \tag{29}$$

Interactions among mobile particles can be introduced as follows: (i) For an ordered structure, the average of all interactions can be simplified by a mean field approximation. (ii) For a disordered structure, the interaction among particles is too complicated to describe exactly. We deal with this by assuming that the solid state electrolyte consists of merely two kind of ions: skeleton ions A and mobile ions B. Then the Hamilton equation of the lattice gas model can be constructed as follows:[1]

$$H = \sum_l \frac{1}{2m_A}\boldsymbol{p}_l^2 + \sum_\lambda \frac{1}{2m_{\rm B}}\boldsymbol{p}_\lambda^2 + \phi(\boldsymbol{r}_l, \boldsymbol{r}_\lambda), \tag{30}$$

where l and λ indicate individual mobile ions A and skeleton ions B, respectively; $\boldsymbol{r}_l$ and $\boldsymbol{r}_\lambda$ represent the displacements of A and B relative to the equilibrium position, respectively; the potential φ includes interactions among all particles. When φ is expanded with respect to displacements u_λ^α (α labels the Cartesian components), the following expressions can be obtained:

$$\begin{aligned} H &= H_A + H_{\rm B} + H', && (31)\\ H_A &= \sum_l \frac{1}{2m_A}\boldsymbol{p}_l^2 + \sum_{l,\lambda} V^0(|\boldsymbol{r}_l - \boldsymbol{r}_\lambda^0|) \\ &\quad + \frac{1}{2}\sum_{l\neq l'} V^1(|\boldsymbol{r}_l - \boldsymbol{r}_{l'}|), && (32)\\ H_{\rm B} &= \sum_l \frac{1}{2m_{\rm B}}\boldsymbol{p}_\lambda^2 + \frac{1}{2}\sum_{\substack{\lambda\lambda' \\ \alpha\alpha'}} C_{\lambda\lambda'}^{\alpha\alpha'} u_\lambda^\alpha u_{\lambda'}^{\alpha'}, && (33)\\ H' &= \sum_{l\lambda\alpha} V_\alpha^2(\boldsymbol{r}_l - \boldsymbol{r}_\lambda^0)u_\lambda^\alpha + \sum_{\substack{l\lambda \\ \alpha\alpha'}} V_{\alpha\alpha'}^3(\boldsymbol{r}_l - \boldsymbol{r}_\lambda^0)u_\lambda^\alpha u_\lambda^{\alpha'}, && (34) \end{aligned}$$

where V_α^2 and $V_{\alpha\alpha'}^3$ arise from the interactions between mobile ions, and skeleton ions; V^1 is the interaction among the mobile ions and the force constant matrix $C_{\lambda\lambda'}^{\alpha\alpha'}$ arises from interactions among skeleton particles.

Let us consider an N-particle system with charges e_n and masses m_n, $n = 1, 2, \ldots, N$. Periodic lattice sites are defined by the position vector $\boldsymbol{q}_{n\alpha}^0$. By introducing the lattice gas representation $a = (n_1, n_2, \ldots, n_N)$, the potential energy can be harmonically approximated as

$$\begin{aligned} V &= V(\boldsymbol{q}_0) + \frac{1}{2}\sum_{\substack{n,\alpha \\ m\beta}} (\boldsymbol{q}_{n\alpha} - \boldsymbol{q}_{n\alpha}^0) m_n^{1/2} \phi_{\alpha\beta}^0(n,m) m_m^{1/2} \\ &\quad \times (\boldsymbol{q}_{n\beta} - \boldsymbol{q}_{n\beta}^0), \end{aligned} \tag{35}$$

with the Kubo formula

$$\sigma_{\alpha\beta}(\omega) = \frac{1}{\Omega}{\rm tr}\left\{QS_{\alpha\beta}(\omega)\right\}, \tag{36}$$

where the oscillator strength matrix Q reads

$$Q(n,m) = \frac{e_n}{m_n^{1/2}}\frac{e_m}{m_m^{1/2}}, \tag{37}$$

and the velocity correlation matrix reads

$$S_{\alpha\beta}(n,m) = \frac{1}{k_{\rm B}T}\left\langle m_n^{1/2} V_{n\alpha}(-{\rm i}\omega - L)^{-1} V_{m\beta} m_m^{1/2}\right\rangle, \tag{38}$$

with the Liouvillian L as

$$L = V\frac{\partial}{\partial q} - \sum_{n,\alpha} m_n^{-1}\frac{\partial V}{\partial q_{n,\alpha}}\frac{\partial}{\partial V_{n,\alpha}}. \tag{39}$$

Then the dynamic conductivity depending on frequency can be obtained as

$$\sigma_{\alpha\beta}(\omega) = \sum_{i=0}^{3} Q{\rm tr}\left\{Q\Lambda_{\alpha\beta}^{(i)}(\omega)\right\}. \tag{40}$$

For $i = 0$,

$$\begin{aligned} \Lambda_{\alpha\beta}^{(0)}(n,m) &= \frac{m_n^{1/2} m_m^{1/2}}{k_{\rm B}T}\frac{1}{2}\sum_{ab} p_a^{\rm eq}\left(l_{n\alpha}^b - l_{n\alpha}^a\right) \\ &\quad \times \Gamma_{ab}^{\rm eq}\left(l_{m\beta}^b - l_{m\beta}^a\right). \end{aligned} \tag{41}$$

For $i = 1$,

$$\begin{aligned} \Lambda_{\alpha\beta}^{(1)}(n,m) &= -\frac{m_n^{1/2} m_m^{1/2}}{k_{\rm B}T} \\ &\quad \times \sum_{ab} p_a^{\rm eq}\left\langle V_{n\alpha}^{a,(1)}(-{\rm i}\omega - L^{\rm eq})_{ab}^{-1} V_{m\beta}^{b,(1)}\right\rangle_a, \\ V_{n\alpha}^{a,(i)} &= \sum_b \Gamma_{ab}^{(i)}\left(l_{n\alpha}^b - l_{n\alpha}^a\right), \\ L_{ab}^{\rm eq} &= \Gamma_{ab}^{\rm eq} - \delta_{ab}\sum_c \Gamma_{ac}^{\rm eq}. \end{aligned} \tag{42}$$

For $i = 2, 3$,

$$\begin{aligned} &\Lambda_{\alpha\beta}^{(i)}(n,m) \\ &= -\frac{m_n^{1/2} m_m^{1/2}}{k_{\rm B}T}\sum_{ab} p_a^{\rm eq}\left\langle V_{n\alpha}^{a,(i)}(-{\rm i}\omega - L)_{ab}^{-1} V_{m\beta}^{b,(i)}\right\rangle_a, \end{aligned} \tag{43}$$

where $p_a^{\rm eq}$ is the equilibrium probability for the occurrence of configuration a; $\Gamma_{ab}^{\rm eq}$ indicates a thermal mean rate with the transitions from $\boldsymbol{r}_a$ to $\boldsymbol{r}_b$; $l_{n\alpha}^a$ represents the average position of the particle n in configuration a with the direction α. The solutions of Eqs. (40)–(43) for some special cases can be found in Ref. [1]. The Monte Carlo (MC) simulation details of the diffusion process are presented in Ref. [230].

The free-ion model of the ordered structure is a single-particle approximation, which results in a typical linear Arrhenius plot with a constant slope, and the behavior of solid state electrolytes are unrelated to the frequency. If we take the free-ion model to analyze the frequency-dependent experimental results and the nonlinear Arrhenius plot for the ionic conductivity, they can be ascribed to the disorder of crystal structure and the Coulomb interaction. Given that only the disorder of crystal structure is involved in the free-ion model, some phenomenological and semi-microscopic approaches have been developed to explain the frequency dependent results. Nevertheless, many experimental phenomena remain that cannot be explained quantitatively.[231–234]

Compared with the free-ion model, the lattice gas model maps the interactions among the many bodies onto the dynamics of a single particle moving in a complex energy landscape. Through the theoretical calculations, the disordered structure and Coulomb interaction can conveniently be taken into consideration to simulate and fit the experimental results, including the nearly constant loss (NCL) in the high frequency region, the quasielastic scattering and NMR. Besides, the literature on fitting the Arrhenius plot with the lattice gas model indicates that low temperature conductivity is affected by both lattice disorder and Coulomb interaction, whereas the high temperature behavior is influenced by Coulomb interaction only, resulting in lower activation energy.[230]

3.3.3. Continuous stochastic model[1,230]

In order to describe the complicated multi-particle dynamics, the system can be simplified as an effective single-particle dynamics model, called continuous stochastic model, as shown in Fig. 6. The movement of ion carriers can be divided into two parts: the vibration located on equilibrium lattice sites, and the diffusion between two sites. The hopping time is not infinitely short, as a result of Coulomb integration. Here, the self-correlation function $G_s(\boldsymbol{r},t)$ is introduced to characterize the single-particle motion completely, and the van Hove correlation function $G(\boldsymbol{r},t)$ to consider the correlation among various particles' motion.[235] With these two correlation functions, the vibration and diffusion of ions can be dealt with simultaneously, and thus the frequency dependent phenomena can be explained.

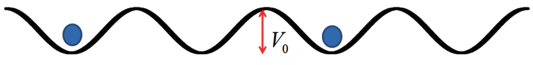


Fig. 6. Ionic motion in flat potential with potential barriers V_0 (adapted from Ref. [1]).

(I) Conductivity

$$\hat{\sigma}(\omega)=\frac{Ne^2}{3k_{\mathrm{B}}TV}\int_0^{\infty} Z(t)\,\mathrm{e}^{-\mathrm{i}\omega t}\,\mathrm{d}t,$$

$$Z(t)=\frac{1}{2}\frac{\mathrm{d}^2}{\mathrm{d}t^2}\int_V r^2\left[G(\boldsymbol{r},t)-\frac{N}{V}\right]\mathrm{d}\boldsymbol{r}, \tag{44}$$

where $Z(t)=\left\langle \sum_{i,j}^{1,\ldots,N} v_i(0)v_j(t)\right\rangle \Big/ N$ is the velocity correlation function. When mediated by $Z(t)$, $\hat{\sigma}(\omega)$ can be calculated from the correlation function $G(\boldsymbol{r},t)$. Note that there exists the frequency threshold ω_{NCL}, and that when $\omega>\omega_{\mathrm{NCL}}$, $\mathrm{Re}\,\hat{\sigma}(\omega)\sim\omega$. The phenomenon is called "nearly constant loss" (NCL) and is equivalent to dielectric loss.

(II) Nuclear magnetic resonance (NMR)

$$\begin{aligned} &T_1^{-1}\propto J(\omega_{\mathrm{L}}),\\ &J(\omega)=\int_{-\infty}^{\infty} G(t)\,\mathrm{e}^{-\mathrm{i}\omega t}\,\mathrm{d}t,\\ &G(t)=\langle m|H_1(t_0)|k\rangle\langle k|H_1(t_0+t)|m\rangle, \end{aligned} \tag{45}$$

where $1/T_1(\omega_{\mathrm{L}},T)$ is the spin-lattice relaxation (SLR) rate caused by the diffusion, and is a function of the Larmor frequency ω_{L} and temperature T. Then

$$\begin{aligned} &1/T_1(\omega_{\mathrm{L}},T)\\ &\sim\begin{cases}\exp(E_1^{\mathrm{SLR}}/k_{\mathrm{B}}T), & T\gg T_{\max}(\omega_{\mathrm{L}}),\\ \omega_{\mathrm{L}}^{n_{\mathrm{SLR}}-2}\exp(-E_2^{\mathrm{SLR}}/k_{\mathrm{B}}T), & T\ll T_{\max}(\omega_{\mathrm{L}}).\end{cases} \end{aligned} \tag{46}$$

The index $n_{\mathrm{SLR}}\geq 0$. According to the Bloembergen–Purcell–Pound (BPP) ansatz[236]

$$\begin{aligned} &G(t)=G(0)\exp(-|t|/\tau_{\mathrm{c}}),\\ &J(\omega)=G(0)\frac{2\tau_{\mathrm{c}}}{1+(\omega\tau_{\mathrm{c}})^2},\\ &\tau_{\mathrm{c}}=\tau_{\mathrm{c}0}\exp(-E_{\mathrm{A}}/k_{\mathrm{B}}T), \end{aligned} \tag{47}$$

where τ_{c} is the mean residence time for particles in the lattice sites. When $E_1^{\mathrm{SLR}}=E_2^{\mathrm{SLR}}$, $1/T_1$ is symmetrical, and when

$$\omega_{\mathrm{L}}\tau_{\mathrm{c}}\approx 1, \tag{48}$$

the function $1/T_1$ reaches its maximum value, and $1/T_1\sim J(\omega)=G(0)\tau_{\mathrm{c}}\sim\exp(-E_{\mathrm{A}}/k_{\mathrm{B}}T)$. Note that here E_{A} is the micro-activation energy, which is usually lower than the macro-activation energy derived from the tracer diffusion coefficient and conductivity diffusion coefficient. When $\omega_{\mathrm{L}}\tau_{\mathrm{c}}\gg 1$, the slope of $1/T_1$ is $\omega_{\mathrm{L}}^{-2}=(\gamma B)^{-2}$, where B is the external magnetic field. However, for the case of disordered structure, or when particle–particle Coulomb interactions occur as well as particle—lattice Coulomb interactions, $1/T_1$ loses its symmetry. Various models were introduced to interpret the asymmetry of spin-lattice relaxation in the disordered structure.[231,237–239]

(III) Quasi-elastic scattering

The coherent and incoherent dynamic structure factors of the mobile ions are given by

$$\begin{aligned} &S(\mathbf{Q},\omega)=(2\pi)^{-1}\iint G(\boldsymbol{r},t)\,\mathrm{e}^{\mathrm{i}(Qr-\omega t)}\,\mathrm{d}\boldsymbol{r}\,\mathrm{d}t,\\ &S_{\mathrm{inc}}(\mathbf{Q},\omega)=(2\pi)^{-1}\iint G_s(\boldsymbol{r},t)\,\mathrm{e}^{\mathrm{i}(Qr-\omega t)}\,\mathrm{d}\boldsymbol{r}\,\mathrm{d}t. \end{aligned} \tag{49}$$

The total dynamic structure factor is

$$S^{\mathrm{tot}}(\mathbf{Q},\omega)=\sigma S(\mathbf{Q},\omega)+\sigma_{\mathrm{inc}}S_{\mathrm{inc}}(\mathbf{Q},\omega), \tag{50}$$

where σ and σ_{inc} are coherent and incoherent scattering cross sections, respectively. For the random walk model, the line shape is Lorentzian, although a deviation in the actual shape usually occurs, which reflects an inherent non-exponential nature of the ionic relaxation processes. Although $S^{\rm tot}(\boldsymbol{Q},\omega)$ is determined by the coherent and incoherent correlation functions $G(\boldsymbol{r},t)$ and $G_{\rm s}(r,t)$, the correlation functions cannot be obtained from $S^{\rm tot}(\boldsymbol{Q},\omega)$ conversely. This is because the correlation functions contain more information than $S^{\rm tot}(\boldsymbol{Q},\omega)$. As a result, it is hard to identify the ionic diffusion mechanism from the dynamic structure factor deviation, without making other assumptions.

Although the continuous stochastic model was phenomenological at first,[240,241] it can be microscopically obtained from the Hamiltonian.[242] Assume that mobile ions move continuously in the skeleton potential V_0, which is driven by the system forces based on the displacement relative to the equilibrium sites of mobile ions. The system's potential is strongly inharmonic when applied the disordered structure or Coulomb interaction, and valleys control oscillation, while barriers control diffusion. The skeleton vibrations ($H_{\rm B}$) are treated as a bath, and the coupling term H' provides the random forces and friction. The interaction among the mobile ions is indirectly considered by being integrated into the bath so that the simplified solution can be written as the Langevin equation. Take one-dimensional motion for example

$$m\ddot{x}+m\gamma\dot{x}-K(x)=f(t), \tag{51}$$

where $K(x)=-\partial V^0/\partial x$ is the systematic force provided by interactions with the rigid skeletons. Both the friction constant γ and the random force $f(t)$ arise from the interactions with the skeleton lattice vibrations and with other mobile ions. More exactly, when the mobile ions and skeletons perform coherent out-of-phase oscillations for a certain time interval, the case should be explicitly treated by solving the coupled Langevin equations rather than the bath simplified model. Here are conclusions, for which the inference can be found in Ref. [1]

$$\sigma(\omega)=n(Ze)^2\mu(\omega), \tag{52}$$

$$\mu(\omega)=\frac{1}{k_{\rm B}T}\sum_{n=0}^{\infty}\frac{\langle v\widehat{L}^n v\rangle}{(-{\rm i}\omega)^{n+1}}, \tag{53}$$

where $\mu(\omega)$ is the mobility dependent on frequency, $\widehat{L}$ is the backward operator, which describes the time evolution of the system and is also called Liouvillian but includes the dispersion term unlike Liouvillian in the classical mechanics. Theoretically, the property of system is determined by the Liouvillian. However, only in several limited cases, e.g., low temperature,[243] small friction[244] and large friction,[245,246] can the analytic solutions with the mobility $\mu(\omega=0)$ be obtained. Besides, the approximate solutions can also be given by introducing the memory function[247–251] or an ensemble of oscillators with a frequency distribution of the Debye type.[240,252]

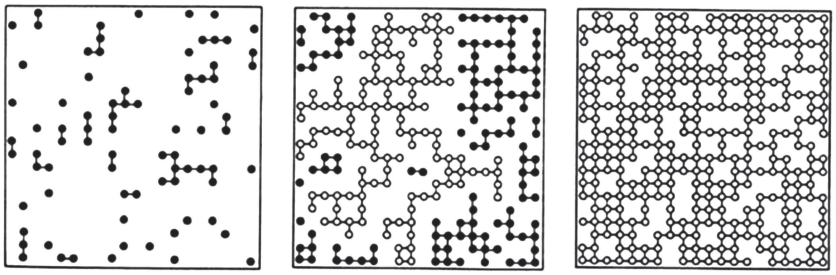
To sum up, theoretically speaking, ion diffusion in a solid state electrolyte is a complicated process. The above methods can give the analytic solutions only under extremely simplified conditions. In order to investigate the ion diffusion in solid state electrolytes quantitatively, one needs to adopt the atomic-scale molecular dynamics[253–255] and semi micro-Monte Carlo simulations.[230,238,256–260]

3.3.4. Percolation model[261]

The models in Sections 3.3.1–3.3.3 focus mainly on the micro-diffusion, or the macro-effects derived from the micro-mechanism. In contrast, the percolation model concentrates more on the macro-diffusion mechanism and is often used to describe the amorphous states (organic polymers, inorganic glasses), composite conductors and porous media.

(I) Site-percolation model

The site-percolation model is usually used to describe inorganic crystals with sites occupied randomly. A sketch of it is shown in Fig. 7. Assuming the site is randomly occupied with the probability p, and the occupied sites connect as the conduction pathway. Thus when p is small, the occupations are either isolated or form small clusters by neighbors, but cannot connect continuously through the whole bulk, and the small clusters are called finite clusters. When p is increased to $p=p_{\rm c}$, infinite clusters are developed by connecting through the bulk and permit macro-electrical current. Here, the threshold $p_{\rm c}$ is essentially critical concentration of the normal-superionic phase transition, and is determined by the type and dimension of the lattice.[262–264] Percolation phase transition belongs to a geometric phase transition, which is a general theory with wide application, thus it can be defined by the geometric parameter.[265] When $p=p_{\rm c}$, finite clusters and infinite clusters are both self-similar, and can be described in terms of fractal theory. With the increase of p, more finite clusters are incorporated into infinite clusters, resulting in a decrease of the volume of finite ones. Now seeing at a longer length scale than that of the infinite clusters, the system can be considered homogeneous, while at the shorter length scale, the system is self-similar. In other words, when $p_{\rm c}<p<1$, the backbone, which consists of the connected infinite clusters (including sites and chemical bonds), can carry macro-electrical current, and the topological distance traversed by current is defined as the chemical distance, whereas the dangling ends, which are connected to the backbone by just one site, carry no current. In this way, the direct current (DC) conductivity is $\sigma_{\rm dc}\sim(p-p_{\rm c})^{\mu}$, where μ is a constant related only to the dimension. When $p=1$, all the sites are part of infinite clusters. Among the common Li-ion solid state electrolytes, perovskite observes this kind of percolation mechanism.[149–151,155]



(a) $p = 0.2$ (b) $p = 0.59$ (c) $p = 0.8$

Fig. 7. Site percolation on a square lattice: The small circles represent the occupied sites for three different concentrations: $p = 0.2$, 0.59, and 0.80. Nearest-neighbor cluster sites are connected by lines representing the bonds. Filled circles are used for finite clusters, while open circles mark the large infinite clusters.[261] (a) $p = 0.2$, (b) $p = 0.59$, (c) $p = 0.8$.

(II) Bond percolation model

Bond percolation model is illustrated in Fig. 8(a), where all the sites have been occupied and the bonds between the sites are connected with the probability q. This model is usually utilized to describe the polymerization. When $q > q_c$, a network of chemical bonds connects thoroughly across the whole bulk; this is the so-called sol–gel transition. The most common derived model is a random resistor network. In addition, when bonds with capacity behavior are considered, the bond percolation model evolves to the equivalent circuit model, the conductivity of which is a frequency dependent complex number. When sites are occupied with the probability p and bonds are linked with the probability q, a more general site-bond percolation model can be obtained.

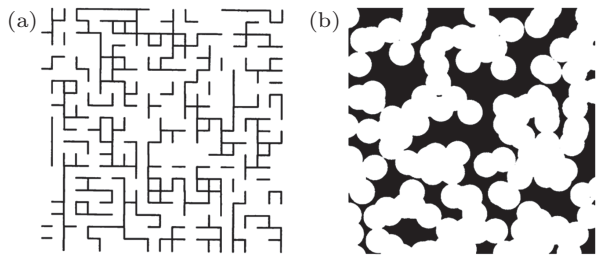


Fig. 8. (a) Bond percolation cluster on a square lattice and (b) continuum percolation of conductive material with circular holes of fixed radius at the percolation threshold.[261]

(III) Continuum percolation model

If two components of a random mixture are not restricted at the discrete sites in a regular lattice but are continuously distributed, as shown in Fig. 8(b), it is a continuum percolation model, also called the Swiss cheese model. The model is usually used to describe porous or composite materials, and the composite solid electrolytes is another important application of percolation model other than the perovskite $(Li_{3x}Ln_{2/3-x}[U + FFFF]_{1/3-2x})TiO_3$ mentioned above.

Only solid–solid composite electrolytes are within the scope of this review. The attention paid to this family can be traced back to 1973, when Liang found an abnormal enhancement of conductivity by dispersing Al_2O_3 particles into a LiI matrix.[42] The space-charge layer theory was developed to explain this phenomenon.[266–270] It assumes a high concentration of interlayer defects between the insulated and conductive phases. As a result, composite electrolytes are considered to be three-phase systems with the conductivity phase A, insulator phase B, and interphase C, among which C has very high conductivity because of the substantial frequency of defects. Figure 9 shows a simplified two-dimensional sketch of a discretized model for such composites, in which from Fig. 9(a) to Fig. 9(b), phase A (white squares) decreases and phase B (grey squares) increases, and phase C (interphase of phase A and phase B, indicated by bold lines) first increases and then decreases. Phases A and B, which follow the corresponding correlated bond percolation models, feature two thresholds p_c^C and $p_c^{C'}$. On one hand, if the percolation threshold of conductivity phase A is p_c^A, then $p_c^C = p_c^A$ is the onset of interphase percolation; on the other hand, $p_c^{C'} = 1 - p_c^A$ indicates the phase transition critical point from conductivity to insulator, which is hard to observe in experiments. Investigations of composite materials are usually based on the continuum percolation model, leading to dynamic critical properties thoroughly different from those resulting from the lattice percolation model (based on site or bond percolation).[271,272] The direct current (DC) conductivity can be obtained by Monte Carlo simulation,[273] whereas the alternating current conductivity can be studied with the renormalization group.[274] For the micro- and nano-crystalline composite conductors, the sizes of both dispersed particles make a significant influence on the diffusion mechanism. For example, if B is microcrystalline, the width of interphase C is negligible as compared with the size of B, which makes it impossible for the C phase to self-connect. As a result, the high conductivity phase cannot occur, so the system is in fact composed of two phases, A and B, and observes the corresponding two-phase percolation model. However, when B is nanocrystalline, the size of insulator B is comparable to the width of interphase C, which results in high probability of a continuous C phase with high total conductivity of the whole bulk. Indris *et al.*[275] used the effective-medium approximation (EMA) to get the DC conductivity,

with the assumption that $P_0(p) = p$, $P_2(p) = (1-p)^{\eta^3}$, and $P_1(p) = 1 - p - P_2(p)$ represent the concentrations of insulator phase, high conductive interphase and conductor phase respectively. Here, $\eta = (R+\lambda)/R$, R is the particle radius ($R \cong 10$ nm for nanoparticles and $R \cong 5$ μm for microparticles), λ is the width of the high conductive interphase, ranging between 1–2 nm

$$\begin{aligned}
&\sigma_{\rm dc}(p) = \sigma_{\rm B}^0 \frac{1}{z-2}\left\{-A + \left[A^2 + 2\tau(z-2-zP_0)\right]^{1/2}\right\},\\
&A = \tau(1-zP_1/2) + \tau(1-zP_2/2),\\
&p_{\rm c} = (z-2)/z,\\
&\tau = \sigma_{\rm A}^0/\sigma_{\rm B}^0.
\end{aligned} \tag{54}$$

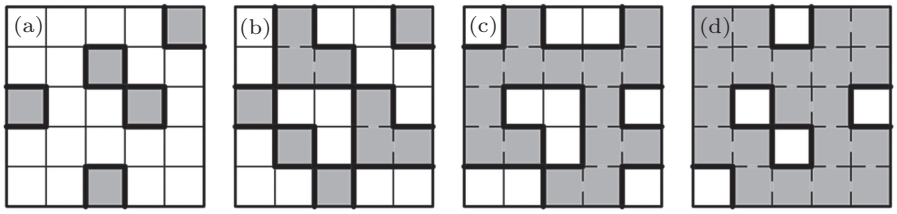


Fig. 9. Illustration of the three-component percolation model for dispersed ionic conductors, for different concentrations p of the insulating material. The insulator is represented by the grey area, the ionic conductor by the white area. The bonds can be highly conducting bonds (A bonds, bold lines), normal conducting bonds(B bonds, thin lines), or insulating (C bonds, dashed lines). (a) $p < p_{\rm c}'$, (b) $p = p_{\rm c}'$, (c) $p = p_{\rm c}''$, and (d) $p > p_{\rm c}''$. Here, $p_{\rm c}'$ is the percolation threshold of highly conducting interphase presented by bold bonds, and $p_{\rm c}''$ is the percolation threshold of insulating material presented by grey area. [261]

4. Experimental methods for characterizing ion transport mechanism in lithium-ion solid state electrolytes

In order to provide insight into the microscopic kinetic process, absorption, reflection and scattering techniques are often used to investigate the interaction of electromagnetic waves or probe particles with matter, as shown in Table 1. AC impedance spectrum measurement of ionic conductivity can span the frequency range from DC to 10 MHz. The information beyond this frequency can be indirectly obtained via low temperature impedance spectrum measurements. Radio wave and microwave detectors are applied to the frequency range of 10 MHz–GHz and higher. The response for even higher frequency can be studied by absorption and reflection of

Table 1. Frequency ranges of phenomena and methods used to study solid state electrolytes.[9]

Name of radiation	λ^{-1}/cm^{-1}	λ	Frequency/Hz		Phenomena and methods
		3 Å	10^{18}		
X-ray		30 Å	10^{17}		photon interaction
Ultraviolet		300 Å	10^{16}		
		3000 Å	10^{15}		
Visible light		3 μm	10^{14}		
Infrared	1000	30 μm	10^{13}		ion vibration
	100	300 μm	10^{12}		Fourier spectroscopy
Far infrared	10		10^{11}		neutron scattering
	1		10^{10}	40 GHz	light scattering
Microwave		30 cm	10^{9}	2 GHz	(Raman, Brillouin)
		3 m	10^{8}		acoustic phonons
Radio shortwave		30m	10^{7}		
medium		300 m	10^{6}	1 MHz	
longwave		3000 m	10^{5}		
			10^{4}		
			10^{3}	1 kHz	AC impedance
			10^{2}		measurements
Alternating current (AC)			10		
			1		
			10^{-1}		electrode diffusion
			10^{-2}		phenomena
			10^{-3}	1 mHz	
				H	
				L	
Direct current (DC)				$10^{-\infty}$	DC measurements

far-infrared, infrared and visible frequency ranges, as well as quasielastic scattering (including Mössbauer spectra based on γ-ray and quasielastic neutron scattering based on neutrons; in the latter, probe particles other than electromagnetic waves, with energy slightly lower than elementary excitation are utilized). The general optical mode of phonon spectra is about 10^{13} Hz for the crystalline phase, which reflects the ion vibration. In the frequency region much higher than the frequency of the ion vibration, i.e., where the interaction between photon and matter is much faster than ion vibration, the x-ray diffraction spectrum (or elastic neutron diffraction spectrum with a wave length similar to x-ray, where the interaction occurs between neutron particle and matter) is determined by the ionic instantaneous configurations, which gives the structure information.[9,194] The frequency dependent experimental methods are illustrated in Fig. 10.

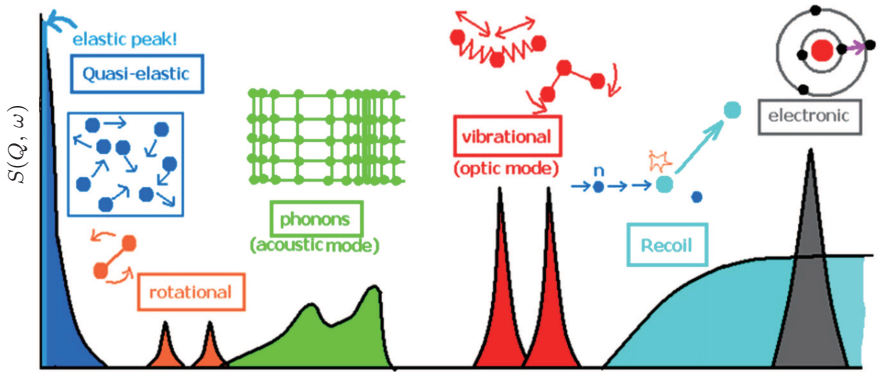


Fig. 10. Map of dynamical modes (from the lecture of 2013 Oxford School on Neutron Scattering, drawn by Victoria Garcia Sakai).[276]

4.1. Crystal structure and lithium-ion occupation pattern

Since many topics of solid state electrolytes are rooted in the crystal structure, as shown in Section 2, e.g., skeletons and mobile ion sublattices, disordered structure resulting from the superionic phase transition and Li-ion displacement arising from phonon mode softening, x-ray diffraction (XRD) is the method of choice to determine the crystal structure; its mechanism is shown in Fig. 11(a). However, it is difficult to detect the light elements by XRD, especially when they are mixed with heavy elements (but in some cases, Li ions in a single crystal can be located[133,138]). By contrast, the kinetic energy of a thermal neutron beam (shown in Fig. 11(a)) is low. As a result, the positions and dynamic features of nearly all elements in the periodic table can be detected by neutron diffraction, including our subject, lithium, as is shown in Fig. 11(c). X-ray and neutron diffraction patterns contain both the periodic structure information (Bragg peaks or Debye lines) from the long-range order and a liquid-like diffuse scattering pattern from the short-range correlation. However, when the studied system is chemically and structurally more complicated, much less information can be extracted about local structure. For such materials, small-angle x-ray scattering (SAX), small-angle neutron scattering (SANS), and first-sharp diffraction peak (FSDP) can be used for distinguishing the intermediate range order, with the magnitude of order ranging from 1 nm to 10 nm. In cases of short-range order, extended x-ray absorption fine structure (EXAFS), which arises from scattering by the near neighbors of excited atom species only, can probe the short-range structural, typological and coordination information between excited atoms and their neighbors, and reveal the relationship between this information and the high conductivity of the materials.

4.2. Lithium-ion conduction pathways

For the superionic conductors, the relaxation time, when ions leave lattice sites and transport across barriers, cannot be ignored. Driven by the temperature, Li ions arrange themselves statistically in an ellipsoid shape around the lattice sites and have opportunities to connect as a pathway at higher temperatures. With the help of high-temperature neutron diffraction (HTND) and the maximum-entropy method (MEM), the Li nuclear-density distribution and even the conduction pathway can be estimated, which was first used by Yamada *et al.* to study $LiFePO_4$[278] and then solid state electrolytes[140,161] as well. XRD, ND, and ND+MEM are always combined to obtain the information about the structure and diffusion mechanism more and more accurately. Taking garnet as an example, the skeleton lattice is initially determined by XRD,[157] then powder ND is applied to confirm the Li ion positions exactly, as very important structure information,[161] and HTND with MEM is subsequently used to map the conduction pathway.[163]

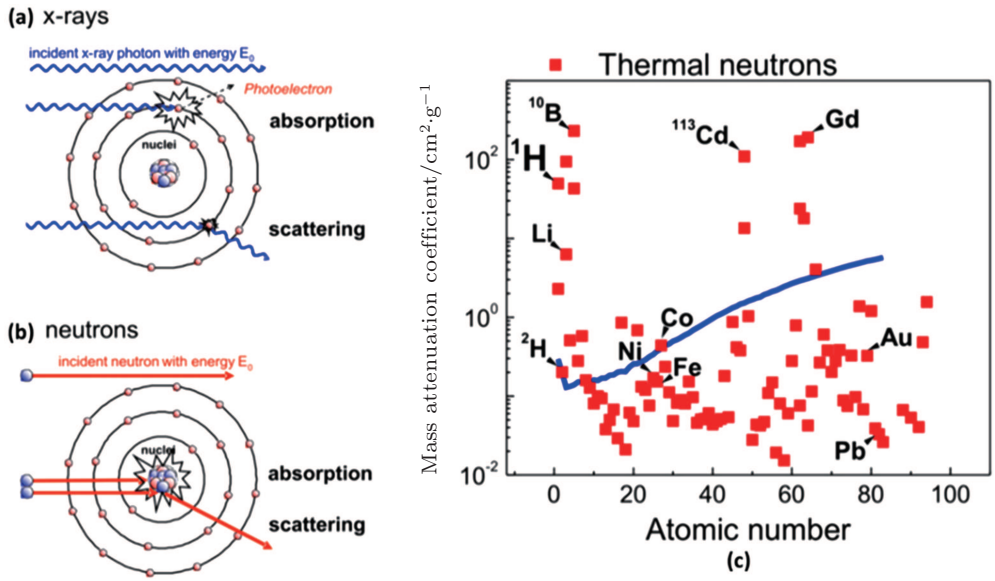


Fig. 11. Left: interaction of matter with (a) x-rays and (b) neutrons. (c) Mass attenuation coefficients for thermal neutrons and 100 keV x-rays for the elements (natural isotopical mixture unless stated differently).[277]

4.3. Lithium-ion conductivity and diffusion coefficient

Methods for measuring the diffusion coefficient can be grouped into two major categories: direct methods based on Fick's laws, and indirect methods not based directly on Fick's laws. As illustrated in Section 3, macroscopic and microscopic diffusion mechanisms are not always consistent with each other, and can be transformed to each other with the correlation factor. Table 2 shows some macroscopic/microscopic and nuclear/non-nuclear methods for studying the diffusion coefficient in solids. And common measurements for investigating diffusion are shown in Fig. 12, which are summed up from the aspect of temporal/special scale.[204]

Table 2. Methods for studying diffusion in solids.[204,279]

	Macroscopic	Microscopic
Nuclear	tracer diffusion	NMR relaxation
	field gradient NMR	β-radiation-detected NMR quasielastic neutron scattering mössbauer spectroscopy
Non-nuclear	DC conductivity	AC conductivity
	mechanical relaxation	

4.3.1. Direct methods[280]

The tracer method is the most direct and accurate technique to determine the (self- or impurity) diffusion coefficient in solids. Since the number of tagged atoms is very small, tracer isotopes will not influence the chemical composition. The isotope can be either radioactive or stable. The best way to determine the concentration-depth profile is to serial-section the sample and then measure the amount of tracer per section. If the diffusion coefficient is very small and the diffusion depth is less than 1 μm, it is hard to section and determine the tracer amount exactly. In addition, several other profiling and detection methods are commonly employed, including secondary ion mass spectrometry (SIMS), electron microprobe analysis (EMPA), Auger electron spectroscopy (AES), Rutherford backscattering spectrometry (RBS), nuclear reaction analysis (NRA), and field gradient nuclear magnetic resonance ((P)FG NMR),[281] details of which can be found Ref. [278] and references identified therein.

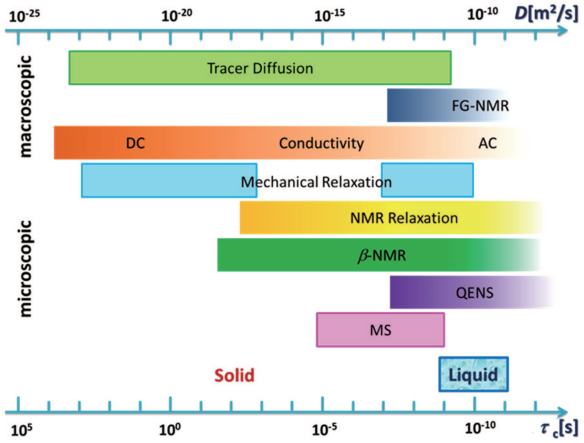


Fig. 12. Typical ranges of the diffusivity D and motional correlation time τ_c of some macroscopic and microscopic methods. FG-NMR: field gradient NMR, β-NMR: β-radiation-detected NMR, QENS: quasielastic neutron scattering, MS: Mössbauer spectroscopy. The hatched bar indicates the transition from solid to liquid, wherein the motional correlation time is reduced by about two orders of magnitude (adapted from Ref. [204]).

4.3.2. Indirect methods

(I) Impedance spectroscopy

As shown in Eq. (8), the self-diffusion coefficient D^* can be determined by D^σ derived from the electrical conductivity and Haven ratio H_R.[204] Note that for the electrode, the problem is more complicated, with the chemical potential, concentration and cross ionic/electronic phenomenological coefficients.[279]

AC impedance spectroscopy is the most common technique for determining conductivity. It can identify the contributions of bulk and grain boundary especially for polycrystalline, and make it possible to investigate how the microstructure affects the overall conductivity.[282] The principle is as follows: apply an AC voltage $U(\omega) = U_0 e^{i\omega t}$ to the sample, and the responding current is $I(\omega) = I_0 e^{i(\omega t+\Phi)}$ with the same frequency as the voltage but a phase shift Φ. As a result, the complex impedance with a real part indicating conductivity and an imaginary part indicating capacity is defined by Ohm's law: $Z(\omega) = U(\omega)/I(\omega) = Z_0 e^{-i\Phi} = Z_0 \cos\Phi - iZ_0 \sin\Phi$, and can be fitted from the equivalent circuit to give the microstructure information.[204]

In addition, by adding a microelectrode or nanoelectrode, the local conductivity of each local point within the bulk and grain boundary can be mapped in spatial scale.[283–286] More specifically, one method is to cover the surface of objects with micro-electrodes, as shown in Fig. 13. The other is to utilize the tip of a conducting atomic force microscope as nanoelectrode, as illustrated in Fig. 14.

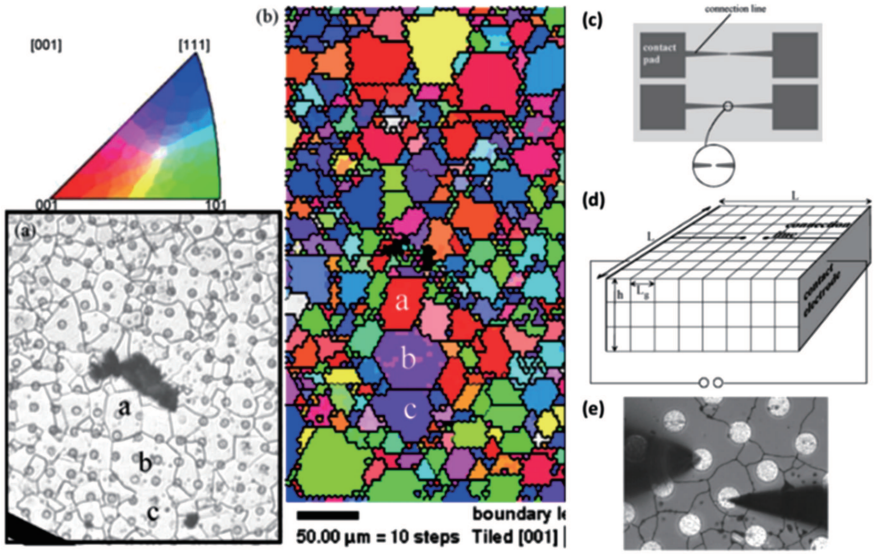


Fig. 13. (a) Polycrystalline $SrTiO_3$ with microelectrodes on the top in the optical microscope, (b) the orientations of the grains, (c) microelectrode, (d) sketch of a model sample, (e) image of circular microelectrodes contacted by tips.[283]

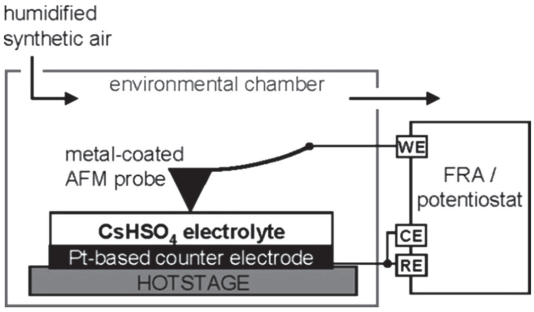


Fig. 14. Schematic drawing of the nanoelectrode setup.[284]

The Hall effect is employed as an alternative method to study conduction behavior.[287–290] Note that this method is suitable to Ag ionic conductors, which have high ionic conductivity and are typical examples of the sublattice melting model. However, as far as we are concerned, the relationship between Hall mobility and conductivity mobility remains unclear. This is because the Hall effect is understood in terms of the quasiliquid model, which is not really true for most ionic conductors. Especially for Li-ion solid electrolytes, the complicated long-range interactions, including those among mobile ions and those between mobile ions and skeleton lattices, can lead to larger deviations.

(II) Mechanical and magnetic relaxation methods[280]

Mechanical relaxation methods are possible because atomic motion in a material can be induced by an external disturbance like applied mechanical stress, either constant or oscillating. In ferromagnetic materials, the interaction between the magnetic moments and local order can give rise to various relaxation phenomena similar to those observed in anelasticity. They are rarely applied to the study of solid electrolytes.

(III) Nuclear methods[291]

Nuclear methods include nuclear magnetic resonance (NMR),[281,292,293] quasielastic Mössbauer spectroscopy (MBS),[294] and quasielastic neutron scattering (QENS).[280,295]

(i) NMR[9,204,292]

NMR is a powerful tool for studying materials. It can probe both the short range and long range motions, and can identify atoms located on inequivalent sites. There are various kinds of NMR, among which FG NMR is usually applied to investigate particle diffusion and particles' interaction with structure in mesoporous medium,[281] and also can be used to measure the long-range correlation in Li-ion solid

state electrolytes with response time scale on the order of milliseconds.[138,296] On the other hand, electrophoretic NMR is usually used to study the charged particles in liquid.[293] Beyond such macroscopic applications, the diffusion process can be investigated by NMR for atomistic time scales, i.e., transient studies and wideline studies.

In transient studies, the sample in a static external magnetic field is exposed to a brief, intense pulse of radio-frequency radiation. This pulse transfers additional energy to nuclei, which leads to a phase correlation of nuclei normal motion in the external magnetic field. Removal of the pulse means that nuclei transfer energy to the surrounding environment, and the phase correlation decays in two characteristic times (spin-lattice relaxation time T_1 and spin–spin relaxation time T_2). The magnitudes of T_1 and T_2 reflect the interaction strength between the nuclei and their environment. The extended methods of transient studies make use of the spin-lattice relaxation in the rotating frame, with the characteristic time $T_{1\rho}$, whose property is between T_1 and T_2, as shown in Fig. 15, and the decay of NMR signal locked in the transverse direction by the second radio frequency pulse is studied. The value of $\tau(T)$ can be obtained from Eq. (48), and τ_0 and E_A can be obtained from Eq. (47). In the light of the random walk model, if the interaction is considered, the results will deviate from the BPP theory as shown in Section 3.3.3, and T_1^{-1} will become asymmetric in Fig. 15. The more obvious deviation occurs in the low-dimensional and disordered system, with a gentler slope at the low temperature. As a result, this deviation study can be used to probe the local disorder.

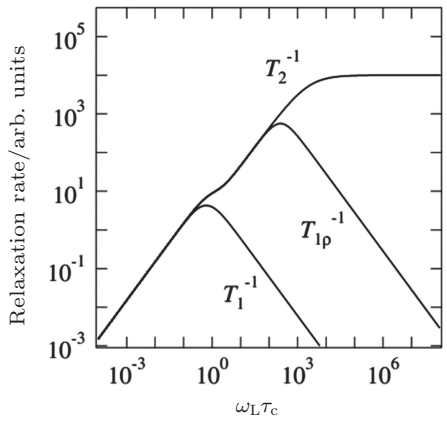


Fig. 15. Schematic of the relaxation rates T_1^{-1}, $T_{1\rho}^{-1}$, and T_2^{-1} versus, $\omega_L\tau_c$ for the three-dimensional diffusion via the random walk model.[292]

In the wideline studies, the sample is exposed to a static external magnetic field and a continuously applied, small radio frequency field. Then the position, width, and shape of the absorption spectrum reflects the interaction between nuclei and their microscopic local surroundings, such as the magnetic moments of adjacent nuclei, electric field gradients, and other components of the compound (e.g., paramagnetic electronic species and conduction electrons). As for the superionic phase, mobile carriers can move "freely" across the skeleton, which leads to the average uniformity of local field everywhere. As a result, $\tau_c^{-1} \geq 2\pi\Delta\nu_R$, and the resonance line $\Delta\nu_R$ is narrowed, called motional narrowing. Owing to $T_2^{-1} \propto J(0) \propto \tau_c$, when $\tau_c^{-1} > \omega_L$ at higher temperature, the extreme motional narrowing occurs and the values of T_1, T_2, and $T_{1\rho}$ are the same, as shown in Fig. 15. This method can be applied to the heterogeneous structure, e.g., nanocrystalline crystalline, to identify the different dynamic performance of carriers in any part of the heterogeneous structure. The spectral density outside the motional narrowing region can be explained by the random walk model.[297,298]

(ii) Quasielastic methods

Compared to "elastic" methods, "quasielastic" methods indicate a small amount of transference of energy, which enables the measurement to probe the dynamic characteristic of elements. Quasielastic neutron scattering (QENS) and uasielastic Mössbauer spectroscopy (QEMS) are common quasielastic techniques, the principle of which has been introduced in Section 3.3.3, presenting the proportional relationship between the spectrum intensity and dynamic structure factor $S^{tot}(\boldsymbol{Q}, \omega)$. If the diffusion in a solid is fast enough, i.e., $D \sim 10^{-14}$–10^{-10} m^2/s for QENS, and $D \sim 10^{-13}$–10^{-7} m^2/s for QEMS, the phenomenon called diffusional broadening occurs, as shown in Fig. 16. That is because the wave train scattered (in the case of QENS) or emitted (in the case of QEMS) by the diffusing atoms can be cut into several wave trains. As all these wave trains arise from the same nucleus, the interference between them depends on the relative orientation between the jump vector and the wave vector.

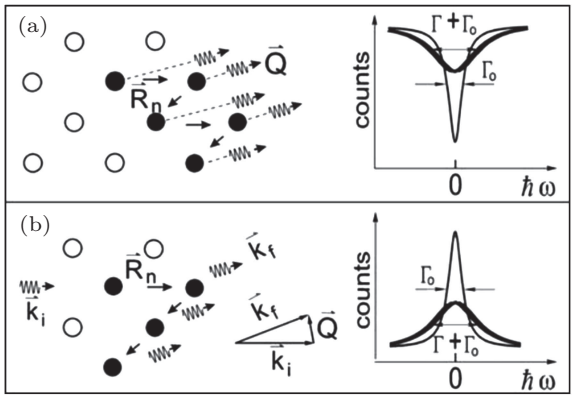


Fig. 16. Simplified, semiclassical explanation of diffusional line broadening for QEMS (a) and QENS (b).[294]

4.4. Complete conductivity spectra[9,194]

As shown in Table 1 and Fig. 10, the frequency dependent techniques to investigate ion transport can be grouped into the low frequency methods and high frequency methods; the former are mainly DC and AC impedance spectroscopy, and the latter involve measurements based on the quasielastic scattering (mentioned above) and based on electromagnetic

waves. Here, we address only the frequency-dependent conductivity measurements, as shown in Fig. 17, and for various methods corresponding to different frequency ranges, they can be collectively called complete conductivity spectra. The measurements variously correspond to the different frequency ranges, although their principles are consistent as introduced in the continuous stochastic model in Section 3.3.3: the complex conductivity $\hat{\sigma}(\omega)$ can be determined by amplitudes and phases of quantities induced by the external field. For impedance spectroscopy, the quantities are voltages and currents, and for other techniques without electrodes, the quantities are complex field amplitudes of electromagnetic wave transmitted or reflected by samples; thus they can be obtained by solving Maxwell's equations with boundary conditions at the interfaces. As $\hat{\sigma}(\omega)$ is the Fourier transform function of the velocity correlation function, it presents the structure at the ionic motional characteristic frequency and indicates certain features of the velocity correlation function. Given that the complete conductivity spectra method spans more than 17 decades on the frequency scale, as shown in Fig. 17, it enables us not only to probe the motion of charged particles across a wide time scale, but also to observe the motion limited at a minimal time scale, thus giving probability to interpret the elementary hopping process.

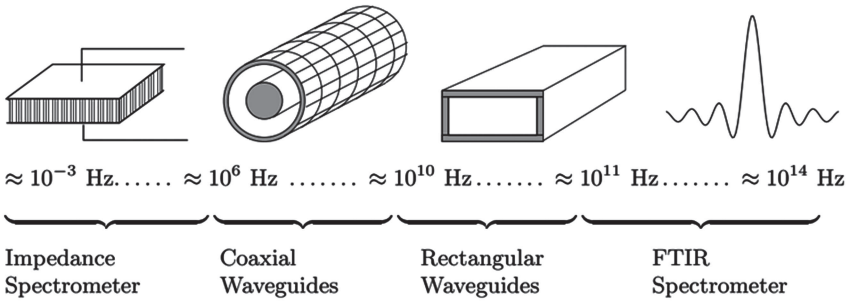


Fig. 17. Schematic overview of different techniques for the measurement of frequency-dependent conductivity.[194]

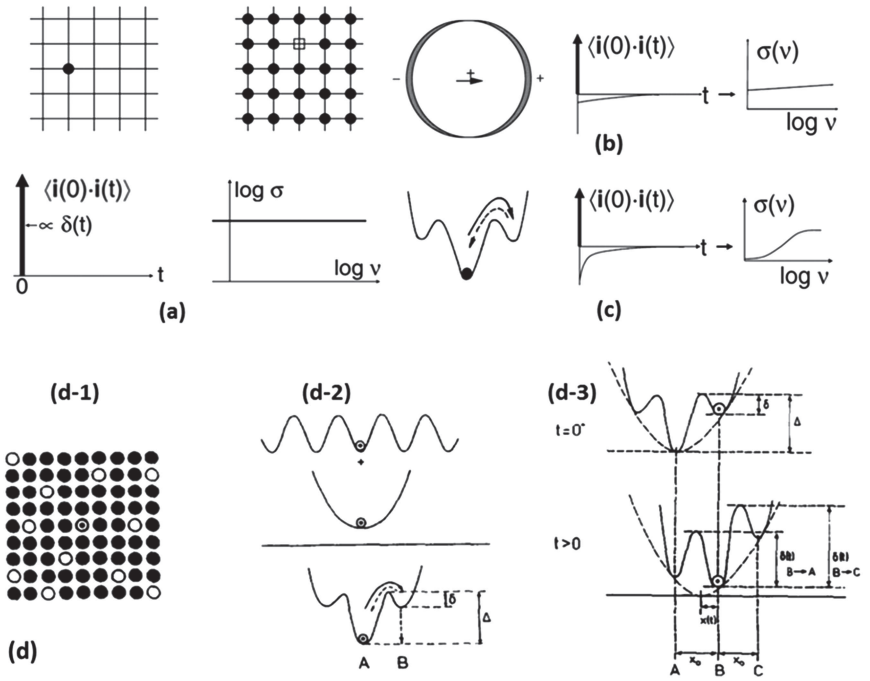


Fig. 18. Schematic comparison of the current density autocorrelation function and the conductivity dispersion in (a) crystals with thermal activating defects, (b) a dilute strong liquid electrolyte, and (c) a structurally disordered solid electrolyte.[194] (d) The jump relaxation model.[299]

A schematic of complete conductivity spectra of various systems is shown in Figs. 18(a)–18(c). Note that the spectra are totally different among crystals with thermal activating defects, dilute strong liquid electrolytes and structurally disordered solid electrolytes. As illustrated in Section 3.1, crystals with the thermal activating defects can be grouped into level two. The point defects diffusion mechanism can be interpreted by the random walk model so that there is no interaction

among the point defects, making the cross terms of correlation function vanish. In addition, without the memory effect, only self-correlation of current is left to be $\delta(t)$, which becomes constant after Fourier transformation, as shown in Fig. 18(a). The dilute strong liquid electrolyte in Fig. 18(b) exhibits the Debye–Hückel–Onsager–Falkenhagen effect. That is, once ions in the solution displace from the equilibrium sites, the following two contributions make them tend to balance: ions hopping backward and neighboring "clouds" with the negative charge hopping forward, leading to a reverse current compared with ions displacement; thus a slight enhancement of conductivity with increasing frequency as the Fourier transform of the correlation function. However, for the disordered solid state electrolytes, the motion of ions is achieved by hopping between different potential valleys, and the "clouds" are the neighboring mobile ions. Accordingly, two relaxation processes exist: ions hopping backward and clouds hopping forward. As a result, for the structurally disordered electrolytes, as shown in Fig. 18(c), the velocity correlation has a sharp peak at $t = 0$, which reflects the self-correlation during the hopping and shows a decaying behavior at $t > 0$, implying a small probability of backward ion hopping; the corresponding mechanism sketch is shown in Fig. 18(d). The striking difference between Figs. 18(b) and 18(c) lies in the relative magnitude between the two contributions mentioned above: the amount of backward flow of charge and thus the resulting dispersion of $\hat{\sigma}(\omega)$ are dramatically larger in the solid than in the dilute liquid electrolyte.

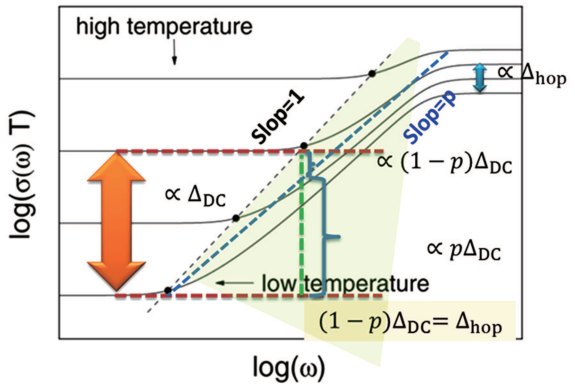


Fig. 19. Sketch of a set of frequency-dependent conductivity isotherms (Adapted from Refs. [194] and [299]).

Figure 19 illustrates the isothermal diagram on the conductivity versus frequency relationship, which shows the characteristic parameters such as the backward hopping probability p, the activation energy of DC impedance spectrum Δ_{DC} and frequency disturbing microscopic hopping Δ_{hop}, and the correlation among them. Here, the segment with the constant slope of p indicates the dispersion related to the frequency mentioned above, or called nearly constant loss (NCL) behavior. Note that the onset frequencies of dispersion at any temperature can be connected to form a straight line with the slope of 1. Since $p < 1$, the activation energy in the high frequency region Δ_{hop} is lower than that in the low frequency Δ_{DC}. As a result, the approximation of the relationship reads: $(1-p)\Delta_{DC} = \Delta_{hop}$, which attributes the non-Arrhenius behavior of DC conductivity to the supercooling of melting ionic crystals. The more detailed description on the characteristic parameters in Fig. 18 can be found in Ref. [194].

5. Factors influencing the ionic conductivity in lithium-ion solid state electrolytes

Seeing from the development history of solid state electrolytes as reviewed above, the conductivities of various conductor families span a wide range, and only a handful of them can attain high enough conductivity, usually with the open structure, which can be regarded as the critical factor leading to the superionic conductors. However, it is still not clear how to evaluate the structure quantitatively, and what is the consequent correlation between the specific structure and the high conductivity. In order to investigate the relationship between structure and performance, the method of high-throughput calculations was developed specially for Li-ion solid state electrolytes.[82,300] Much more work is in process on effective data mining.[301]

For enhancing the performance of the known solid state electrolytes, efforts are usually focused on higher carrier concentration, more sites suitable for Li-ion occupation, and the connective conduction pathway caused by the former two aspects meeting the requirement of the percolation model. Figure 20 shows two strategies: compositional complexity and morphological complexity. Note that with the reduction of material size, the distinction between them is blurred.

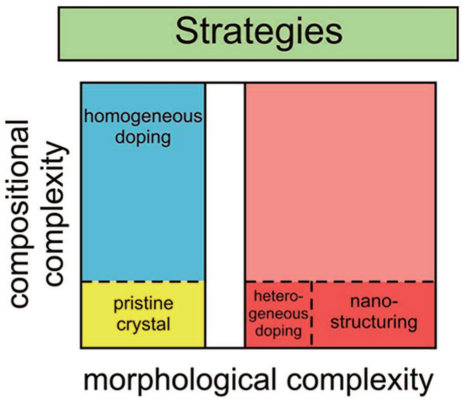


Fig. 20. Besides varying simple state parameters, such as pressure and temperature (electric field, etc.), the variation of morphological complexity evolves, in addition to the well-known strategy of varying chemical complexity, to a more powerful method in materials engineering.[302]

From the compositional aspect, doping and substituting by elements with different valence states, concerning the knowledge of defect chemistry, is one of the most common

and effective ways to enhance the conductivity of solid state electrolytes. Besides, the structural parameters can usually be finely tuned by dopants and substitutions with different ionic radius within the concentration range of solid solution, and the parameters, or the size of the "bottleneck" in the Li-ion conduction pathway, can be optimized to the certain values for higher conductivity. In addition, the element types of dopants and substitutions located at the skeleton sites have the different interaction with mobile Li ions, and weaker interaction usually enables Li ions to transport more freely.

From the morphological aspect, other effective methods to increase the ionic conductivity are applying glass state or glass-ceramic state instead of crystalline state, as well applying composite materials. Moreover, in all-solid-state batteries' applications, there exists the interphase problem derived from matching the electrolytes and electrodes (both cathodes and anodes, and the latter are usually referred to as SEI, i.e., solid electrolyte interphase), leading to the striking high resistance, which can even become the most severe limitation of the full cell's conductivity. As a result, decreasing, or even eliminating the interphase resistance, will enhance the full cell performance effectively.

5.1. Structural disorder

The development history of glass and polymer and ionic transport are reviewed in detail in Ref. [303]. The structure characterization techniques of amorphous solid electrolytes are similar to those of crystal electrolytes, with the emphasis placed on the short-range and medium-range order, which is of critical importance for Li-ion diffusion in the amorphous state.[304] Ionic conduction is the process that the locally (at atomic scale) ordered lattice ions are excited to the disordered neighboring sites, then collectively diffuse in macroscopic scale. That is, the disorder and the collective motion are the key points with the following relationship: the correlation of independent point defects is weak, while for the amorphous materials with abundant defects, the interaction cannot be neglected among mobile ions and even among mobile ions and skeleton ions. The experimental techniques for studying amorphous ionic conductors are shown in Fig. 21, and the space-time hierarchy structure leads to complicated dynamic results depending on techniques of different time-space window. Among them, the time scale of radio frequency (10^{-9} s–10^{-3} s: kHz–GHz) is the characteristic region, where there exist universal frequency responses to amorphous ionic/electronic conductivity as well as NCL mentioned above, with the possible correlational motion of mobile ions, and/or dynamical effect of the random structure.

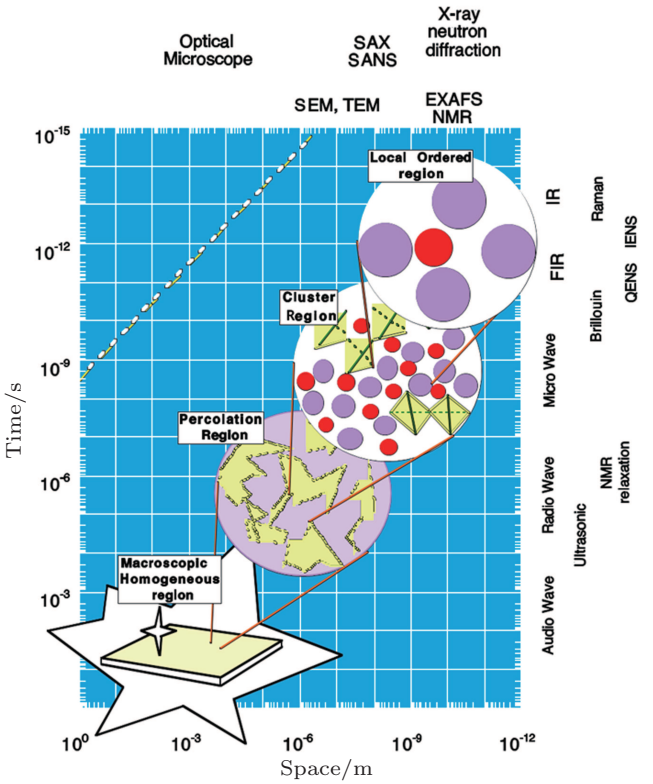


Fig. 21. Space-time hierarchy structure of amorphous ionic conductor experimental techniques (The original image is from Ref. [303], and the daptation is from Prof. Kawamura Junichi's private mail).

For the crystal with ordered structure, the ionic conductivity is often expressed by Arrhenius type law as: $\sigma_{\mathrm{DC}}T = A_\sigma \exp(-E_\sigma/k_{\mathrm{B}}T)$. However, for the disordered glasses and polymers, and even some crystalline solid state electrolytes with Li ions and "vacancies" randomly occupied, the conductivity expression will deviate from the typical Arrhenius type (i.e., the relationship between the logarithm of conductivity and the inverse of temperature deviates from linear), and the consequent examples with curved Arrhenius relationships are shown in Figs. 2 and 4. In this way, the behavior can be better expressed by the Vogel–Fulcher–Tammann (VFT) equation or the Williams–Landel–Ferry (WLF) equation as

$$\sigma_{\mathrm{DC}}T \propto \exp(-E/k_{\mathrm{B}}(T-T_0)). \tag{55}$$

When $T_0 = 0$, equation (55) reduces to the normal Arrhenius equation. This equation can be explained by a configurational entropy theory,[305] or a free-volume theory.[306,307] In the configurational entropy theory, the transition state is supposed to form by the correlational fluctuation of atomic (or ionic) configuration; the configurational entropy reads: $S_{\mathrm{C}} \sim \Delta C_{\mathrm{p}}/T + \mathrm{const}$, and the transition probability per unit time can be written as $\nu_i = \nu_i^0 \exp(b/TS_{\mathrm{C}})$; then equation (55) can be obtained. In the free-volume theory, molecular transport occurs only when the voids having a volume V greater than some critical volume V^*, and the free volumes distribute randomly in liquid. Then the temperature dependence of the average free volume V^{f} is approximately $V^{\mathrm{f}} = V_0\alpha^{\mathrm{f}}(T-T_0)$, where α^{f} is

the thermal expansion coefficient of the free volume in the liquid state; T_0 is the temperature at which the free volume vanishes and V_0 is the volume of the liquid at T_0. Therefore, the diffusion coefficient is written as $D = D_0(\gamma V^*/V^{\rm f})$, which can also be reorganized to Eq. (55). When the barrier potential effect is considered,[308] only atoms with energy higher than the barrier potential $E_{\rm V}$ can hop out of the local equilibrium sites effectively, and thus the diffusion coefficient can be rewritten as $D = D_0[-(\gamma V^*/V^{\rm f}) + (E_{\rm V}/kT)]$, which can be used to fit the Arrhenius plot of polymers[309,310] and glasses[311,312] well. All above efforts are attempting to fit the experimental curve, and by revising the diffusion coefficient equation, the mechanism causing the deviation is supposed. In fact, the transport mechanism differs greatly in different materials. Taking Li-ion solid state electrolytes as an example, of the inorganic glasses the Li ions' mobility usually approaches 1 while the mobility of the polymers is much less than 1 for both cation and anion transport. The greater difference lies in the ion hopping mechanism: for the disordered inorganic solid, the motion can be explained by the lattice gas model or continuous stochastic model presented in Section 3.3; for the polymers, the ionic motion is mediated by the peristalsis of segments and fluctuation of skeleton ions, which provide the ions conduction pathway randomly. Moynihan and Angell identified the different transport mechanisms between polymers and glasses by using the concepts of "coupled" and "decoupled",[313–317] and explain successfully why the inorganic solid state electrolytes can work under the glass transition temperature $T_{\rm g}$.

The present review concentrates on the discussion of inorganic solid state electrolytes. At the time scale of mobile carrier diffusion, the crystal skeleton is supposed to be highly stable, while the interaction between skeleton and mobile ions cannot be ignored.[239] As compared with Eq. (55), Arrhenius behavior in inorganic glasses can by expressed as

$$\sigma(T) = T^m \sigma_0 \exp\left(-\frac{\Delta E}{kT}\right), \quad (m = 0 \quad \text{or} \quad -1), \qquad (56)$$

which can fit the experimental results better, and is called the Rasch–Hinrichsen relationship.[318,319] In the theoretical model presented in Section 3.3, analytic solutions to the diffusion mechanism problems in the disordered solid can be obtained only with some difficulty, for the following reasons.[303]

(I) From the aspect of nonequilibrium thermodynamics, glass transition is naturally fluctuation-freeze resulting from the sudden change of external parameters (such as temperature). Ergodic to non-ergodic transition phenomenon is also a frontier in statistical mechanics, and the relaxation of the transition critical region is neither exponential nor linear.[313]

(II) The process of ions vibrating and diffusing in the energy landscape with random barriers and random wells can be phenomenologically expressed by the two-state model and percolation model introduced in Sections 3.3.1 and 3.3.4. However, amorphous materials have short-range order although without long-range order compared to crystal. In other words, they also have the microscopic structure and are not exactly random in fact. Moreover, other than short-range order of the skeleton-similarity in glasses, in crystalline Li ion conductors, such as perovskite and garnet types, semi-disorder of Li-ion sublattice occurs. In this case, of the probability ellipsoids located near the equilibrium sites, the occupied rate of Li ions decreases with the increase of the radius.

(III) Correlation effect is among the most challenging problems, including the mobile ions, mobile ions' correlation as well as mobile ions and skeleton ions' correlation. This is because many-body interaction has to be considered,[313] which is more significant for classical particles with large volume and mass than for quantum particles as electrons. Generally speaking, the interaction involves the backward correlation mentioned with regard to complete conductivity spectra[239,320] and concerted migration, usually studied by calculations.[4,5]

(IV) Silver and copper ion conductors usually exhibit higher conductivity, which is quite counterintuitive because Ag and Cu have larger mass and larger radius. In this way, quantum mechanical or chemical bond analysis may be helpful for us to obtain a better knowledge of ionic conduction.

In order to explain the experimental results, some phenomenological and semi-microscopic methods have beenthe introduced, including lattice gas model mentioned above, coupling scheme proposed by Ngai *et al.*,[231] the jump relaxation model proposed by Funke,[299] the diffusion-controlled relaxation model proposed by Elliott and Owens,[234] and so on. Besides the above theoretical models, numerical simulation methods such as MD and MC also play important roles.

Although no final conclusion for ion diffusion in disordered structures can be theoretically drawn, and the experimental results can usually be explained only phenomenologically, experiments do indicate that amorphous materials of certain systems show higher conductivity. The increase of conductivity may result from the substantial defects for the inorganic glasses or may be attributed to a means of fabrication of glasses that is good for eliminating pores and suspending grain boundaries. In addition, during the process of glass preparation, because of the freezing of thermal fluctuation, the heterogeneous structures form intrinsically.[321–323] Moreover, when the crystalline materials mix into, or segregate from glass basement, the conductivity of product is further enhanced, which may arise from the enrichment of defects surrounding the crystalline materials or to the heterogeneity effect introduced below in composite materials. In this case, the percolation model must be taken into consideration for the

ion diffusion, not only in homogeneity, but also with the preference in certain regions.[230,261,324]

5.2. Composite materials

As shown in Fig. 22, the interest of composite materials, which can increase the conductivity effectively) can be traced back to 1973, when Liang found that the Li-ion conductivity in LiI can be enhanced by dispersing insulating Al_2O_3 particles into the LiI matrix.[42] Now it is widely accepted that the enhancement of conductivity arises from the interphase region. Composite materials can be grouped into three catalogues proposed by Wagner:[326] (i) immiscible second phase, e.g., Al_2O_3 in LiI;[42] (ii) two phases proposed by Wagner, which can form a limited solid solution with a certain miscibility gap, and reach the equilibrium in the separation region of phase diagram, e.g., AgI–AgBr system;[327,328] (iii) polycrystalline material of single phase proposed by Maier, containing grain boundary with the same single phase, e.g., silver halides polycrystalline.[329] Composite electrolytes were reviewed in Ref. [266], and the common kinds of composite materials are shown in Fig. 23 (from Ref. [325]),

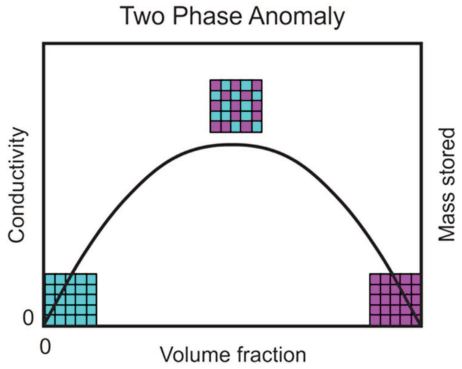


Fig. 22. Qualitative sketch of the two-phase anomaly of effective composite conductivity and storage capacity based on redistribution processes (contact equilibrium) at the interfaces. Strictly speaking, percolation effects lead to modification in the shape for the transport case.[302]

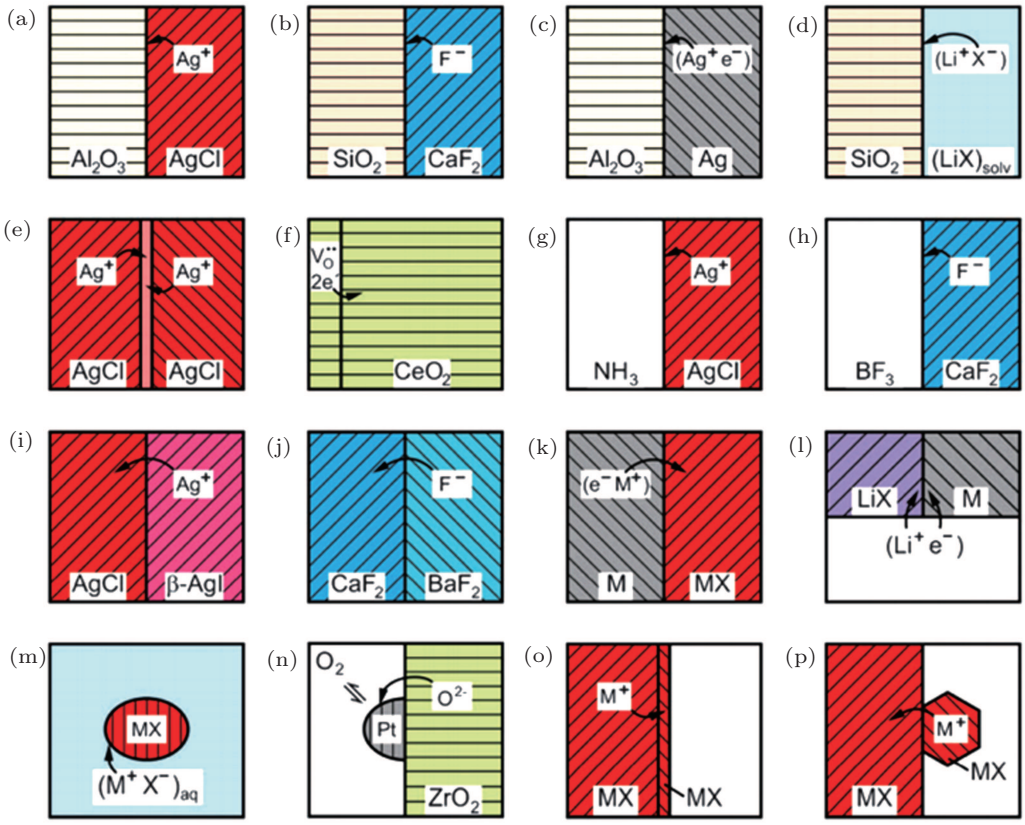


Fig. 23. Examples of ionic space charge effects at various contacts. Introduction of (a) Al_2O_3 and (b) SiO_2 particles into (a) AgCl (b) CaF_2, leading to vacancy enriched regions that provide highly conductive pathways; (c) addition of alkaline Al_2O_3 to metal Ag, leading to the an adsorption of Ag^+ resulting in vacancy enriched regions, and enhancing Ag^+ conductivity which can compete with e^- conductivity; (d) addition of acidic SiO_2 to Li-salt containing polymers or liquids, leading to an adsorption of the anions resulting in breaking ion pairs and enhancing Li^+ conductivity; (e) the simple grain boundaries in AgCl, adsorbing Ag^+ and increasing the silver vacancy concentration in the vicinity; (f) the simple grain boundaries in CeO_2, where electrons accumulated, inverting the O^{2-} conductivity invert to n-type conductivity; additions of (g) NH_3 and (h) BF_3 as (g) Ag^+ and (h) F^- attractors, resulting in the contamination of the grain boundaries to accumulate the mobile carries such as (g) Ag^+ and (h) F^- respectively; the inhomogeneous grain boundary between (i) AgCl and β-AgI, (j) CaF_2 and BaF_2, and (k) M (metal) and MX, accumulating Ag^+, F^-, and M^+ respectively; (l) the inhomogeneous grain boundary between LiX and M (metal), where Li^+ accumulated at LiX side while e^- at M side, leading to the mixed electronic–ionic conductor at interfaces; (m) addition of MX particles into M^+X^- aqueous solution, leading to an adsorption of $(M^+X^-)_{aq}$; (n) addition Pt as the catalyzer to accumulate O^{2-} at the surface; MX with the (o) two-dimensional and (p) zero-dimensional (point contacting) homogeneous interphase MX, adsorbing M^+ (o) at interphase and (p) host matrix respectively.[325]

which indicates very different interphases depending on various kinds of composites, resulting in the difference in mechanisms of conductivity enhancement. In fact, as concluded by Wagner,[326] the phenomenon mentioned above may be attributed to multifaceted reasons, such as the formation of space charge layers (SCL), an enhanced dislocation density, or the formation of new phases. Among them, SCL theory proposed by Maier is generally acceptable.[267–270] As illustrated in SCL theory, in order to keep the charge neutrality in the bulk, cation and anion defects are locally equal, even with different formation enthalpies. However, the constraint above is relaxed due to grain-boundary or interface charged as the result of the different electrochemical potential of both sides, thus the concentrations of cation and anion defects can be different. This results in the formation of a SCL. The unbalanced defect concentrations decay from the interface to the interior, and Debye screening length (λ) can be defined as

$$\lambda = \sqrt{\frac{\varepsilon_0 \varepsilon_r RT}{2(zF)^2 C_b}}, \tag{57}$$

where ε_0 and ε_r are respective permittivities of vacuum and sample, C_b is the concentration of the majority carrier in the bulk, z is the charge, and F is the Faraday constant.

For the materials controlled by interface, the interphase region can be enlarged by diminishing the particle size, which belongs to Nanoionics theory. Maier proposes that the size effects are classified into two kinds as shown in Fig. 24:[302,330] the explicit and implicit size effects. The explicit size effect refers to the direct geometrical influence on resistive (related to transport) and capacitive (related to storage) performance. In contrast, the implicit size effect concerns the dependence on the effective material parameters, especially in the heterogeneous case, where the superposition of the various local conductivities may be complex based on heterogeneous doping (or called higher-dimensional doping) and the performance is influenced by volume fraction, as shown in Fig. 23,

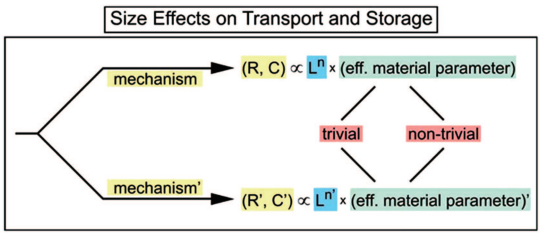


Fig. 24. Explicit and implicit size dependence of resistive and capacitive elements that are required to describe (electro) chemical transport or storage.[302]

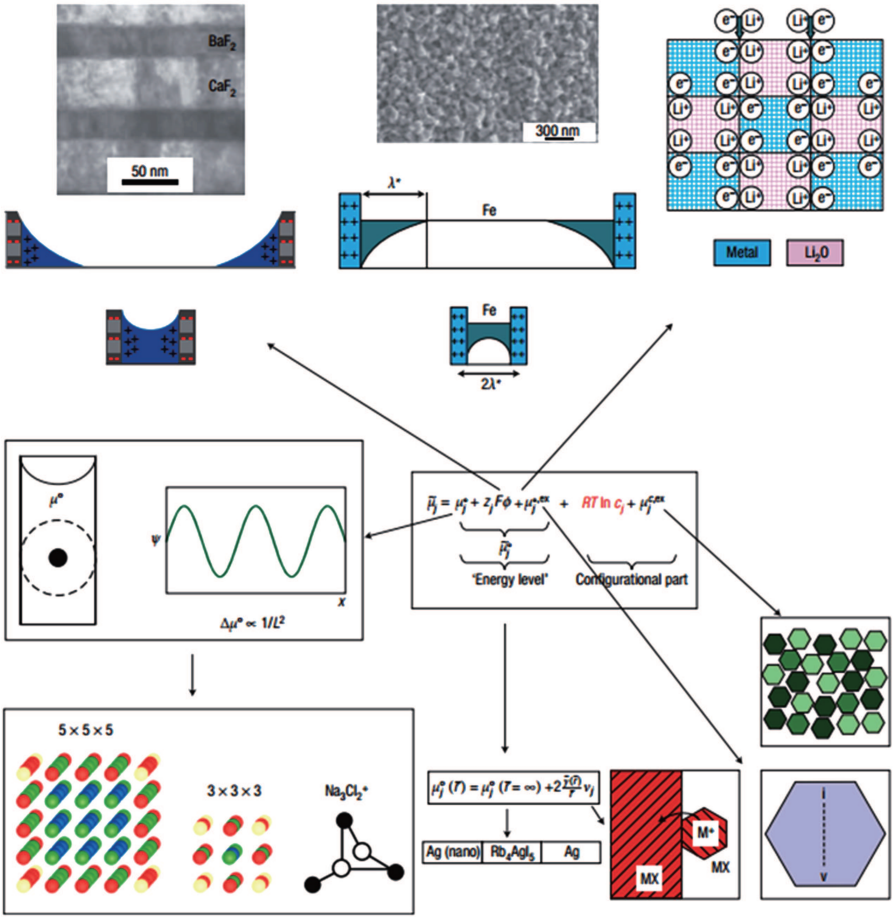


Fig. 25. Size effects classified according to their contribution to the total chemical potential.[331]

which can be explained by the percolation model. The implicit size effect can be further grouped into trivial size effects and non-trivial size effects.[330] The former indicates the situation where the local effect is the same as isolated interface, and the latter in contrast indicates the situation where space charge layers overlap, interfaces perceive each other, and ascribed to the quantum effect that the decreased size induces the increase of non-local electrons.[331]

In addition to the charge carriers redistribution at the grain boundaries, another important influence on concentration variations is the formation (free) energy, or more precisely speaking, the standard chemical potentials. The two aspects above are not independent, for the formation of grain boundaries is often ascribed to the defects relaxation induced by (electro) chemistry. By considering the macroscopic and microscopic effects related to the size comprehensively, size effects can be classified according to their contribution to the total chemical potential, as shown in Fig. 25.

Note that there is no clear distinction between disordered and composite materials, because the former can be regarded as the limit of the latter, when all atoms have lost the long-range order and the whole macroscopic system consists only of grain boundaries. As a result, the percolation model must be considered in various space scales to account for the different degrees of mixing from atomistic to mesoscopic to macroscopic levels, corresponding to glass to polycrystalline/glass-ceramic to classic mixture with the miscibility gap.

5.3. Interphase between solid state electrolyte and electrode

In considering the solid electrolytes in contact with the electrode materials, the critical problem lies in the interface with usually small, and even point contact area. For the thin film batteries fabricated by RF sputtering, via the strict control of preparation process, the layers of electrolyte and electrode can be dense and basically free of grain boundaries and are in close contact with each other at atomic scale. For all-solid-state batteries with the sandwich structure, if oxides are provided as solid state electrolytes, the electrodes should be fabricated by mixing electrolyte materials into electrode materials. Then the primitive loose mixture with sandwich structure is sintered to enlarge the contact area and eliminate the interface resistance. In contrast, since sulfides have good ductility, with Yong's modulus between polymers and oxide ceramics,[332,333] their grain boundary resistance can be reduced only by the cold pressing,[332–334] and they can contact with other materials (including electrodes and the other compositions in composite electrolytes) closely.[335] Another method to improve the physical contact of solid–solid phases is to modulate the materials' morphology.[336] When Li metal or Li–In alloy is applied as the anode, because of the good ductility of metal, the physical contact is no longer the most critical problem, but is replaced by the preferential consideration of chemical stability, electrochemical stability and space charge layer.

5.3.1. Solid state electrolyte/anode interphase and mixing transport

The solid state electrolytes are electronic insulator with the Li-ion mobility as 1, although at the interface with electrodes, the complicated ionic–electronic mixed conductivity occurs as the result of electron tunneling or (electro)chemical reaction. This effect is especially significant when the solid state electrolyte is in contact with the anode.

Carbon as anode and organic electrolytic solution as electrolyte are usually applied in Li-ion batteries these days, and the formation of SEI (solid electrolyte interphase) film on the surface of carbon anodes contribute mostly to their application. SEI film grows at the cost of capacity loss, and restricts rate performance; as a result, it is expected that SEI film can be stable and compact after the initial charge–discharge cycle, to prevent electrons from penetrating into organic electrolytic solution to promote the decomposition of electrolyte accompanied by the growth of SEI film. Investigated by *ab initio* calculations of the microscopic mechanism of the formation of SEI film, the rate of electron tunneling is obtained, indicating that in the nonadiabatic regime the reorganization of solvent molecules can slow the electron transfer.[337] The makeup of this film is so complicated[338] that the Li-ion transport mechanism within it is hard to study. Li_2CO_3 as the principal inorganic constituent has extremely low conductivity[2–5] and is not at all a "superionic conductor". The Li-ion transport mechanism is studied by calculation,[4,5,339,340] ascribing the conductivity to the interstitial Li ions hopping by means of "knock-off".[4,5,339] However, Li can diffuse in the form of atoms,[4] concerning the electronic–ionic mixed transport, and resulting in the continuous growth of SEI film.

It is generally accepted that one of the advantages of inorganic solid electrolytes lies in their probable wide electrochemical window, because it would prohibit the formation of SEI film. However, this conclusion was questioned by a recent study. By applying electron energy loss spectroscopy (EELS) combined with scanning transmission electron microscopy (STEM) to investigate a solid state battery with LIPON as the electrolyte, an interface layer can be obviously observed between LiPON and Si anode. Note that as compared with energy dispersive x-ray (EDX), EELS has a higher resolution for light elements such as Li, which is an advantage for investigating Li-ion batteries, as shown in Fig. 26. Figure 27 shows the concurrence of Li, P, Si, and the mutual diffusion directly indicates that a chemical reaction takes place at the interface.

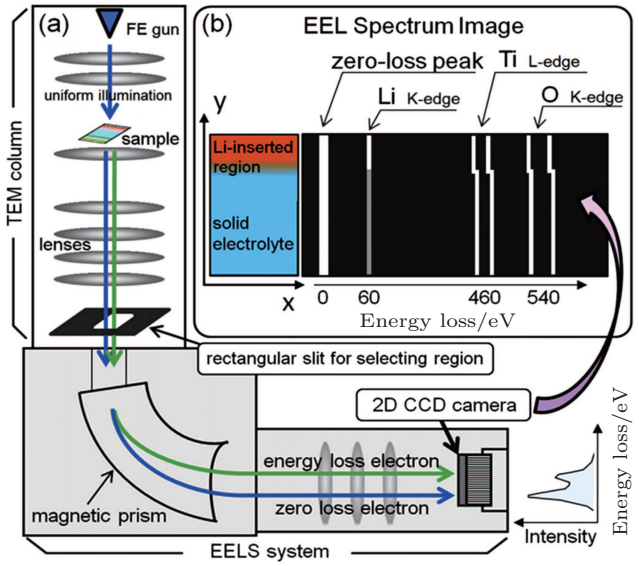


Fig. 26. Spatially resolved electron energy-loss spectroscopy in transmission electron microscopy mode (SR-TEM-EELS).[341]

Among the oxide solid state electrolytes, the perovskite and NASICON families usually have high conductivity. However, the compositions with highest conductivity of both of them contain Ti with variable valence which can be reduced. Moreover, the Li intercalation reaction is experimentally confirmed.[343,344] Therefore, when NASICON is used as solid state electrolyte, Li anode can be precipitated *in situ* opposite the cathode side by the first cycle charging, as shown in Fig. 28, and the change of Ti valence state corresponds to the electron transfer.

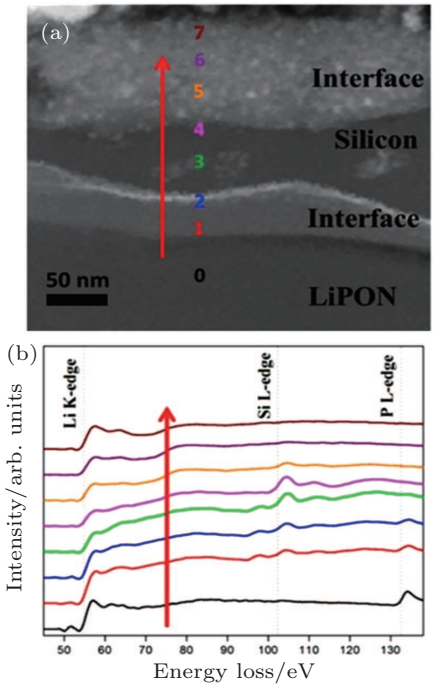


Fig. 27. Cross-sectional image of the Si/interphase/LIPON by (a) SEM and (b) EELS.[342]

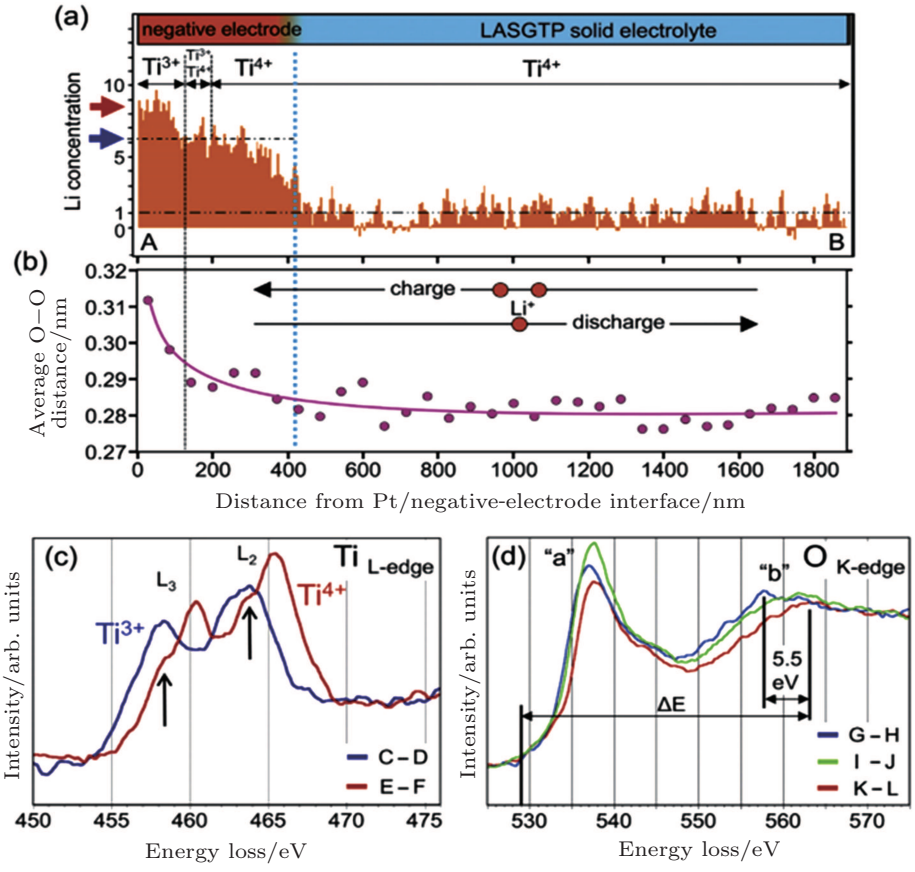


Fig. 28. Li concentration profile and its effects on Ti and O. (a) One-dimensional Li concentration profile with Ti^{4+} and Ti^{3+} regions; (b) profile of average O–O distance; (c) spectra of Ti_{L-edge}, showing the Ti^{3+} and Ti^{4+} features; (d) spectra of O-*K*-edge, both peaks "a" and "b" are shifted by the Li insertion in the negative electrode.[341]

Some sulfide solid state electrolytes, especially those containing Ge (e.g., glass-ceramics with Ge[345] and crystalline $Li_{10}GeP_2S_{12}$[132]) or Si,[100,345,346] whose reduction potentials are higher than Ti^{4+}, can even react with graphite anode.

In conclusion, the solid state electrolytes must be selected by their electrochemical windows according to the electrode materials, or different electrolytes are selected for either-side contact with anodes and electrodes, to satisfy the requirement of prohibiting reduction at the anode as well as oxidization at the cathode side.[100,132,345]

5.3.2. Solid state electrolyte/cathode interphase and space charge layer

Owing to the development of sulfide solid electrolytes, the problem related to the grain boundary is basically solved, and conductivity is no longer the restriction. At present, the greater challenge is about the interface, including: the mutual diffusion caused by the different electronegativity at either side of interface, the uncertainty of interphase structure arising from the crystal lattice mismatch, the thermal activating point/line/plane defects (including space charge layer).[348] In addition, at the time scale, the dynamic process that charge and mass transfer during the charging–discharging will result in the new problems, and at the space scale, the interface with thickness of nanometers results in "small size effect", which is categorized into nanoionics.[325,331] All mentioned above add the difficulty to the experiments and calculations.

As was first proposed by Takada research group,[349] it is the interface between the solid electrolyte and cathode, rather than the electrolyte itself that limits the high rate performance of sulfide solid electrolytes with high conductivity, and the mechanism is shown in Fig. 29. Since S in the electrolyte layer has the weaker Li ions bound ability than O in the cathode layer, Li ions at the electrolyte side of interface are depleted, resulting in the increase of resistance. Takada *et al.* found a "slope" at the start of charging in the CV measurement that is similar to the behavior of capacitors. Then they coat the cathodes with various materials (including $Li_4Ti_5O_{12}$,[349,350] $LiTaO_3$,[350] $LiNbO_3$,[350,351] and so on) and with different thicknesses, and AC conductivity is measured to affirm the positive effect by coating. In order to investigate the microscopic mechanism of the performance improvement, Takata collaborating with Haruyama[352] investigated the space charge layer effect at the $LiCoO_2/\beta$-Li_3PS_4 and $LiCoO_2/LiNbO_3/\beta$-Li_3PS_4 interfaces with density functional theory (DFT). Results indicate that along the interface, Li ions deplete at the β-Li_3PS_4 side, and accumulate at the $LiCoO_2$ side (which is a little different from the traditional opinion that Li ions accumulate in the $LiCoO_2$ bulk), giving rising to the formation of the space charge layer forms in the thermodynamic equilibrium. Now consider the dynamic process, when at the start of discharging, the space charge layer prevents Li ions from

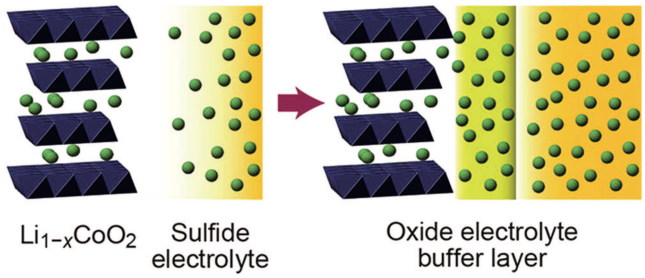


Fig. 29. Schematic of the reduction mechanism of electrode resistance at a 4 V cathode/sulfide electrolyte interface.[347]

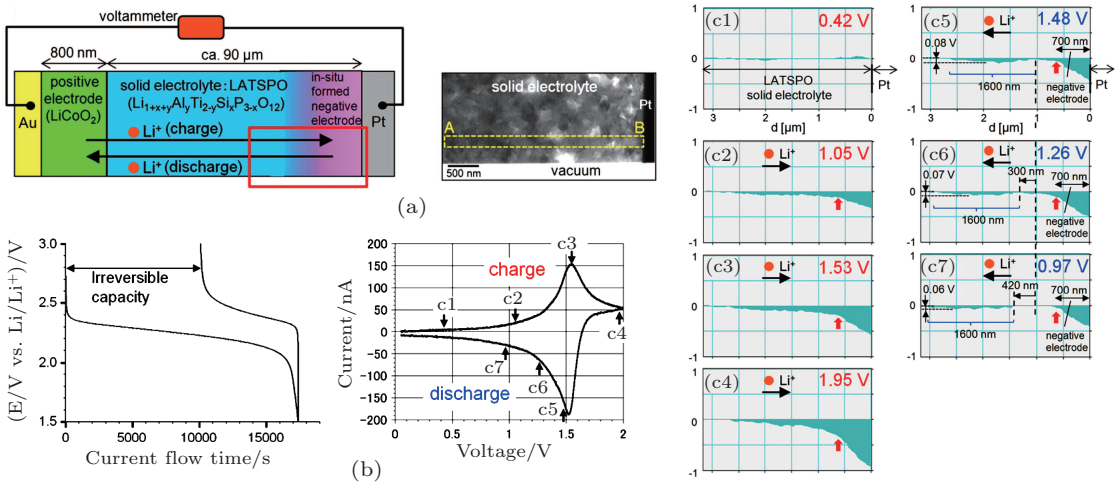


Fig. 30. (a) Preparation of the solid-state lithium battery, left: schematic illustration of the sample, and right: TEM image around the LATSPO/Pt interface; (b) macroscopic measurement of the battery reaction, left: initial Li-insertion/extraction reaction of the LATSPO/Pt half-cell at 3.0–1.5 V (versus Li/Li^+), $I = 5$ μA (electrode area: 0.785 cm^2), and right: initial cyclic volt ammogram (40 $mV{\cdot}min^{-1}$) measured in the TEM. (c) Electric potential distribution during the initial CV measurement. Panels (c1)–(c7) in the right indicate the distributions on the negative side along the line "A–B" in panel (a). The applied voltages between the current collectors correspond to the points c1–c7 indicated in the right of panel (b). Potential (V) is given on the vertical axis.[354]

intercalating into $LiCoO_2$, and makes them further collect at interface, which results in the behavior similar to capacitors. The $LiNbO_3$ buffer layer effectively mitigates the formation of a space charge layer, and restrains the capacitor behavior at the primary charging stage. However, in Ref. [352], the interface construction is oversimplified, for the structure parameters at two sides of interface vary considerably, which may lead to an intolerable difference in strains and stresses to be relaxed in some atomic layers. In fact, the interphases contain diverse forms, and can be influenced by the crystal structure, lattice parameters, and the properties of component elements.[270] Thanks to the development of advanced electron holographic techniques, the space charge layer can be directly observed, and it extends to solid state electrolyte by hundreds of nanometers, which is significantly deeper than that in traditional liquid,[353–355] as shown Fig. 30.

6. Conclusion and outlook

6.1. Material systems

At present, the material systems related to Li-ion conductors are finite. A number of them have relatively high conductivity, and even reach up to that of electrolytic solution, as shown in Figs. 1 and 2.

As for the application of solid state electrolytes in all-solid-state batteries, the film batteries with LiPON as electrolyte have good cycling performance,[6,92] although it is costly to scale up,[6,88] beyond requirements of most electrochemical energy storage devices.

Another promising system is about sulfide solid state electrolytes with the high conductivity and negligible grain boundary, even when prepared by cold pressing. The main limitation of the system is its stability to electrodes, including the (electro)chemical reaction and space charge layer problems. One effective solution is to apply different solid state electrolytes to satisfy various demands of cathodes and anodes,[100,132,345] and another is to introduce the buffer layer into the interface between the electrode and electrolyte.[349–351]

Considering the environmental safety of the fabricating process and practical applications, oxides often attract the more extensive attention. However, oxides usually have high grain boundary resistance, and the higher density with less grain boundary can only be obtained by sintering at high temperature for a long time, resulting in higher cost. Replacing the ceramic by glass or glass-ceramic is an effective and economical way to eliminate the grain boundaries.[75–78] In addition, oxides usually have higher mechanical strength, leading to the point contact with electrodes and high interface resistance. One solution is to mix the oxides and sulfides together and take advantage of both of them: low resistance of bulk and grain boundary, together with high chemical stability, and can be fabricated by cold pressing with the lower cost. In addition, the good ductility of the mixture contributes to the better physical contact with electrodes.[335] As for the NASICON and perovskite families, the compositions with highest conductivity usually contain Ti^{4+}, which is not stable to anodes with low potential.[343,344] LLZO in the garnet family has relatively high conductivity, free from Ti, resulting in good chemical stability. However, when LLZO is applied in an all-solid-state battery, the interface resistance is usually very high due to the bad physical contact and space charge layer effect. Also, another reason was proposed by a recent study, which indicates that low conductivity can arise from the formation of Li_2CO_3 in the condition of humidity.[356] If this is so, smaller bulk and more boundaries can increase the conductivity, and fine control of structure can be realized during the preparation process.[357]

For inorganic materials, the interface contact resistance is always a difficult problem. In addition, despite the higher hardness of inorganic materials, they are short of flexibility, which causes many challenges in the practical applications of full cells: How to match the volume change with electrodes during the Li ions' intercalating/deintercalating? How to match the thermal expansion arising from the increase of temperature under work? For (hybrid) electrical vehicles and other mobile devices, how to solve the ceramic fragmentation and short circuit problems ascribed to sudden shock? Considering all the problems above, organic polymers have unrivalled superiority in the aspects of flexibility and elasticity. Combining the advantages of polymers and ceramics may be the silver bullet.[266,358–361] Common polymers used today have a narrow electrochemical window and low conductivity, and the large volume fraction restricts the energy density. In contrast, liquid electrolytes (including organic electrolytic solution and ionic liquid) promise to reach higher conductivity. In addition, they may have better wettability of electrodes, and can improve the contact performance greatly by adding a relatively small amount in response to the safety problem (for organic electrolytic solution). Therefore, the composition of liquid and solid may be a further direction for research.[362]

6.2. Synthesis and characterization

For a certain material system, optimizing the composition and doping ratio is usually an important to improve conductivity. However, exploring the optimizal point in the composition phase diagram is very difficult and requires much work for a long time. The combinatorial materials science infrastructure is set up to raise the efficiency. Dahn research group in Canada used the 64-channel combinatorial electrochemical cell for high-throughput screening of materials for use as Li-ion rechargeable battery electrodes.[363] The technique was also applied to study the solid-solution $LiFe_{1-x}Mn_xPO_4$ cathodes.[364] Now, Xiaodong Xiang and Peter Schultz of Lawrence Berkeley National Lab have developed and improved the Combinatorial Material Processing to realize the simultaneous growth and characterization of thousands of compositions of novel material.[365–368] Another high-throughput

synthesis and characterization method, called the Diffusion-Multiple Approach, was developed by Jicheng Zhao of General Electric Company (GE).[369–372]

Experimental methods to investigate the diffusion mechanism can be grouped into direct measurement and indirect measurement. The former is mainly based on tracer atom detection, although all the methods employed so far, such as serial sectioning or SIMS depth profiling, are destructive and *ex situ*. Indirect methods usually give the average results of microscopic mechanism, without spatial resolution for polycrystals. The methods adopting microelectrodes or nanoelectrodes can map the full space and find the statistical relationship between conductivity and structure in various microstructures.[284] Annular bright field imaging using aberration-corrected scanning transmission electron microscopy (ABF-STEM) is the best method so far to detect Li, providing the opportunity to picture the atomic space motion. However, for the application in solid state electrolytes, difficulty occurs for the low electronic conductivity of samples, leading to e-beam damage.[342] Note that it is still questionable whether the damage can be controlled. Further, 4D ultrafast electron microscopy introduces the time dimension,[373] which becomes a new hot spot of the development of electron microscopy after ABF-STEM. This method combines the TEM in atomic resolution with ultrafast laser technologies as well as *in situ* technique and can realize the spatial resolution in pm and time resolution in ps. Scanning tunnel microscopy (STM) can be applied to *in situ* observation of Li-ion motion at the surface, as well as motion induced by electric field. If experiments can be designed for *in situ* dynamic study, it will be of great help to understand the transport mechanism. However, the problem still lies in the low electronic conductivity of sample.

6.3. Theory and calculation

From the development history of solid electrolytes, it seems that the understanding of ion diffusion mechanism may be driven by the emergence of novel materials. Ions rather than electrons become the mobile carriers, leading to the set up of defect chemistry. In order to explain the abnormal high conductivity, sublattice melting picture was introduced. In order to interpret the anomalies in experiments, such as the broadening of quasielastic spectral line, and the odd relationship between the conductivity and frequency in the high frequency region, multiple dynamic models were proposed with the consideration of many-body interaction. The ion diffusion mechanism models were continually revised with the improvement of characterization methods, although the current theoretical model cannot give the analytic solution. Therefore, it is a great challenge to build effective simplified models to balance the accuracy and time cost. In fact, the mechanisms of various systems are quite different. So the key to building rational models is to extract more effective information from experiments and characterization.

There are still important problems that cannot be solved by current experimental methods, considering the technological limits and the time and monetary cost. In contrast, along with the rapid development of computer technology and information science, theory–model–calculation-simulation has become a powerful supplement of experiments. The Materials Genome Initiative (MGI) aims at integrating the experiment, calculation and database together, among which calculation is important.[374,375] As defined by Alpaydin in 2004, machine learning is "programming computers to optimize a performance criterion using example data or past experience". With the process of machine learning, the ultimate goal of MGI is to realize the rational design of materials, including the discovery of novel materials as well as the performance optimization (e.g., interface design or size design, and so on) of existing ones. Note that when the size is reduced to nanometers, the material properties usually change abnormally due to size effects. Quantification of the size effect is influenced by the specific size and shape of materials, which adds two dimensions to the structure–performance relationship. Recently, Qian *et al.* proposed the concept of Nanomaterials Genome Initiative (NMGI) with the consideration of the size and shape dimension, as shown in Fig. 31, which provides new insight to the modulation in nanometers.[376]

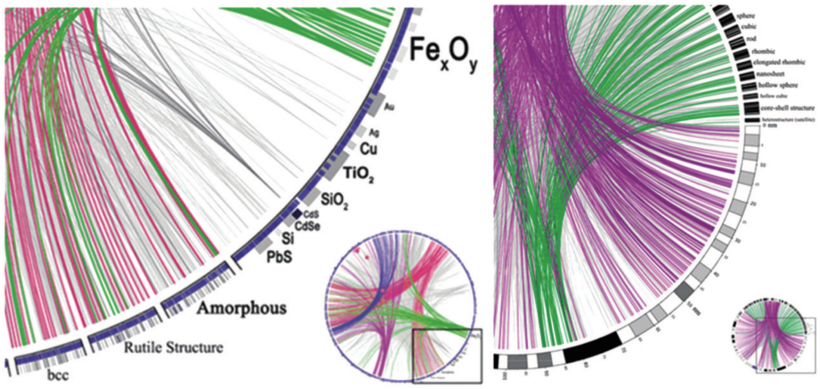


Fig. 31. Circos diagram of Nanomaterials Genome (a) composition-structure and (b) size-shape relations.[376]

References

[1] Salamon M B 1979 *Physics of Superionic Conductors* (Berlin, Heidelberg: Springer-Verlag GmbH)
[2] Dissanayake M A K L and Mellander B E 1986 *Solid State Ion.* **21** 279
[3] Shannon R D, Taylor B E, English A D and Berzins T 1977 *Electrochim. Acta* **22** 783
[4] Shi S Q, Qi Y, Li H and Hector L G 2013 *J. Phys. Chem. C* **117** 8579
[5] Shi S Q, Lu P, Liu Z Y, Qi Y, Hector L G, Li H and Harris S J 2012 *J. Am. Chem. Soc.* **134** 15476
[6] Wang B, Bates J B, Hart F X, Sales B C, Zuhr R A and Robertson J D 1996 *J. Electrochem. Soc.* **143** 3203
[7] Knauth P and Tuller H L 2002 *J. Am. Ceram. Soc.* **85** 1654
[8] Takada K 2013 *Acta Mater.* **61** 759
[9] Hagenmuller P and van Gool W 1978 *Solid Electrolytes: General Principles, Characterization, Materials, Applications* (New York, San Fransisco, London: Academic Press)
[10] Owens B B 2000 *J. Power Sources* **90** 2
[11] Thangadurai V and Weppner W 2006 *Ionics* **12** 81
[12] Faraday M 1833 *Philos. Trans. R. Soc. London* **123** 23
[13] Faraday M 1838 *Philos. Trans. R. Soc. London* **128** 83
[14] Hittorff 1851 *Annalen der Physik* **60** 1
[15] Gaugain J M 1853 *Comptes Rendus Hebdomadaires des Séances de L'Académie des Sciences* **37** 584
[16] Warburg E 1884 *Ann. Phys.* **257** 622
[17] Nernst W 1900 *Zeit. Elektrochem.* **6** 41
[18] Nernst W (*Material for Electric-Lamp Glowers*, U.S. Patent) 685730 [1901]
[19] Wagner C 1943 *Naturwissenschaften* **31** 265
[20] Haber F and Moser A 1905 *Zeitschrift für Elektrochemie und Angewandte Physikalische Chemie* **11** 593
[21] Katayama M 1907 *Zeit. Phys. Chem.* **61** 566
[22] Schottky W (*Zur Stromlieferung Geeignetes Galvanisches Element Bzw, Elementkette*, German Patent) 650224 [1937]
[23] Baur E and Preiss H 1937 *Zeitschrift für Elektrochemie* **43** 727
[24] Takahasi T, Ito K and Iwahara M 1965 *Rev. Energie Primaire, Journées Int. d'Etude des Pilesà Combustible, Bruxelles* **3** 42
[25] Tubandt C and Lorenz E 1914 *Z. Phys. Chemie* **87** 513
[26] Tubandt C and Eggert S 1920 *Zeitschrift für Anorganische und Allgemeine Chemie* **110** 196
[27] Strock L W 1935 *Z. Phys. Chem. B-Chem. E* **31** 132
[28] Joffé A 1923 *Ann. Phys.* **377** 461
[29] Frenkel J 1926 *Z. Phys.* **35** 652
[30] Wagner C and Schottky W 1930 *Z. Phys. Chem. B-Chem. E* **11** 163
[31] Wagner C 1933 *Z. Phys. Chem. B-Chem. E* **22** 181
[32] Schmalzried H and Wagner C 1962 *Fehlordnung in Ternären Ionenkristallen. Zeitschrift für Physikalische Chemie* **31** 198
[33] Kiukkola K and Wagner C 1957 *J. Electrochem. Soc.* **104** 379
[34] Bradley J N and Greene P D 1966 *Trans. Faraday Soc.* **62** 2069
[35] Takahashi T, Yamamoto O, Yamada S and Hayashi S 1979 *J. Electrochem. Soc.* **126** 1654
[36] van Gool W and Division N A T O S A 1973 *Fast ion Transport in Solids: Solid State Batteries and Devices (Proceedings of The NATO Sponsored Advanced Study Institute on Fast Ion Transport in Solids, Solid State Batteries and Devices)* (North Holland Pub. Co.)
[37] Yu Y and Kummer J T 1967 *Journal of Inorganic and Nuclear Chemistry* **29** 2453
[38] Kamaya N, Homma K, Yamakawa Y, Hirayama M, Kanno R, Yonemura M, Kamiyama T, Kato Y, Hama S, Kawamoto K and Mitsui A 2011 *Nat. Mater.* **10** 682
[39] Zintl E and Brauer G 1935 *Zeitschrift für Elektrochemie und Angewandte Physikalische Chemie* **41** 102
[40] Alpen U V, Rabenau A and Talat G H 1977 *Appl. Phys. Lett.* **30** 621
[41] Boukamp B A and Huggins R A 1976 *Phys. Lett. A* **58** 231
[42] Liang C C 1973 *J. Electrochem. Soc.* **120** 1289
[43] Wagner J B 1989 *Composite Solid Ion Conductors. High Conductivity Solid Ionic Conductors* pp. 146–165
[44] Maier J 1995 *Prog. Solid State Chem.* **23** 171
[45] Schneider A A, Harney D E and Harney M J 1980 *J. Power Sources* **5** 15
[46] Hartwig P, Rabenau A and Weppner W 1981 *J. Less-Common. Met.* **78** 227
[47] Poulsen F W 1981 *Solid State Ion.* **2** 53
[48] Andersen N H, Kjems J K and Poulsen F W 1982 *Phys. Scripta* **25** 780
[49] Nakamura O and Goodenough J B 1982 *Solid State Ion.* **7** 119
[50] Matsuo M, Nakamori Y, Orimo S, Maekawa H and Takamura H 2007 *Appl. Phys. Lett.* **91** 224103
[51] Epp V and Wilkening M 2010 *Phys. Rev. B* **82** 020301(R)
[52] Maekawa H, Matsuo M, Takamura H, Ando M, Noda Y, Karahashi T and Orimo S I 2009 *J. Am. Chem. Soc.* **131** 894
[53] Pizzini S 1971 *J. Appl. Electrochem.* **1** 153
[54] West A R 1973 *J. Appl. Electrochem.* **3** 327
[55] Goodenough J B, Hong H Y P and Kafalas J A 1976 *Mater. Res. Bull.* **11** 203
[56] Hong H Y P 1976 *Mater. Res. Bull.* **11** 173
[57] Taylor B E, English A D and Berzins T 1977 *Mater. Res. Bull.* **12** 171
[58] Thangadurai V and Weppner W 2002 *Ionics* **8** 281
[59] Cretin M and Fabry P 1999 *J. Eur. Ceram. Soc.* **19** 2931
[60] Anantharamulu N, Rao K K, Rambabu G, Kumar B V, Radha V and Vithal M 2011 *J. Mater. Sci.* **46** 2821
[61] Lin Z X, Yu H J, Li S C and Tian S B 1986 *Solid State Ion.* **18–19** 549
[62] Lin Z X and Tian S B 1983 *Solid State Ion.* **9–10** 809
[63] Subramanian M A, Subramanian R and Clearfield A 1986 *Solid State Ion.* **18–19** 562
[64] Sobiestianskas R, Dindune A, Kanepe Z, Ronis J, Kezionis A, Kazakevicius E and Orliukas A 2000 *Mat. Sci. Eng. B-Solid* **76** 184
[65] Aono H, Sugimoto E, Sadaoka Y, Imanaka N and Adachi G Y 1990 *J. Electrochem. Soc.* **137** 1023
[66] Aono H, Sugimoto E, Sadaoka Y, Imanaka N and Adachi G Y 1989 *J. Electrochem. Soc.* **136** 590
[67] Bounar N, Benabbas A, Bouremmad F, Ropa P and Carru J C 2012 *Physica B* **407** 403
[68] Stenina I A, Kislitsyn M N, Pinus I Y, Haile S M and Yaroslavtsev A B 2006 *Defect and Diffusion Forum* **249** 255
[69] Li S C, Cai J Y and Lin Z X 1988 *Solid State Ion.* **28–30** Part 2 1265
[70] Aono H, Sugimoto E, Sadaoka Y, Imanaka N and Adachi G Y 1992 *Bull. Chem. Soc. Jpn.* **65** 2200
[71] Paris M A, MartinezJuarez A, Iglesias J E, Rojo J M and Sanz J 1997 *Chem. Mater.* **9** 1430
[72] Aono H, Sugimoto E, Sadaoka Y, Imanaka N and Adachi G Y 1993 *Solid State Ion.* **62** 309
[73] Chowdari B V R, Radhakrishnan K, Thomas K A and Rao G V S 1989 *Mater. Res. Bull.* **24** 221
[74] Aono H, Sugimoto E, Sadaoka Y, Imanaka N and Adachi G 1991 *Solid State Ion.* **47** 257
[75] Hosono H and Abe Y 1991 *Solid State Ion.* **44** 293
[76] Fu J 1997 *Solid State Ion.* **96** 195
[77] Leo C J, Chowdari B V R, Rao G V S and Souquet J L 2002 *Mater. Res. Bull.* **37** 1419
[78] Bucheli W, Arbi K, Sanz J, Nuzhnyy D, Kamba S, Varez A and Jimenez R 2014 *Phys. Chem. Chem. Phys.* **16** 15346
[79] Hong H Y P 1978 *Mater. Res. Bull.* **13** 117
[80] Bruce P G and West A R 1980 *Mater. Res. Bull.* **15** 379
[81] Rodger A R, Kuwano J and West A R 1985 *Solid State Ion.* **15** 185
[82] Fujimura K, Seko A, Koyama Y, Kuwabara A, Kishida I, Shitara K, Fisher C A J, Moriwake H and Tanaka I 2013 *Adv. Energy Mater.* **3** 980
[83] Kanehori K, Matsumoto K, Miyauchi K and Kudo T 1983 *Solid State Ion.* **9–10** Part 2 1445
[84] Miyauchi K, Matsumoto K, Kanehori K and Kudo T 1983 *Solid State Ion.* **9–10** Part 2 1469
[85] Wang B, Chakoumakos B C, Sales B C, Kwak B S and Bates J B 1995 *J. Solid State Chem.* **115** 313
[86] Bates J B, Dudney N J, Gruzalski G R, Zuhr R A, Choudhury A, Luck C F and Robertson J D 1993 *J. Power Sources* **43** 103
[87] Bates J B, Dudney N J, Lubben D C, Gruzalski G R, Kwak B S, Yu X and Zuhr R A 1995 *J. Power Sources* **54** 58
[88] Bates J B, Dudney N J, Neudecker B, Ueda A and Evans C D 2000 *Solid State Ion.* **135** 33
[89] Neudecker B J, Zuhr R A and Bates J B 1999 *J. Power Sources* **81–82** 27
[90] Neudecker B J, Dudney N J and Bates J B 2000 *J. Electrochem. Soc.* **147** 517
[91] Yu X, Bates J B, Jellison G E and Hart F X 1997 *J. Electrochem. Soc.* **144** 524
[92] Li J, Ma C, Chi M, Liang C and Dudney N J 2014 *Adv. Energy Mater.*

[93] Senevirathne K, Day C S, Gross M D, Lachgar A and Holzwarth N A W 2013 *Solid State Ion.* **233** 95
[94] Ribes M, Barrau B and Souquet J L 1980 *J. Non-Cryst. Solids* **38–39** Part 1 271
[95] Mercier R, Malugani J P, Fahys B and Robert G 1981 *Solid State Ion.* **5** 663
[96] Wada H, Menetrier M, Levasseur A and Hagenmuller P 1983 *Mater. Res. Bull.* **18** 189
[97] Kennedy J H, Sahami S, Shea S W and Zhang Z 1986 *Solid State Ion.* **18–19** Part 1 368
[98] Pradel A and Ribes M 1986 *Solid State Ion.* **18–19** Part 1 351
[99] Machida N, Maeda H, Peng H and Shigematsu T 2002 *J. Electrochem. Soc.* **149** A688
[100] Takada K, Nakano S, Inada T, Kajiyama A, Sasaki H, Kondo S and Watanabe M 2003 *J. Electrochem. Soc.* **150** A274
[101] Aotani N, Iwamoto K, Takada K and Kondo S 1994 *Solid State Ion.* **68** 35
[102] Hayashi A, Yamashita H, Tatsumisago M and Minami T 2002 *Solid State Ion.* **148** 381
[103] Iwamoto K, Aotani N, Takada K and Kondo S 1995 *Solid State Ion.* **79** 288
[104] Takada K, Aotani N, Iwamoto K and Kondo S 1996 *Solid State Ion.* **86–88** Part 2 877
[105] Komiya R, Hayashi A, Morimoto H, Tatsumisago M and Minami T 2001 *Solid State Ion.* **140** 83
[106] Mercier R, Malugani J P, Fahys B, Douglade J and Robert G 1982 *J. Solid State Chem.* **43** 151
[107] Mercier R, Malugani J P, Fahys B, Robert G and Douglade J 1982 *Acta Crystallogr. B* **38** 1887
[108] Tachez M, Malugani J P, Mercier R and Robert G 1984 *Solid State Ion.* **14** 181
[109] Kanno R, Hata T, Kawamoto Y and Irie M 2000 *Solid State Ion.* **130** 97
[110] Kanno R and Maruyama M 2001 *J. Electrochem. Soc.* **148** A742
[111] Murayama M, Kanno R, Kawamoto Y and Kamiyama T 2002 *Solid State Ion.* **154–155** 789
[112] Murayama M, Kanno R, Irie M, Ito S, Hata T, Sonoyama N and Kawamoto Y 2002 *J. Solid State Chem.* **168** 140
[113] Kobayashi T, Imade Y, Shishihara D, Homma K, Nagao M, Watanabe R, Yokoi T, Yamada A, Kanno R and Tatsumi T 2008 *J. Power Sources* **182** 621
[114] Ohta N, Takada K, Osada M, Zhang L Q, Sasaki T and Watanabe M 2005 *J. Power Sources* **146** 707
[115] Homma K, Yonemura M, Kobayashi T, Nagao M, Hirayama M and Kanno R 2011 *Solid State Ion.* **182** 53
[116] Gobet M, Greenbaum S, Sahu G and Liang C D 2014 *Chem. Mater.* **26** 3558
[117] Liu Z C, Fu W J, Payzant E A, Yu X, Wu Z L, Dudney N J, Kiggans J, Hong K L, Rondinone A J and Liang C D 2013 *J. Am. Chem. Soc.* **135** 975
[118] Inada T, Kobayashi T, Sonoyama N, Yamada A, Kondo S, Nagao M and Kanno R 2009 *J. Power Sources* **194** 1085
[119] Matsumura T, Nakano K, Kanno R, Hirano A, Imanishi N and Takeda Y 2007 *J. Power Sources* **174** 632
[120] Hayashi A, Ishikawa Y, Hama S, Minami T and Tatsumisago M 2003 *Electrochem. Solid St.* **6** A47
[121] Hayashi A, Hama S, Minami T and Tatsumisago M 2003 *Electrochem. Commun.* **5** 111
[122] Mizuno F, Hayashi A, Tadanaga K and Tatsumisago M 2005 *Electrochem. Solid St.* **8** A603
[123] Mizuno F, Hayashi A, Tadanaga K and Tatsumisago M 2005 *Adv. Mater.* **17** 918
[124] Mizuno F, Hayashi A, Tadanaga K and Tatsumisago M 2006 *Solid State Ion.* **177** 2721
[125] Hayashi A, Minami K and Tatsumisago M 2010 *J. Solid State Electr.* **14** 1761
[126] Seino Y, Takada K, Kim B C, Zhang L, Ohta N, Wada H, Osada M and Sasaki T 2005 *Solid State Ion.* **176** 2389
[127] Sur U K 2011 *Curr. Sci.* **101** 1129
[128] Kato Y, Kawamoto K, Kanno R and Hirayama M 2012 *Electrochemistry* **80** 749
[129] Whiteley J M, Woo J H, Hu E, Nam K W and Lee S H 2014 *J. Electrochem. Soc.* **161** A1812
[130] Hassoun J, Verrelli R, Reale P, Panero S, Mariotto G, Greenbaum S and Scrosati B 2013 *J. Power Sources* **229** 117
[131] Mo Y, Ong S P and Ceder G 2012 *Chem. Mater.* **24** 15
[132] Shin B R, Nam Y J, Oh D Y, Kim D H, Kim J W and Jung Y S 2014 *Electrochim. Acta* **146** 395
[133] Kuhn A, Koehler J and Lotsch B V 2013 *Phys. Chem. Chem. Phys.* **15** 11620
[134] Du F, Ren X, Yang J, Liu J and Zhang W 2014 *J. Phys. Chem. C* **118** 10590
[135] Adams S and Rao R P 2012 *J. Mater. Chem.* **22** 7687
[136] Xu M, Ding J and Ma E 2012 *Appl. Phys. Lett.* **101** 031901
[137] Hu C H, Wang Z Q, Sun Z Y and Ouyang C Y 2014 *Chem. Phys. Lett.* **591** 16
[138] Bron P, Johansson S, Zick K, auf der Guenne J S, Dehnen S and Roling B 2013 *J. Am. Chem. Soc.* **135** 15694
[139] Nishino S, Fujiwara T and Yamasaki H 2014 *Phys. Rev. B* **90** 024303
[140] Kwon O, Hirayama M, Suzuki K, Kato Y, Saito T, Yonemura M, Kamiyama T and Kanno R 2015 *J. Mater. Chem. A* **3** 438
[141] Ong S P, Mo Y, Richards W D, Miara L, Lee H S and Ceder G 2013 *Energy Environmental Science* **6** 148
[142] Kato Y, Saito R, Sakano M, Mitsui A, Hirayama M and Kanno R 2014 *J. Power Sources* **271** 60
[143] Kuhn A, Gerbig O, Zhu C, Falkenberg F, Maier J and Lotsch B V 2014 *Phys. Chem. Chem. Phys.* **16** 14669
[144] Wang Z Q, Wu M S, Liu G, Lei X L, Xu B and Ouyang C Y 2014 *Int. J. Electrochem. Sci.* **9** 562
[145] Latie L, Villeneuve G, Conte D and Leflem G 1984 *J. Solid State Chem.* **51** 293
[146] Inaguma Y, Chen L Q, Itoh M, Nakamura T, Uchida T, Ikuta H and Wakihara M 1993 *Solid State Commun.* **86** 689
[147] Inaguma Y, Chen L Q, Itoh M and Nakamura T 1994 *Solid State Ion.* **70–71** Part 1 196
[148] Itoh M, Inaguma Y, Jung W H, Chen L Q and Nakamura T 1994 *Solid State Ion.* **70–71** Part 1 203
[149] Inaguma Y, Matsui Y, Shan Y J, Itoh M and Nakamura T 1995 *Solid State Ion.* **79** 91
[150] Inaguma Y and Itoh M 1996 *Solid State Ion.* **86–88** 257
[151] Katsumata T, Matsui Y, Inaguma Y and Itoh M 1996 *Solid State Ion.* **86–88** 165
[152] Yashima M, Itoh M, Inaguma Y and Morii Y 2005 *J. Am. Chem. Soc.* **127** 3491
[153] Emery J, Buzare J Y, Bohnke O and Fourquet J L 1997 *Solid State Ion.* **99** 41
[154] Jay E E, Rushton M J D, Chroneos A, Grimes R W and Kilner J A 2015 *Phys. Chem. Chem. Phys.* **17** 178
[155] Inaguma Y, Seo A and Katsumata T 2004 *Solid State Ion.* **174** 19
[156] Bohnke O 2008 *Solid State Ion.* **179** 9
[157] Mazza D 1988 *Mater. Lett.* **7** 205
[158] Thangadurai V, Kaack H and Weppner W J F 2003 *J. Am. Ceram. Soc.* **86** 437
[159] Narayanan S, Ramezanipour F and Thangadurai V 2012 *J. Phys. Chem. C* **116** 20154
[160] Thangadurai V, Adams S and Weppner W 2004 *Chem. Mater.* **16** 2998
[161] Cussen E J 2006 *Chem. Commun.* 412
[162] van Wullen L, Echelmeyer T, Meyer H W and Wilmer D 2007 *Phys. Chem. Chem. Phys.* **9** 3298
[163] Han J T, Zhu J L, Li Y T, Yu X H, Wang S M, Wu G, Xie H, Vogel S C, Izumi F, Momma K, Kawamura Y, Huang Y, Goodenough J B and Zhao Y S 2012 *Chem. Commun.* **48** 9840
[164] Xu M, Park M S, Lee J M, Kim T Y, Park Y S and Ma E 2012 *Phys. Rev. B* **85** 052301
[165] Bernstein N, Johannes M D and Hoang K 2012 *Phys. Rev. Lett.* **109** 109
[166] Jalem R, Yamamoto Y, Shiiba H, Nakayama M, Munakata H, Kasuga T and Kanamura K 2013 *Chem. Mater.* **25** 425
[167] Wang X P, Gao Y X, Xia Y P, Zhuang Z, Zhang T and Fang Q F 2014 *Phys. Chem. Chem. Phys.* **16** 7006
[168] Meier K, Laino T and Curioni A 2014 *J. Phys. Chem. C* **118** 6668
[169] Santosh K C, Longo R C, Xiong K and Cho K 2014 *Solid State Ion.* **261** 100
[170] Zheng Z, Fang H, Yang F, Liu Z K and Wang Y 2014 *J. Electrochem. Soc.* **161** A473

[171] Ribeiro J F, Sousa R, Carmo J P, Gonçalves L M, Silva M F, Silva M M and Correia J H 2012 *Thin Solid Films* **522** 85
[172] Reinacher J, Berendts S and Janek J 2014 *Solid State Ion.* **258** 1
[173] Ohta S, Kobayashi T and Asaoka T 2011 *J. Power Sources* **196** 3342
[174] Murugan R, Thangadurai V and Weppner W 2007 *Angew. Chem.-Int. Edit.* **46** 7778
[175] Shimonishi Y, Toda A, Zhang T, Hirano A, Imanishi N, Yamamoto O and Takeda Y 2011 *Solid State Ion.* **183** 48
[176] Jin Y and McGinn P J 2011 *J. Power Sources* **196** 8683
[177] Bernstein N, Johannes M D and Hoang K 2012 *Phys. Rev. Lett.* **109** 205702
[178] Xie H, Alonso J A, Li Y, Fernández-Díaz M T and Goodenough J B 2011 *Chem. Mater.* **23** 3587
[179] Teng S, Tan J J and Tiwari A 2014 *Curr. Opin. Solid St. M* **18** 29
[180] Kim S, Hirayama M, Taminato S and Kanno R 2013 *Dalton Trans.* **42** 13112
[181] Ahn C W, Choi J J, Ryu J, Hahn B D, Kim J W, Yoon W H, Choi J H and Park D S 2015 *J. Electrochem. Soc.* **162** A60
[182] Djenadic R, Botros M, Benel C, Clemens O, Indris S, Choudhary A, Bergfeldt T and Hahn H 2014 *Solid State Ion.* **263** 49
[183] Jin Y and McGinn P J 2013 *J. Power Sources* **239** 326
[184] Kato T, Hamanaka T, Yamamoto K, Hirayama T, Sagane F, Motoyama M and Iriyama Y 2014 *J. Power Sources* **260** 292
[185] Zhao Y S and Daemen L L 2012 *J. Am. Chem. Soc.* **134** 15042
[186] Reckeweg O, Blaschkowski B and Schleid T 2012 *Zeitschrift für Anorganische und Allgemeine Chemie* **638** 2081
[187] Emly A, Kioupakis E and van der Ven A 2013 *Chem. Mater.* **25** 4663
[188] Mouta R, Melo M Á B, Diniz E M and Paschoal C W A 2014 *Chem. Mater.* **26** 7137
[189] Mouta R, Silva R X and Paschoal C W A 2013 *Acta Crystallogr. B* **69** 439
[190] Zhang Y, Zhao Y S and Chen C F 2013 *Phys. Rev. B* **87** 134303
[191] Braga M H, Ferreira J A, Stockhausen V, Oliveira J E and El-Azab A 2014 *J. Mater. Chem. A* **2** 5470
[192] Schroeder D J, Hubaud A A and Vaughey J T 2014 *Mater. Res. Bull.* **49** 614
[193] Funke K 2013 *Sci. Technol. Adv. Mater.* **14** 043502
[194] Funke K, Cramer C and Wilmer D 2005 *Concept of Mismatch and Relaxation for Self-Diffusion and Conduction in Ionic Materials with Disordered Structures*, in: Heitjans P and Kärger J eds., *Diffusion in Condensed Matter* (The Netherlands: Springer) p. 857
[195] Kim S, Yamaguchi S and Elliott J A 2009 *MRS Bull.* **34** 900
[196] Casciola M, Costantino U, Merlini L, Andersen I G K and Andersen E K 1988 *Solid State Ion.* **26** 229
[197] Johnston W V, Wiedersi H and Lindberg G W 1969 *J. Chem. Phys.* **51** 3739
[198] Pardee W J and Mahan G D 1974 *J. Chem. Phys.* **61** 2173
[199] Lederman F L, Salamon M B and Peisl H 1976 *Solid State Commun.* **19** 147
[200] Graham L J and Chang R 1975 *J. Appl. Phys.* **46** 2433
[201] Nagao M and Kaneda T 1975 *Phys. Rev. B* **11** 2711
[202] Leung K M and Huber D L 1979 *Phys. Rev. Lett.* **42** 452
[203] Mehrer H 2007 *Diffusion in Solids: Fundamentals, Methods, Materials, Diffusion-Controlled Processes* (Berlin, Heidelberg: Springer)
[204] Heitjans P and Indris S 2003 *J. Phys.: Condens. Matter* **15** R1257
[205] Murch G E 2005 *Diffusion Kinetics in Solids, Phase Transformations in Materials* (Berlin, Heidelberg: Wiley-VCH Verlag GmbH & Co. KGaA) p. 171
[206] Barber M N and Ninham B W 1970 *Random and Restricted Walks: Theory and Applications* (New York, London, Paris: Gordon and Breach)
[207] Weiss G H 1994 *Aspects and Applications of the Random Walk* (North-Holland: North-Holland)
[208] van Kampen N G 2011 *Stochastic Processes in Physics and Chemistry* (Netherlands: Elsevier Science)
[209] Spitzer F 2001 *Principles of Random Walk* (New York: Springer)
[210] Spohn H 2011 *Large Scale Dynamics of Interacting Particles* (Berlin, Heidelberg: Springer)
[211] Kingery W 2013 *Introduction to Ceramics* (John Wiley & Sons)
[212] Shin H C and Pyun S I 2001 *Electrochim. Acta* **46** 2477
[213] Tang S B, Lai M O and Lu L 2008 *J. Alloy. Compd.* **449** 300
[214] Striebel K A, Deng C Z, Wen S J and Cairns E J 1996 *J. Electrochem. Soc.* **143** 1821
[215] Julien C, Camacho-Lopez M A, Escobar-Alarcon L and Haro-Poniatowski E 2001 *Mater. Chem. Phys.* **68** 210
[216] Bouwman P J, Boukamp B A, Bouwmeester H J M and Notten P H L 2002 *J. Electrochem. Soc.* **149** A699
[217] Jang Y I, Neudecker B J and Dudney N J 2001 *Electrochem. Solid-State Lett.* **4** A74
[218] Xia H, Lu L and Ceder G 2006 *J. Power Sources* **159** 1422
[219] Iriyama Y, Inaba M, Abe T and Ogumi Z 2001 *J. Power Sources* **94** 175
[220] Xie J, Imanishi N, Matsumura T, Hirano A, Takeda Y and Yamamoto O 2008 *Solid State Ion.* **179** 362
[221] Murch G E 1982 *Solid State Ion.* **7** 177
[222] Sato H 1977 *Some Theoretical Aspects of Solid Electrolytes*, in: Geller S ed., *Solid Electrolytes*, Vol. 21 (Berlin, Heidelberg: Springer) p. 3
[223] Kehr K, Mussawisade K, Schütz G and Wichmann T 2005 *Diffusion of Particles on Lattices*, in: Heitjans P and Kärger J eds., *Diffusion in Condensed Matter* (The Netherlands: Springer)
[224] Haus J W and Kehr K W 1987 *Phys. Rep.* **150** 263
[225] Kutner R and Sosnowska I 1977 *J. Phys. Chem. Solids* **38** 741
[226] Kehr K W, Richter D and Swendsen R H 1978 *J. Phys. F: Met. Phys.* **8** 433
[227] Anderson I S, Heidemann A, Bonnet J E, Ross D K, Wilson S K P and Mckergow M W 1984 *J. Less-Common Met.* **101** 405
[228] Spitzer F 1970 *Adv. Math.* **5** 246
[229] Liggett T M 1999 *Stochastic Interacting Systems: Contact, Voter and Exclusion Processes*, Vol. 324 (Berlin, Heidelberg, New York, Barcelona, Hong Kong, Milan, Paris, Singapore, Tokyo: Springer Science & Business Media)
[230] Bunde A, Dieterich W, Maass P and Meyer M 2005 *Ionic Transport in Disordered Materials*, in: Heitjans P and Kärger J eds., *Diffusion in Condensed Matter* (The Netherlands: Springer) p. 813
[231] Ngai K L and Kanert O 1992 *Solid State Ion.* **53–56** 936
[232] Funke K and Hermeling J 1987 *J. Electrochem. Soc.* **134** C511
[233] Funke K and Riess I 1984 *Z Phys. Chem. Neue. Fol.* **140** 217
[234] Elliott S R and Owens A P 1991 *Phys. Rev. B* **44** 47
[235] van Hove L 1954 *Phys. Rev.* **95** 249
[236] Bloembergen N, Purcell E M and Pound R V 1948 *Phys. Rev.* **73** 679
[237] Gobel E, Mullerwarmuth W, Olyschlager H and Dutz H 1979 *J. Magn. Reson.* **36** 371
[238] Knodler D, Pendzig P and Dieterich W 1996 *Solid State Ion.* **86–88** 29
[239] Funke K 1993 *Prog. Solid State Chem.* **22** 111
[240] Huberman B A and Sen P N 1974 *Phys. Rev. Lett.* **33** 1379
[241] Fulde P, Pietronero L, Schneider W R and Strassler S 1975 *Phys. Rev. Lett.* **35** 1776
[242] Mori H 1965 *Prog. Theor. Phys.* **33** 423
[243] Kramers H A 1940 *Physica* **7** 284
[244] Wert C A 1950 *Phys. Rev.* **79** 601
[245] Ivanchen Y and Zilberma L 1969 *Sov. Phys. Jetp.-Ussr* **28** 1272
[246] Ambegaokar V and Halperin B I 1969 *Phys. Rev. Lett.* **22** 1364
[247] Bruesch P, Strassler S and Zeller H R 1975 *Phys. Status Solidi A* **31** 217
[248] Mahan G D and Roth W L 1976 *Superionic Conductors* (New York, London: Plenum Press)
[249] Bruesch P, Pietronero L and Zeller H R 1976 *J. Phys. C-Solid State* **9** 3977
[250] Bruesch P, Pietronero L, Strassler S and Zeller H R 1977 *Phys. Rev. B* **15** 4631
[251] Bruesch P, Pietronero L, Strassler S and Zeller H R 1977 *Electrochim. Acta* **22** 717
[252] Sen P N and Huberman B A 1975 *Phys. Rev. Lett.* **34** 1059
[253] Lammert H, Kunow M and Heuer A 2003 *Phys. Rev. Lett.* **90** 215901
[254] Habasaki J and Hiwatari Y 2004 *Phys. Rev. B* **69** 144207
[255] Vogel M 2004 *Phys. Rev. B* **70** 094302
[256] Maass P, Petersen J, Bunde A, Dieterich W and Roman H E 1991 *Phys. Rev. Lett.* **66** 52
[257] Meyer M, Maass P and Bunde A 1993 *Phys. Rev. Lett.* **71** 573
[258] Maass P, Meyer M and Bunde A 1995 *Phys. Rev. B* **51** 8164
[259] Petersen J and Dieterich W 1992 *Philos. Mag. B* **65** 231
[260] Maass P, Meyer M, Bunde A and Dieterich W 1996 *Phys. Rev. Lett.* **77** 1528

[261] Bunde A and Kantelhardt J 2005 *Diffusion and Conduction in Percolation Systems*, in: Heitjans P and Kärger J eds., *Diffusion in Condensed Matter* (The Netherlands: Springer) p. 895

[262] Havlin S, Bunde A, Bunde A and Havlin S 1991 *Fractals and Disordered Systems* (Berlin, Heidelberg, New York: Springer)

[263] Stauffer D and Aharony A 1994 *Introduction to Percolation Theory* (Florida: CRC Press)

[264] Aharony A and Stauffer D 2003 *Introduction to Percolation Theory* (London, Philadelphia: Taylor & Francis)

[265] Stanley H E 1996 *Fractals and Multifractals: The Interplay of Physics and Geometry*, in: Bunde A and Havlin S eds., *Fractals and Disordered Systems* (Berlin Heidelberg: Springer) p. 1

[266] Agrawal R C and Gupta R K 1999 *J. Mater. Sci.* **34** 1131

[267] Maier J 1987 *Solid State Ion.* **23** 59

[268] Maier J 1995 *Solid State Ion.* **75** 139

[269] Maier J 1995 *Prog. Solid State Chem.* **23** 171

[270] Roman H E 1990 *J. Phys.: Condens. Matter* **2** 3909

[271] Roling B and Murugavel S 2005 Bulk and Interfacial Ionic Conduction in $LiAlSiO_4$ Glass Ceramics Containing Nano- and Microcrystallites *Zeitschrift für Physikalische Chemie/International Journal of Research in Physical Chemistry and Chemical Physics* (Vol. 219) p. 23

[272] Roman H E, Bunde A and Dieterich W 1986 *Phys. Rev. B* **34** 3439

[273] Blender R and Dieterich W 1987 *J. Phys. C: Solid State Phys.* **20** 6113

[274] Indris S, Heitjans P, Roman H E and Bunde A 2000 *Phys. Rev. Lett.* **84** 2889

[275] Sakai V G 2013 *Quasi-Elastic Neutron Scattering*

[276] Strobl M, Manke I, Kardjilov N, Hilger A, Dawson M and Banhart J 2009 *J. Phys. D: Appl. Phys.* **42** 243001

[277] Yamada A and Yashima M 2009 *J. Crystallogr. Soc. Jpn.* **51** 175

[278] Heitjans P 1986 *Solid State Ion.* **18–19** 50

[279] Mehrer H 2005 *Diffusion: Introduction and Case Studies in Metals and Binary Alloys*, in: Heitjans P and Kärger J eds., *Diffusion in Condensed Matter* (The Netherlands: Springer) p. 3

[280] Kärger J and Stallmach F 2005 *PFG NMR Studies of Anomalous Diffusion*, in: Heitjans P and Kärger J eds., *Diffusion in Condensed Matter* (The Netherlands: Springer Berlin Heidelberg) p. 417

[281] Barsoukov E and Macdonald J R 2005 *Impedance Spectroscopy: Theory, Experiment, and Applications* (Hoboken: Wiley)

[282] Fleig J, Rahmati B, Rodewald S and Maier J 2010 *J. Eur. Ceram. Soc.* **30** 215

[283] Louie M W, Hightower A and Haile S M 2010 *Acs Nano* **4** 2811

[284] Fleig J and Maier J 1999 *Phys. Chem. Chem. Phys.* **1** 3315

[285] Lee W, Prinz F B, Chen X, Nonnenmann S, Bonnell D A and O'Hayre R P 2012 *MRS Bull.* **37** 659

[286] Read P L and Katz E 1960 *Phys. Rev. Lett.* **5** 466

[287] Kaneda T and Mizuki E 1972 *Phys. Rev. Lett.* **29** 937

[288] Liou Y J, Hudson R A, Wonnell S K and Slifkin L M 1990 *Phys. Rev. B* **41** 10481

[289] Stuhrmann C H J, Kreiterling H and Funke K 2002 *Solid State Ion.* **154–155** 109

[290] Schatz G and Weidinger A 1996 *Nuclear Condensed Matter Physics: Nuclear Methods and Applications* (University of Michigan: Wiley)

[291] Heitjans P, Schirmer A and Indris S 2005 *NMR and β-NMR Studies of Diffusion in Interface-Dominated and Disordered Solids*, in: Heitjans P and Kärger J eds., *Diffusion in Condensed Matter* (The Netherlands: Springer) p. 367

[292] Holz M 2005 *Field-Assisted Diffusion Studied by Electrophoretic NMR*, in: Heitjans P and Kärger J eds., *Diffusion in Condensed Matter* (The Netherlands: Springer) p. 717

[293] Vogl G and Sepiol B 2005 *The Elementary Diffusion Step in Metals Studied by the Interference of Gamma-Rays, X-Rays and Neutrons*, in: Heitjans P and Kärger J eds., *Diffusion in Condensed Matter* (The Netherlands: Springer) p. 65

[294] Springer T and Lechner R 2005 *Diffusion Studies of Solids by Quasielastic Neutron Scattering*, in: Heitjans P and Kärger J eds., *Diffusion in Condensed Matter* (The Netherlands: Springer) p. 93

[295] Kuhn A, Duppel V and Lotsch B V 2013 *Energy & Environmental Science* **6** 3548

[296] Stockmann H J 1989 *J. Phys.: Condens. Matter* **1** 5101

[297] Borgs P, Kehr K W and Heitjans P 1995 *Phys. Rev. B* **52** 6668

[298] Funke K 1997 *Solid State Ion.* **94** 27

[299] Gao J, Chu G, He M, Zhang S, Xiao R, Li H and Chen L 2014 *Sci. China Phys. Mech. Astron.* **57** 1526

[300] Wang Y, Richards W D, Ong S P, Miara L J, Kim J C, Mo Y and Ceder G 2015 *Nat. Mater.* **14** 1026

[301] Maier J 2014 *Chem. Mater.* **26** 348

[302] Kawamura J, Asayama R, Kuwata N and Kamishima O 2006 *Physics of Solid State Ionics,* Sakuma T and Takahashi H eds., ISBN: 81-308-0070-5 pp. 193–246

[303] Takahashi H 2006 *Physics of Solid State Ionics,* Sakuma T and Takahashi H eds., ISBN: 81-308-0070-5 pp. 303–321

[304] Adam G and Gibbs J H 1965 *J. Chem. Phys.* **43** 139

[305] Cohen M H and Turnbull D 1959 *J. Chem. Phys.* **31** 1164

[306] Turnbull D and Cohen M H 1970 *J. Chem. Phys.* **52** 3038

[307] Macedo P and Litovitz T 1965 *J. Chem. Phys.* **42** 245

[308] Miyamoto T and Shibayama K 1973 *J. Appl. Phys.* **44** 5372

[309] Watanabe M, Sanui K, Ogata N, Kobayashi T and Ohtaki Z 1985 *J. Appl. Phys.* **57** 123

[310] Souquet J L, Levy M and Duclot M 1994 *Solid State Ion.* **70–71** 337

[311] Souquet J L, Duclot M and Levy M 1998 *Solid State Ion.* **105** 237

[312] Angell C A 1989 *Phnomenology of Fast Ion Conducting Glasses: Fast and Confusions. High Conductivity Solid Ionic Conductors* pp. 89–113

[313] Angell C 1983 *Solid State Ion.* **9–10** 3

[314] Angell C A 1986 *Solid State Ion.* **18–19** Part 1 72

[315] Zhang S, Chang Z, Xu K and Angell C A 2000 *Electrochim. Acta* **45** 1229

[316] Angell C 1992 *Annual Rev. Phys. Chem.* **43** 693

[317] Varshneya A K 1993 *Fundamentals of Inorganic Glasses* (United Kingdom: Elsevier)

[318] Rawson H 1967 *Inorganic Glass-Forming Systems*, Vol. 2 (London: Academic Press)

[319] Bunde A, Maass P, Roman H, Dieterich W and Petersen J 1990 *Solid State Ion.* **40** 187

[320] Richert R 1997 *J. Phys. Chem. B* **101** 6323

[321] Angell C A 1991 *J. Non-Crystall. Solids* **131–133** Part 1 13

[322] Roland B, Gerald H, Thomas J, Fei Q and Hans S 2000 *J. Phys.: Condens. Matter* **12** A383

[323] Kirkpatrick S 1973 *Rev. Mod. Phys.* **45** 574

[324] Maier J 2009 *Phys. Chem. Chem. Phys.* **11** 3011

[325] Wagner J B 1989 *Composite Solid Ion Conductors. High Conductivity Solid Ionic Conductors* (Singapore, New Jersey, Lodon, Hongkong: World Scienfic) p. 146

[326] Shahi K and Wagner J B 1982 *J. Phys. Chem. Solids* **43** 713

[327] Khandkar A, Tare V B, Navrotsky A and Wagner J B 1984 *J. Electrochem. Soc.* **131** 2683

[328] Maier J 1986 *Ber. Bunsen. Phys. Chem.* **90** 26

[329] Maier J 1987 *Mater. Chem. Phys.* **17** 485

[330] Maier J 2014 *Faraday Discussions* **6** 17

[331] Maier J 2005 *Nat. Mater.* **4** 805

[332] Hayashi A, Noi K, Sakuda A and Tatsumisago M 2012 *Nat. Commun.* **3** 856

[333] Sakuda A, Hayashi A and Tatsumisago M 2013 *Sci. Rep. Uk* **3** 2261

[334] Seino Y, Ota T, Takada K, Hayashi A and Tatsumisago M 2014 *Energy & Environmental Science* **7** 627

[335] Rangasamy E, Sahu G, Keum J K, Rondinone A J, Dudney N J and Liang C D 2014 *J. Mater. Chem. A* **2** 4111

[336] Trevey J E, Stoldt C R and Lee S H 2011 *J. Electrochem. Soc.* **158** A1282

[337] Leung K, Qi Y, Zavadil K R, Jung Y S, Dillon A C, Cavanagh A S, Lee S H and George S M 2011 *J. Am. Chem. Soc.* **133** 14741

[338] Aurbach D 2000 *J. Power Sources* **89** 206

[339] Qi Y 2013 *Abstracts of Papers of the American Chemical Society* **246** 340-COMP

[340] Iddir H and Curtiss L A 2010 *J. Phys. Chem. C* **114** 20903

[341] Yamamoto K, Yoshida R, Sato T, Matsumoto H, Kurobe H, Hamanaka T, Kato T, Iriyama Y and Hirayama T 2014 *J. Power Sources* **266** 414

[342] Santhanagopalan D, Qian D, McGilvray T, Wang Z Y, Wang F, Camino F, Graetz J, Dudney N and Meng Y S 2014 *J. Phys. Chem. Lett.* **5** 298

[343] Delmas C, Nadiri A and Soubeyroux J L 1988 *Solid State Ion.* **28–30** Part 1 419

[344] Shan Y J, Inaguma Y and Itoh M 1995 *Solid State Ion.* **79** 245

[345] Takada K, Inada T, Kajiyama A, Sasaki H, Kondo S, Watanabe M, Murayama M and Kanno R 2003 *Solid State Ion.* **158** 269

[346] Kennedy J H and Zhang Z M 1988 *Solid State Ion.* **28–30** 726

[347] Takada K 2013 *Langmuir* **29** 7538
[348] Yamada H, Oga Y, Saruwatari I and Moriguchi I 2012 *J. Electrochem. Soc.* **159** A380
[349] Ohta N, Takada K, Zhang L Q, Ma R Z, Osada M and Sasaki T 2006 *Adv. Mater.* **18** 2226
[350] Takada K, Ohta N, Zhang L Q, Fukuda K, Sakaguchi I, Ma R, Osada M and Sasaki T 2008 *Solid State Ion.* **179** 1333
[351] Takada K, Ohta N, Zhang L Q, Xu X X, Hang B T, Ohnishi T, Osada M and Sasaki T 2012 *Solid State Ion.* **225** 594
[352] Haruyama J, Sodeyama K, Han L Y, Takada K and Tateyama Y 2014 *Chem. Mater.* **26** 4248
[353] Yamamoto K, Iriyama Y, Asaka T, Hirayama T, Fujita H, Fisher C A J, Nonaka K, Sugita Y and Ogumi Z 2010 *Angew. Chem. Int. Edit.* **49** 4414
[354] Yamamoto K, Iriyama Y, Asaka T, Hirayama T, Fujita H, Nonaka K, Miyahara K, Sugita Y and Ogumi Z 2012 *Electrochem. Commun.* **20** 113
[355] Yamamoto K, Hirayama T and Tanji T 2013 *Microscopy* **62** S29
[356] Cheng L, Crumlin E J, Chen W, Qiao R, Hou H, Franz L S, Zorba V, Russo R, Kostecki R, Liu Z, Persson K, Yang W, Cabana J, Richardson T, Chen G and Doeff M 2014 *Phys. Chem. Chem. Phys.* **16** 18294
[357] Cheng L, Chen W, Kunz M, Persson K, Tamura N, Chen G and Doeff M 2015 *ACS Applied Materials & Interfaces* **7** 2073
[358] Fergus J W 2010 *J. Power Sources* **195** 4554
[359] Croce F, Appetecchi G B, Persi L and Scrosati B 1998 *Nature* **394** 456
[360] Wieczorek W, Florjanczyk Z and Stevens J R 1995 *Electrochim. Acta* **40** 2251
[361] Kasemagi H, Aabloo A, Klintenberg M K and Thomas J O 2004 *Solid State Ion.* **168** 249
[362] Bhattacharyya A J and Maier J 2004 *Adv. Mater.* **16** 811
[363] Fleischauer M D, Hatchard T D, Rockwell G P, Topple J M, Trussler S, Jericho S K, Jericho M H and Dahn J R 2003 *J. Electrochem. Soc.* **150** A1465
[364] Roberts M R, Vitins G, Denuault G and Owen J R 2010 *J. Electrochem. Soc.* **157** A381
[365] Schultz P G and Xiang X D 1998 *Curr. Opin. Solid St. M* **3** 153
[366] Xiang X D 1999 *Annu. Rev. Mater. Sci.* **29** 149
[367] Amis E J, Xiang X D and Zhao J C 2002 *MRS Bull.* **27** 295
[368] Xiang X D and Takeuchi I 2003 *Combinatorial Materials Synthesis*, Vol. 1 (New York: CRC Press)
[369] Zhao J C 2001 *Adv. Eng. Mater.* **3** 143
[370] Zhao J C 2005 *Annu. Rev. Mater. Res.* **35** 51
[371] Zhao J C, Jackson M R, Peluso L A and Brewer L N 2002 *Jom-J. Min. Met. Mat. S.* **54** 42
[372] Zhao J C 2014 *Chin. Sci. Bull.* **59** 1652
[373] Mohammed O F, Yang D S, Pal S K and Zewail A H 2011 *J. Am. Chem. Soc.* **133** 7708
[374] Hautier G, Fischer C C, Jain A, Mueller T and Ceder G 2010 *Chem. Mater.* **22** 3762
[375] Jain A, Hautier G, Moore C J, Ong S P, Fischer C C, Mueller T, Persson K A and Ceder G 2011 *Comp. Mater. Sci.* **50** 2295
[376] Qian C, Siler T and Ozin G A 2015 *Small* **11** 64